Published online: March 30, 2020

IMR Press

Review

Microneurosurgical techniques and perioperative strategies utilized to optimize experimental supracollicular decerebration in rats

George Zaki Ghali[1,2] and Michael George Zaki Ghali[3,4,*]

[1] *United States Environmental Protection Agency, Arlington, Virginia, 22202, USA*

[2] *Department of Toxicology, Purdue University, West Lafayette, Indiana, 47907, USA*

[3] *Department of Neurological Surgery, Baylor College of Medicine, Houston, Texas, 77030, USA*

[4] *Department of Neurobiology and Anatomy, Drexel University College of Medicine, Philadelphia, Pennsylvania, 19129, USA*

*Correspondence: mgzghali@gmail.com (Michael George Zaki Ghali)

DOI:10.31083/j.jin.2020.01.1153

Decerebration permits neurophysiological experimentation absent the confounding effects of anesthesia. Use of the unanesthetized decerebrate preparation *in vivo* offers several advantages compared with recordings performed in reduced slice preparations, providing the capacity to perform extracellular and intracellular neuronal recordings in the presence of an intact brainstem network. The decerebration procedure typically generates variable degrees of blood loss, which often compromises the hemodynamic stability of the preparation. We describe our microsurgical techniques and discuss microsurgical pearls utilized in order to consistently generate normotensive supracollicularly decerebrate preparations of the rat, exhibiting an augmenting pattern of phrenic nerve discharge. In brief, we perform bilateral ligation of the internal carotid arteries, biparietal craniectomies, securing of the superior sagittal sinus to the overlying strip of bone, removal of the median strip of bone overlying the superior sagittal sinus, supracollicular decerebrative encephalotomy, removal of the cerebral hemispheres, and packing of the anterior and middle cranial fossae with thrombin soaked gelfoam sponges. Hypothermia and potent inhalational anesthesia ensure neuroprotection during postdecerebrative neurogenic shock. Advantages of our approach include a bloodless and fast operation with a nil percent rate of operative mortality. We allow animal arterial pressure to recover gradually in parallel with gentle weaning of anesthesia following decerebration, performed contemporaneously with the provision of the neuromuscular antagonist vecuronium. Anesthetic weaning and institution of vecuronium should be contemporaneous, coordinate, gentle, gradual, and guided by the spontaneous recovery of the arterial blood pressure. We describe our microsurgical techniques and perioperative management strategy designed to achieve decerebration and accordingly survey the literature on techniques used across several studies in achieving these goals.

Keywords

Operative; technique; microsurgery; strategy; approach; vascular; supracollicular; neurophysiology; decerebration; rat

1. Introduction

The use of anesthesia significantly attenuates neuronal firing rate and neural network oscillatory synchrony, thus confounding the study of a variety of neurophysiological processes, especially those evaluating brainstem and spinal cord modulation of respiratory rhythm generation and pattern formation, sympathetic tone, cardiovagal premotoneuronal outflow, locomotor activity, nociception, and hippocampal theta oscillations (Sapru and Krieger, 1979). Parenterally administered (e.g., etomidate, propofol, urethane, alpha-chloralose, ketamine, pentobarbital) and inhaled (e.g., halothane, enflurane, isoflurane, sevoflurane, desflurane, nitrous oxide) anesthetics significantly reduce neuronal action potential discharge frequency, manifesting as reductions of firing rate and spectral power of neural activity in peripheral neurograms and single-unit recordings (Sapru and Krieger, 1979). Mechanisms underlying the suppressive effects of anesthetics include potentiation of GABAergic signaling, suppression of N-methyl-*D*-aspartate (NMDA)- and non-N-methyl-*D*-aspartate-dependent glutamatergic signaling, antagonism of neurolemmal membrane calcium ion channels, and modifications of neural plasmalemmal membrane fluidity (Kotani and Akaike, 2013; Petrenko et al., 2014). On a network level, anesthetics reduces the oscillatory synchrony between and amongst the sympathetic oscillators and the respiratory central pattern generator, thus compromising the principal neural output of studies seeking to interrogate mechanisms contributing to the regulation of arterial pressure and heart rate and generation of the breathing rhythm (Sapru and Krieger, 1979). Thus, it becomes readily apparent that results obtained using an anesthetized model may not be generalizable to the native awake state, a common theme observed across studies interrogating neural networks generating breathing and autonomic output (Ghali and Marchenko, 2016a,b; Ghali, 2017a,b,c,d, 2015, 2018, 2019a,c; Ghali and Beshay, 2019; Marchenko et al., 2012).

Journal of Integrative Neuroscience

The investigator is accordingly left with two alternatives to the use of anesthetized models. These include awake (Mueller et al., 2019) and unanesthetized decerebrate (or decorticate) animal preparations (Ghali and Marchenko, 2016a,b; Ghali, 2015, 2019a,c; Marchenko et al., 2012, 2016; Sherrington, 1898). Electrophysiological studies in the awake animal, while the most reflective and revelatory of true underlying mechanistic underpinnings of a given physiological process may consequently prove technically challenging and cumbersome to perform when attempting to obtain multiple concurrent recordings of central neuronal and efferent nerve discharge. Importantly, the concurrent use of multiple neuronal and neural efferent recordings elucidates fundamental and essential mechanistic underpinnings and neural network behavior of brainstem and spinal cord circuitry generating and modulating the breathing rhythm, sympathetic tone, and cardiovagal premotoneuronal outflow (Ghali and Marchenko, 2016a,b; Ghali, 2017a,b,c,d, 2015, 2018, 2019a,c; Ghali and Beshay, 2019; Marchenko et al., 2012). Successfully obtaining extracellular and intracellular recordings of individual units and peripheral neural efferent activity requires absolute mechanical stability and perfect electrophysiological isolation (Marchenko et al., 2012). Experimental decerebrate preparations accordingly represent a useful, though nevertheless technically-demanding (Ghali and Marchenko, 2016a,b; Ghali, 2015; Marchenko et al., 2012, 2016), alternative to the use of awake preparations in neurophysiological studies evaluating neural control of breathing (Bezdudnaya et al., 2018; Christakos et al., 1991; Cohen, 1975; Decima and von Euler, 1969; Ghali and Marchenko, 2013, 2015, 2016a,b; Ghali, 2017c,d, 2015, 2018; Ghali et al., 2019; Marchenko and Rogers, 2009, 2007, 2006a,b; Zielinski and Gebber, 1975) and autonomic (Destefino et al., 2011; Ghali, 2017a,b, 2019a; Marchenko and Sapru, 2003; Reynolds et al., 2019; Tsuchimochi et al., 2009) output. We accordingly suggest use of the decerebrate preparation may prove revelatory of subtleties of novel network mechanisms, not otherwise demonstrable in the anesthetized condition.

Decerebrative removal of the cerebral hemispheres (i.e., cerebrectomy) effectively annihilates the animal's capacity to consciously perceive noxious stimuli (Silverman et al., 2005), though brainstem propriobulbar circuitry continues to generate and organize reflexive spinoreticulospinal reflexes to painful stimuli. Removal of the cerebrum accordingly permits the safe and ethical gradual weaning of anesthetic and thus observe neural network behavior in its native unanesthetized state (Ghali and Marchenko, 2015, 2016a,b; Ghali, 2015, 2019a,c; Marchenko et al., 2012; Marchenko and Rogers, 2009, 2007, 2006a,b). Given greater ease of performing the microsurgical steps requisite to achieve appropriate hemostasis and prevent hemorrhage, the decerebration procedure yields significantly less blood loss and has consequently proven routine and commonplace across several larger animal species including dogs (Zuperku et al., 2019), cats (Amemiya and Yamaguchi, 1984; Christakos et al., 1991; Iwakiri et al., 1995; Iwamura et al., 1969; Kawahara et al., 1993; Medvedev and Stepochkina, 1975; Montano et al., 1992; Richardson and Mitchell, 1982), and rabbits (Clarke et al., 1988; Waites et al., 1996), having provided among the most critical insights regarding neural network mechanisms contributing to the genesis of respiratory, sympathetic, cardiovagal, and locomotor rhythmic discharge.

Massive intraoperative blood loss and a general paucity of studies specifically detailing the steps of the decerebration approach and preemptive strategies to prevent intraoperative hemorrhage represent the principal impediments to the effective and faithful use of the decerebrative procedure in rats and other small animals, yielding hypotensive preparations (Woolf, 1984) and significantly compromising the brainstem neural networks generating the breathing rhythm and sympathetic oscillations. Should the internal carotid arteries and superior sagittal sinus not be securely ligated, the cranium would fill rapidly with blood within a matter of seconds following decerebrative transection, having thus rendered the procedure classically impractical to perform in rats and mice. Studies have accordingly previously reported mortality rates approaching 50% (Fouad and Bennett, 1998). Many researcherss have consequently abandoned the use of this technique in smaller animal models or preferred anesthetized preparations given consequent massive blood loss and transection-related neurogenic brainstem shock, frequently yielding vasopressor-dependent hypotensive animals which do not survive for an appreciable period sufficient to permit neural recordings and experimental interventions. Studies have accordingly developed variant modifications of the technique in order to mitigate blood loss or technically simplify the procedure (Sapru and Krieger, 1978). In direct contradistinction, our experience generally yields normotensive or hypertensive animals which may remain stable in excess of fourteen hours (Ghali and Marchenko, 2015, 2016a,b; Ghali, 2015; Marchenko et al., 2012; Marchenko and Rogers, 2009, 2007, 2006a,b). In general agreement and concordance with our assessment, Dobson and Harris (2012) suggest the general lack of a detailed description of decerebration has also prevented more prevalent and facile use of this procedure in smaller mammals. The operative steps of classic mechanical decerebration were described with intermediate detail across several neurophysiological studies conducted in rats (de Almeida et al., 2010; Tsuchimochi et al., 2010). Decerebration may be effectively performed utilizing a variety of techniques and approaches, though typically involves mechanical transection of the neuraxis at a mid- or supra- (Ghali and Marchenko, 2015, 2016a,b; Ghali, 2015; Marchenko et al., 2012; Marchenko and Rogers, 2009, 2007, 2006a,b) collicular levels.

We have extensively utilized the unanesthetized supracollicularly decerebrate preparation of the adult rat with extraordinary success in our laboratory, strikingly revelatory of several novel and profound insights into the mechanistic underpinnings of the neural control of breathing (Ghali and Marchenko, 2015, 2016a,b; Ghali, 2015, 2019c; Marchenko et al., 2012) and blood pressure (Ghali, 2019a), not previously demonstrable through the use of anesthetized preparations (Ghali and Marchenko, 2015, 2016a,b; Ghali, 2015; Marchenko et al., 2012; Marchenko and Rogers, 2009, 2007, 2006a,b). Utilizing the unanesthetized decerebrate preparation of the rat, we systematically characterized a group of phrenic motoneurons discharging with high frequencies correlating with the high frequency spectral band in phrenic nerve discharge (Fig. 1) (Ghali and Marchenko, 2013; Ghali, 2017c; Marchenko et al., 2012) and demonstrated spontaneous preinspiratory activity in hypoglossal discharge in vagus-intact preparation during hyperoxic normocapnic conditions accentuated and cross-modally modulated by vagotomy and hypercapnia (Fig. 2) (Ghali

and Marchenko, 2016b; Ghali, 2015, 2019c), recovery of spontaneous crossed phrenic activity in population neural efferent discharge following high cervical hemisection (Figs. 3 and 4) (Ghali and Marchenko, 2015; Ghali, 2017d), spinal respiratory rhythm generation following high cervical transection (Fig. 5-8) (Ghali and Marchenko, 2016a), and recovery of arterial blood pressure to values approximating normal levels following high cervical transection (Fig. 9) (Ghali, 2019a). Marchenko et al., 2016 provided the strongest evidence supporting respiratory rhythmogenesis and pattern formation require fast inhibitory synaptic neurotransmission in anesthetized adult rats *in vivo* and unanesthetized decerebrate juvenile rats *in situ*. Neurophysiological studies evaluating neural control of gastrointestinal (Darling and Ritter, 2009), respiratory (Zhou et al., 1996), and nociceptive (Dobson and Harris, 2012) function may accordingly actualize significant benefit through the use of this preparation. In this discussion, we will accordingly evaluate the physiological and microsurgical variables governing successful decerebration in order to encourage and facilitate the widespread use of this experimental animal model in an economical, efficient, and systematically-reproducible manner.

2. Ghali Marchenko approach: microsurgical technique

2.1 General surgical preparation

All methods and procedures were approved by the Drexel University Institutional Animal Care and Use Committee, which oversees Drexel University's AAALAC International-accredited animal program. Experiments were conducted upon spontaneously-breathing Sprague-Dawley adult male rats (330-480 g) anesthetized with isoflurane (Matrix; 4-5% induction, 2.0-2.5% maintenance) vaporized in hyperoxia (97.5-98% fractional inspiration of O_2) via a snout mask. We recorded electrocardiogram (EKG) activity via three small subcutaneous electrodes placed in the classic Einthoven positions using conventional amplification and filtering settings (Neurolog; Digitimer, Hertfordshire, United Kingdom) and monitored using audio amplification (model AM10; Grass Instruments) and an oscilloscope. We maintained anesthetic depth at a level such that limb withdrawal reflexes and changes in sinoatrial nodal period in response to pinches of the distal hindlimb were eliminated. Following incision of the tracheal cartilage using electrocautery and tracheo-luminal cannulation using an atraumatic glass tube, animals were mechanically ventilated (respiratory rate: 45-65 cycles/min; tidal volume: 2.5-3.0 mL per breath; Columbus Apparatus) using the same gas mixture (Table 1). Cannulae were introduced into the right femoral artery and vein in order to record arterial pressure and intravenously infuse fluids and drugs, respectively. During the initial general surgical preparation and neural recordings, we maintained rectal temperature at 37.0 $\pm$ 0.1 °C through the use of the surgical lamp. The phrenic nerves were accessed and dissected from the brachial plexus and investing translucent fascia via a cervical pre-scalene approach. We visually identified the common carotid, external carotid, and internal carotid arteries and dissected investing soft tissue encasing the bifurcation of the common carotid artery in the high cervical region (Fig. 10). Soft tissue investing the vessels was gently incised, separated, and removed using sharp and fine microdissection. We identified the proximal extent of the occipital artery emanating from the proximal extent of the external carotid artery and clearly distinguished it from the proximal extent of the internal carotid artery. We ligated the internal carotid arteries bilaterally rostrally with respect to the origins of the pterygopalatine artery effectively preserving the integrity of the baroreceptor-rich carotid sinuses and chemoreceptor-rich carotid bodies (Fig. 11). We occasionally reapproximated the precervical soft tissues in anatomic layers utilizing continuous 6-0 silk suture. We reapproximated the ventral midline rostrocaudally-oriented midline cervical incision utilizing continuous 4-0 silk sutures placed through the cutis and subcutis. We subsequently situated the animal prone in a stereotaxic device and placed lateromedially mobilizable titanium bars in the external acoustic meati bilaterally to achieve head fixation.

2.2 Neurosurgical technique

Rigid head fixation allows the surgeon to trephine the animal under mechanically stable conditions, though should not be excessively overzealous to an extent which significantly compromises presympathetic bulbospinal excitatory synaptic drive conveyed to somatodendritic neuronal membranes of intermediolateral cell column preganglionic sympathetic neurons monosynaptically and polysynaptically through interposed interneuronal relays and generate consequent reductions of the arterial blood pressure. Bilateral everting scalp retraction utilizing 4-0 silk suture follows rostrocaudally oriented sagitally-approximated incision using scissors (Fig. 12). Microdissection of epicranial soft tissue (Fig. 13) proceeds utilizing blunt instruments and that surrounding the margins of the cranial convexity proceeds utilizing bipolar electrocautery (Fig. 14). A diamond drill bit generates generous biparietal craniectomy windows leaving a narrow segment of medianly situated overlying the parietal extent of the superior sagittal sinus (Figs. 15-19). We microsurgically carve concave cuts in the narrow segment of bone overlying the superior sagittal sinus lateromedially using a smaller diamond bit at the four angles between the superior sagittal sinus (SSS)-adjacent the medial sagittal and caudal transverse margins bordering the craniectomy windows and in order to thin the area, thus rendering continuous the two sets of bays (rostral and caudal) (Fig. 18). We subsequently sharply incise the variably tense dura mater covering the left and right parietal lobes of the cerebral hemispheres. Some bleeding may ensue from transection of the dural vessels, though should not alarm the veteran and seasoned investigator (Fig. 19) and may be effectively curtailed by gently placing a cold thrombin-soaked gelfoam sponge on the oozing region and sufficiently suspend the microsurgical impulse to permit the native therapeutically-activated procoagulant pathways to generate platelet-fibrin thrombi in the transected ends of the fine dural vessels. We subsequently thread a 6-0 or 4-0 silk suture needle through one parietal lobe, beneath the superior sagittal and paired anterior cerebral arteries, through the falx cerebri, and ventrodorsally through the substance and surface of the contralateral parietal lobe (Fig. 19). We use the same thread to ligate the superior sagittal sinus to the overlying narrow median segment of bone in the bay areas of thinned cancellous and compact calvarial bone. We repeat this maneuver in order to rostrally and caudally ligate the superior sagittal sinus.

At this juncture, the remainder of the procedure may take on one of several permutative variations. Osteotomy of the narrow

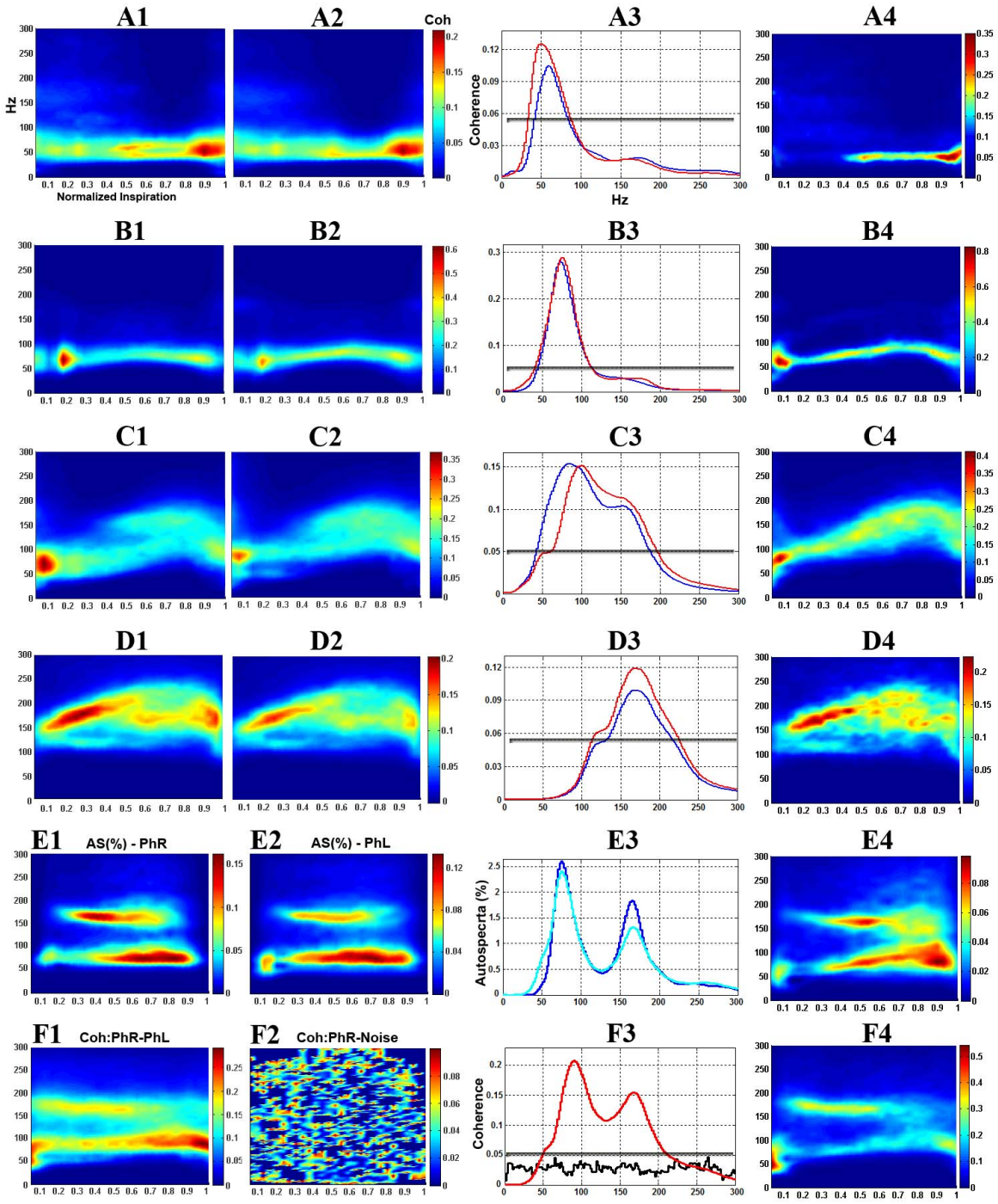

Figure 1. Dynamic phrenic motoneuron-phrenic nerve (PhMN-PhN) coherence in the unanesthetized supracollicularly decerebrate rat. A1-D1: Smoothed pseudo Wigner-Ville Distribution (SPWVD) time frequency representation (TFR) population-averaged PhMN-ipsilateral PhN coherence. A2-D2: population-averaged PhMN-contralateral PhN coherence. A3-D3: Time-averaged (reconstructed from SPWVD TFR) PhMN-PhN coherence for ipsilateral (red) and contralateral (blue) sides. A4-D4: Representative individual PhMN-PhN (ipsilateral) coherence. A1-A4: low frequency (LF) PhMNs. B1-B4: medium frequency (MF) PhMNs. C1-C4: high frequency (HF) PhMNs. D1-D4: high frequency PhMNs with background tonic activity (HF+BG). E1, E2: normalized (%) TFR autospectra of population-averaged right (E1) and left (E2) PhNs. E3: reconstructed autospectra for right (cyan) and left (blue) PhN. E4: normalized (%) autospectrum of an individual PhN. F1: TFR coherence between population-averaged left (PhNL) and right (PhNR) phrenic nerves. F2: control, showing coherence between right PhN and band-limited (0-5,000 Hz) white noise. F3: reconstructed PhNR-PhNL (red) and PhNR-noise (black) coherence. F4: TFR coherence between individual pairs of left and right PhNs (same animal). *Gray lines* in A3-D3 and F3 indicate the top 95% confidence threshold for coherence. Modified with permission from Marchenko et al. (2012).

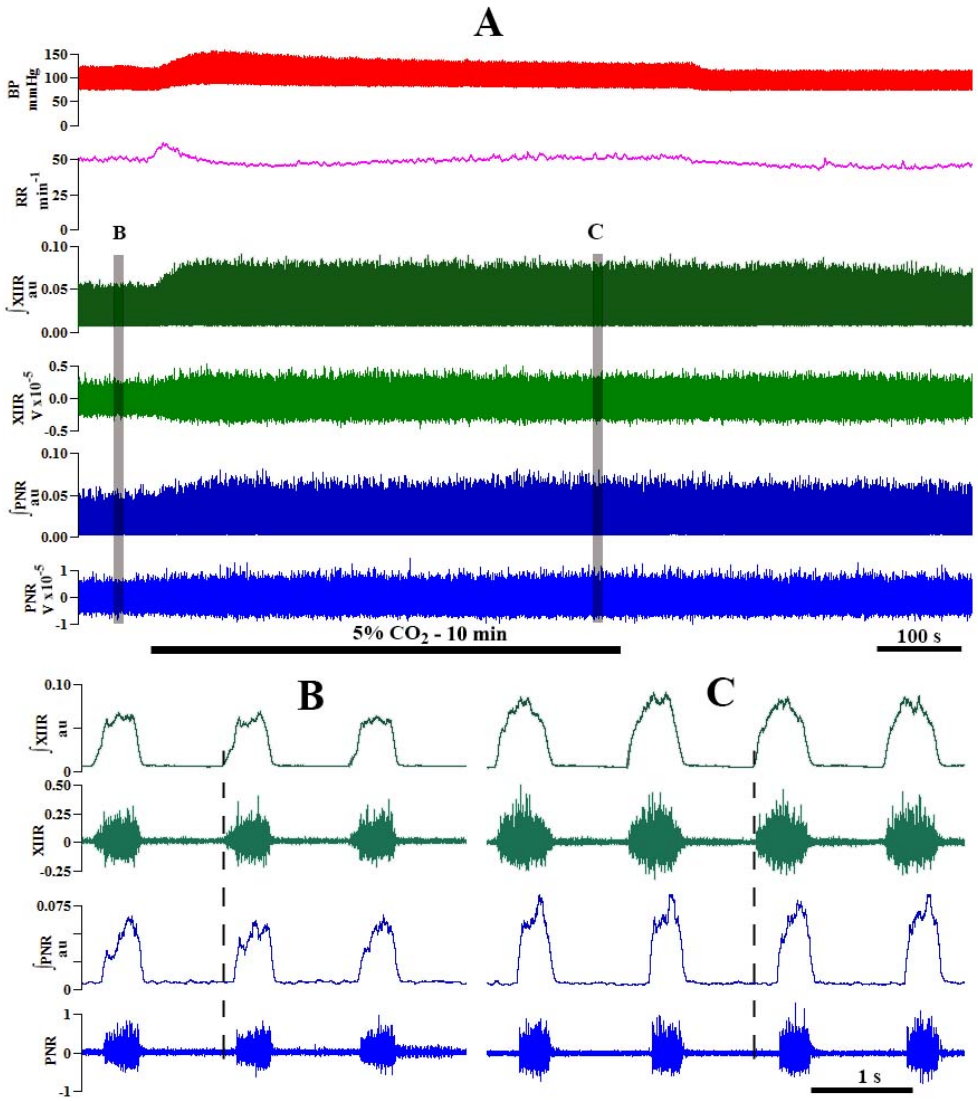

Figure 2. Responses of phrenic and hypoglossal nerve activity to hypercapnia in the vagotomized unanesthetized supracollicularly decerebrate rat. A: Compressed recording. Top trace represents blood pressure (BP; mm Hg). Second trace represents fictive neural breathing frequency or respiratory rate (RR; min^{-1}). B: control recording during hyperoxic (100% O_2) normocapnia (from first segment highlighted in gray in 'A'). C: experimental recording during hyperoxic (95% O_2) 5% hypercapnia (from second segment highlighted by gray in 'A'). Right phrenic nerve (PNR), hypoglossal nerve (XIIR); PNR and XIIR raw activity (volts); ∫ - integrated PNR and XIIR activity (arbitrary units; au). Modified with permission from Ghali and Marchenko (2016b).

median segment of bone overlying the superior sagittal sinus between the ligatures may be performed and the interposed osseous wedge microsurgically drilled using a diamond drill bit connected to a high-speed surgical drill and removed. Rostral and caudal ligation of the superior sagittal sinus (Fig. 20) permits transective interruption utilizing iridectomy scissors (Fig. 21). Alternatively, the bone overlying the superior sagittal sinus may be left in place. The former strategy facilitates decerebrative encephalotomy and the latter marginally reduces operative time. When performing osteotomy and double ligation and transection of the SSS, diencephalo-mesencephalic transection may be performed via a single motion by insertively advancing a microspatula into cerebral parenchyma at the supracollicular level approximately 2.0 to 2.5 mm rostral to the level of lambda and carrying the transection laterally across the midline (akin to cutting cake), while avoiding severing the posterior communicating arteries at the cranial base (Fig. 22). When maintaining the narrow median segment of bone overlying the superior sagittal sinus in place, two motions are consequently required in order to successfully perform the encephalotomy - the first motion advances the microspatula through one craniectomy window underneath the superior sagittal sinus into the contralateral posteroinferolateral sphenosquamous suture between the middle and posterior cranial fossae, then carrying the transection ipsilaterally using the same motion repeated through the contralateral parietal craniectomy window.

Removal of supratentorial cerebral tissue rostral to the transverse rostral transected surface of the mesencephalon via aspirative suctioning follows encephalotomy. Temporal, frontal, and oc-

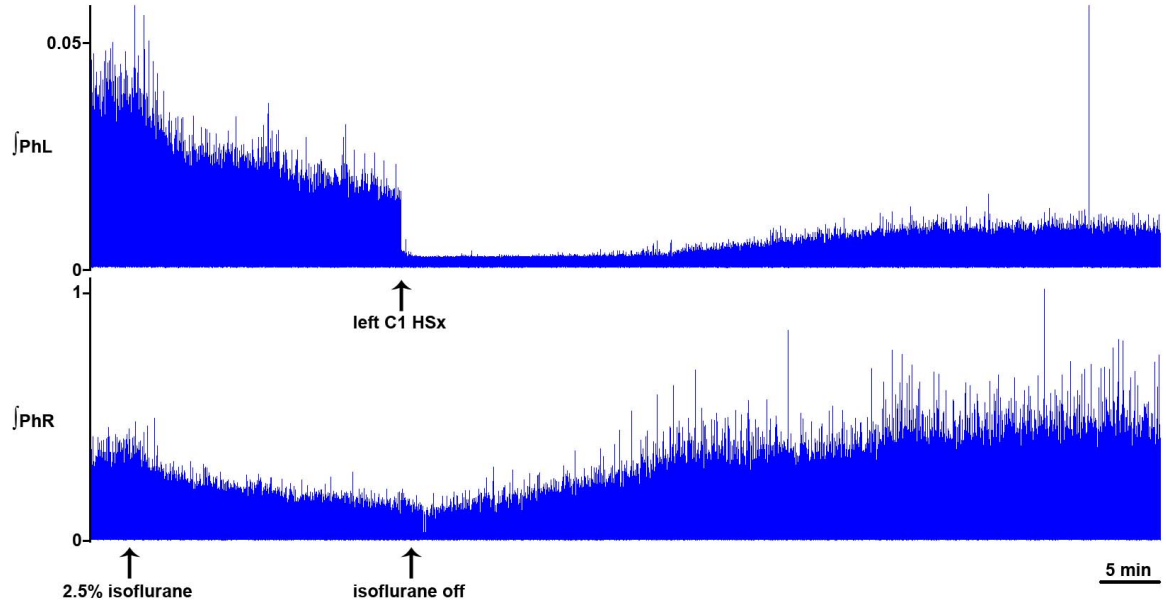

Figure 3. Dynamic changes in phrenic motor output following C_1 hemisection in the unanesthetized supracollicularly decerebrate rat. Readministration of isoflurane anesthesia in the decerebrate condition immediately preceding C1 hemisection attenuates PhN amplitude bilaterally. C1 hemisection of the upper cervical spinal cord performed under isoflurane anesthesia abolishes bursting in the ipsilateral phrenic neurogram. Acute recovery of bursting in the phrenic nerve discharge ipsilateral to C1 hemisection commences within minutes, and progresses during the course of several hours, following C1 myelic injury. PhL, left phrenic nerve; PhR, right phrenic nerve; HSx, hemisection; phrenic nerve amplitude is shown in millivolts (mV). Timescale bar is shown in lower right hander corner. Modified with permission from Ghali and Marchenko (2015).

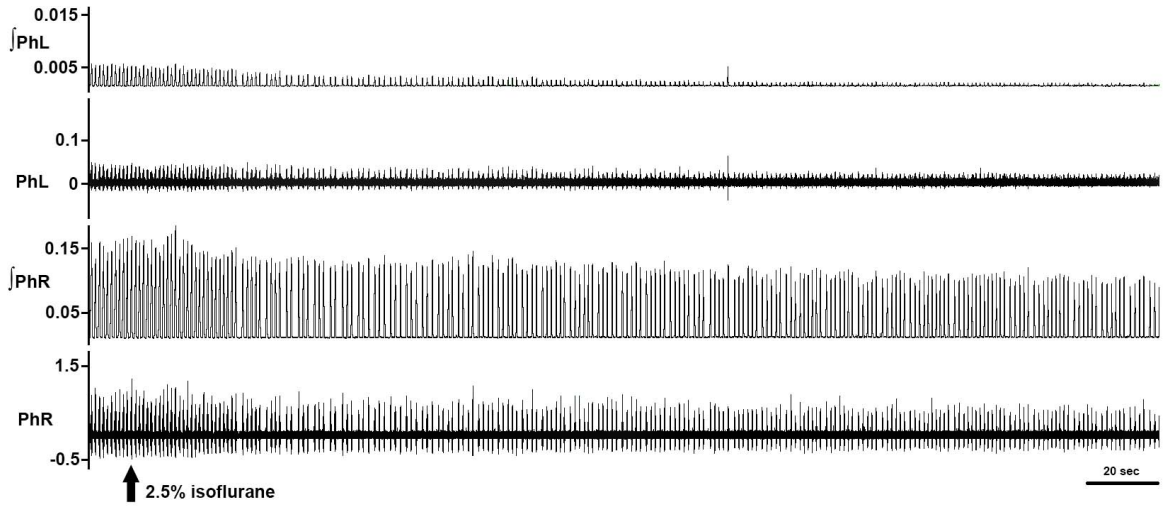

Figure 4. Isoflurane attenuates crossed phrenic nerve activity in the C1-hemisected unanesthetized supracollicularly decerebrate rat. Readministration of isoflurane potent inhalational anesthesia two hours following a hemisection potently attenuates amplitude of rhythmic bursting in phrenic nerve discharge bilaterally and nearly abolishes recovery of spontaneous crossed phrenic nerve activity in PhN ipsilateral to HSx (PhL). PhL, left phrenic nerve; PhR, right phrenic nerve; phrenic nerve amplitude is shown in millivolts (mV). Timescale bar is shown in lower right hander corner. Modified with permission from Fig. 5 of Ghali and Marchenko (2015).

cipital lobectomies follows incipient aspirative parietal lobectomy (Fig. 22). Aspiration of the occipital lobe proceeds *sans* injury to the rhombencephalon by maintaining the suction tip at the most superficial aspect of the caudal margins of the parietal craniectomy windows. The anterior and middle cranial fossae are packed with gelfoam soaked in cold thrombin solution following suctioning of the cerebral parenchyma (Fig. 23). Underpacking of the cranial cavity should be avoided in order to ensure effective skull base hemostasis and mechanically preclude rebleeding and overpacking of the cranial cavity should be avoided in order to prevent transforaminal herniation of the parenchymal contents of the posterior cranial fossa (Fig. 24). Initial post-decerebrative recovery of ani-

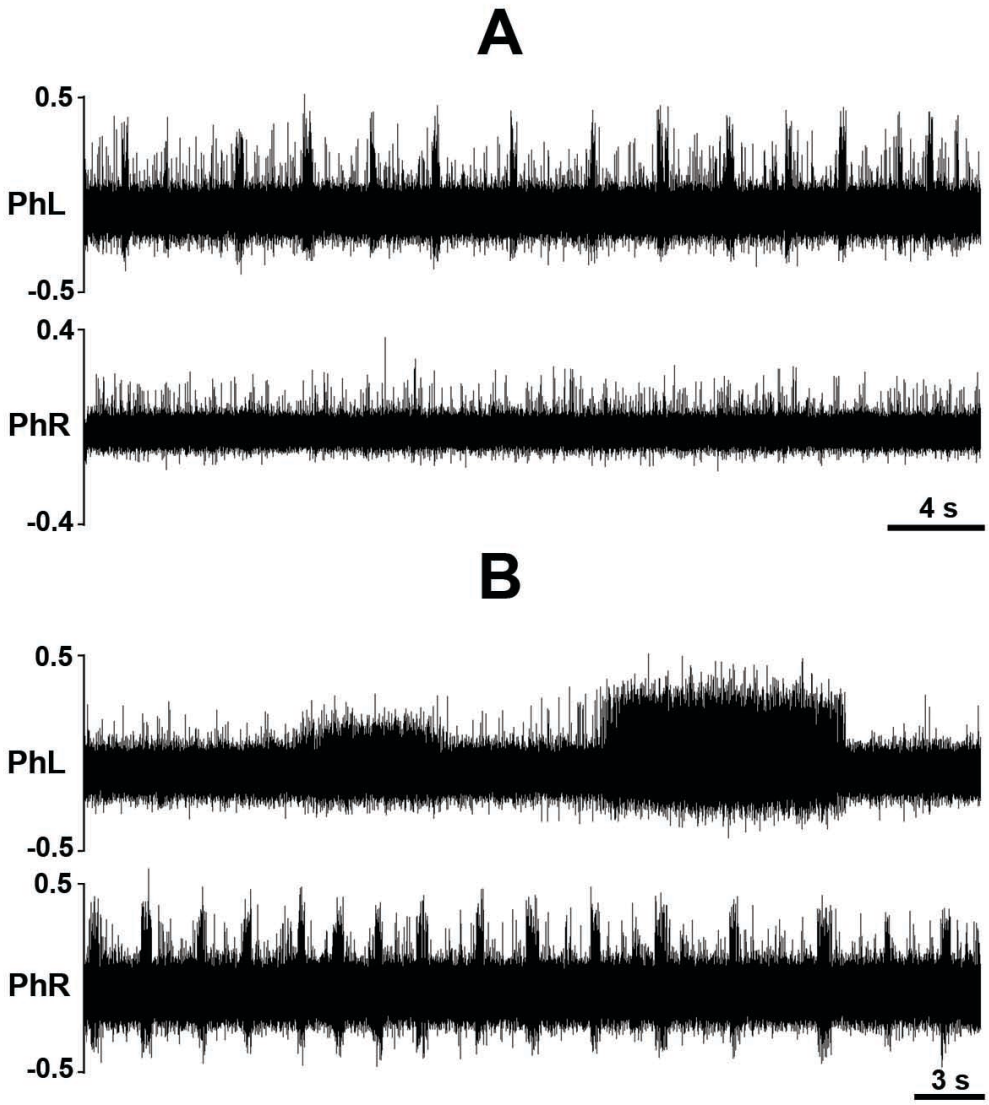

Figure 5. Phasic bursting in the phrenic nerve discharge and phrenic slow oscillations in C_1 transected unanesthetized supracollicularly decerebrate rat. A: Unilateral phasic bursting with background tonic activity in left phrenic nerve discharge and irregular (i.e., tonic) activity in right phrenic nerve discharge. B: Slow oscillations in left phrenic nerve bursting and phasic discharge with tonic background activity in right phrenic nerve discharge. Slow oscillations manifest in left phrenic neurogram curiously exhibit a frequency bearing striking resemblance with the central tendency of arteriolar oscillations (vasogenic autorhythmicity) (~ 0.05 Hz). The finding may evidence common propagation of arteriogenic oscillations to, and/or interactions between, propriospinal interneuronal microcircuit oscillators generating respiratory-related rhythmic bursting and sympathetic activity. PhL, left phrenic nerve; PhR, right phrenic nerve. Modified with permission from Fig. 3 of Ghali and Marchenko (2016a).

mal arterial blood pressure, sympathetic activity, and neural network synchrony proceeds at the same anesthetic depth. Weaning and eventual withdrawal of anesthesia should proceed slowly during the course of approximately one hour to the extent permitted by hemodynamic condition. We typically reduce the level of isoflurane anesthesia in quantal decrements of approximately 0.5% every 15 to 20 minutes, though we encourage the custom design and individualization of perioperative management of anesthetics fitting the instinct of the investigator. The incipient development of "neurophysiologist instinct" typically requires one to have extensively conducted neural recordings in decerebrate animal preparations. Prior to complete withdrawal of isoflurane anesthesia, we characteristically administer a bolus injection of 2 mg/kg vecuronium bromide (0.4 mg/mL) followed by intravenous infusion (4 mg $kg^{-1}\,h^{-1}$) of the same alternately dissolved in Ringer-Locke solution or artificial cerebrospinal fluid. Preservation of parenchymal between the mesencephalic locomotor region, (comprised of pedunculopontine and cuneiform nuclei), and medullary reticulospinal units may permit locomotor activity in the unanesthetized decerebrate condition. We have occasionally observed forelimb and hindlimb locomotor activity representing nascent soi-disant "attempts" at running in the event of anesthetic weaning *sans* commensurate administration of neuromuscular-type nicotinic acetylcholinergic antagonist [Nota Bene: We have used vecuronium to

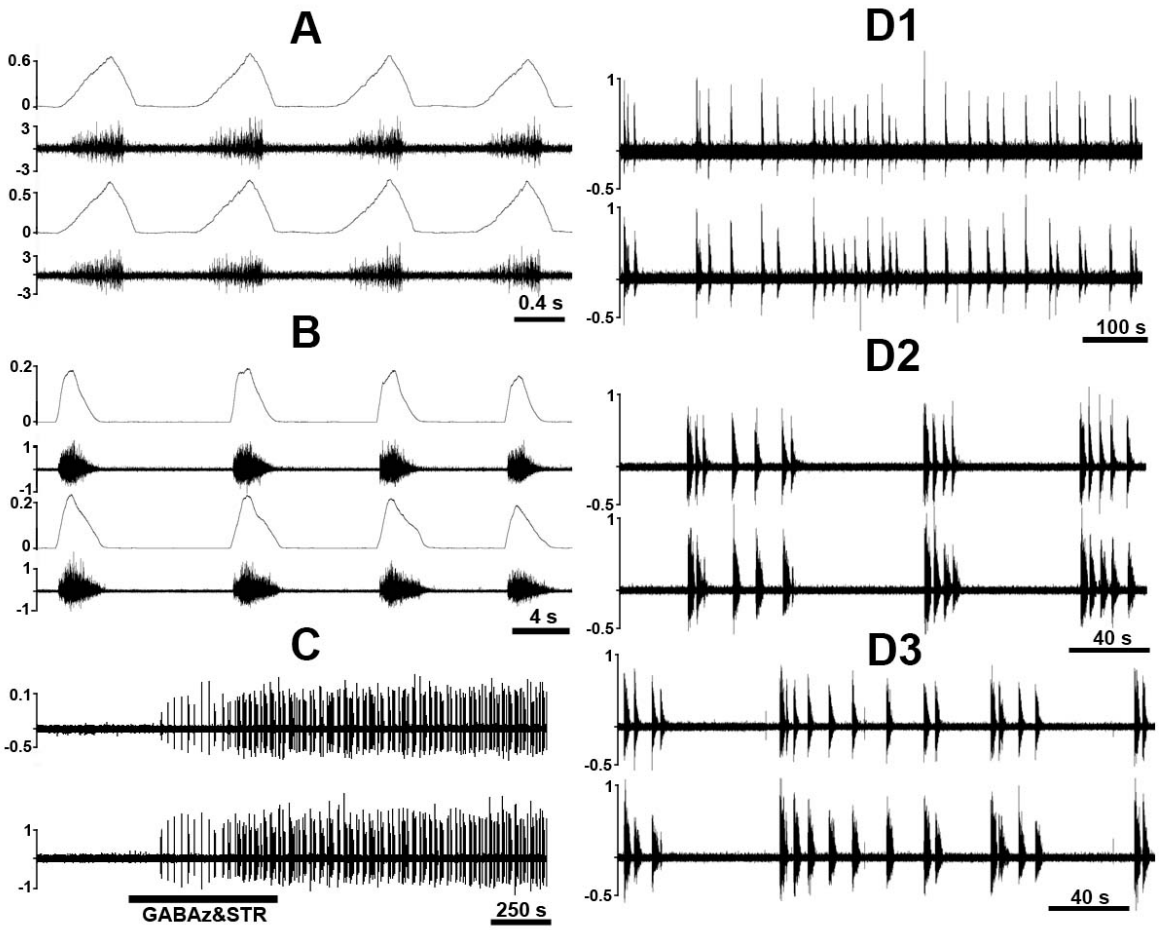

Figure 6. Chemical disinhibition of C1-C2 pre-phrenic interneurons via topical treatment of upper cervical spinal segments C1 and C2 with a cocktail of gabazine (GABAz) and strychnine (STR) elicits phasic bursting in PhN discharge in the unanesthetized supracollicularly decerebrate rat following C_1-spinalization. A: Eupneic phrenic nerve bursting. B: GABAz/STR-induced PhN bursting. C: Compressed recording illustrating phrenic nerve activity elicited in response to GABAz/STR disinhibition of C1-C2 pre-phrenic interneurons. D1-D3: Evolutionary dynamics of GABAz/STR-induced bursting in PhN discharge from slow sub-regular rhythmic-like bursting activity with occasional bursting doublets (D1), to a rhythm exhibiting cluster-like grouping of phasic bursts (D2), and a return to pseudo-regular rhythmic-like activity (D3). Note inconsistency of cycle length and phrenic burst amplitude during GABAz/STR-induced phrenic bursting compared with the normal eupneic rhythm and differences in burst shape of the former (decrementing spatiotemporal dynamics) compared with the latter (augmenting or ramp-like pattern). PhL, left phrenic nerve; PhR, right phrenic nerve; PhN integrated activity (!PhN) is shown in arbitrary units. Modified with permission from Fig. 9 of Ghali and Marchenko (2016a).

achieve effective neuromuscular antagonism and flaccid paresis, though the effects of rocuronium appear to wear off extremely rapidly in our experimental preparation. We do not have a satisfactory nor adequate way to explain this, though we posit rapid metabolism or ligand-receptor mismatching could putatively prevent rocuronium from effectively achieving neuromuscular antagonism sufficient to permit neuronal and neural recordings in the unanesthetized preparation of the decerebrate rat].

Decerebration was successfully performed in all animals *sans* bleeding or neurogenic shock refractory to resuscitative maneuvers. Arterial blood pressure recovered to normotensive or slightly hypertensive values in all animals following decerebration (Fig. 2). Electrophysiological recordings and experimental interventions were typically conducted 1 to 2 hours following decerebrative encephalotomy. Neural recordings of hypoglossal and phrenic nerve efferent activity exhibiting a high ratio between the spatiotemporally dynamic amplitude of rhythmic phrenic bursting and background tonic noise were successfully obtained across all experiments (Fig. 3). Monophasic recordings of hypoglossal and phrenic neural efferent activity revealed regularly rhythmic bursting synchronized with the ventilator cycle. Hypoglossal neural efferent activity demonstrated regularly rhythmic bursting and an augmenting pattern of preinspiratory inspiratory discharge and phrenic neural efferent activity evidenced an augmenting pattern of inspiratory discharge, with variable postinspiratory activity. We venture to propose the presence of an augmenting pattern of phrenic nerve discharge represents an unparalleled metric indicating integrity of brainstem propriobulbar and bulbospinal circuitry.

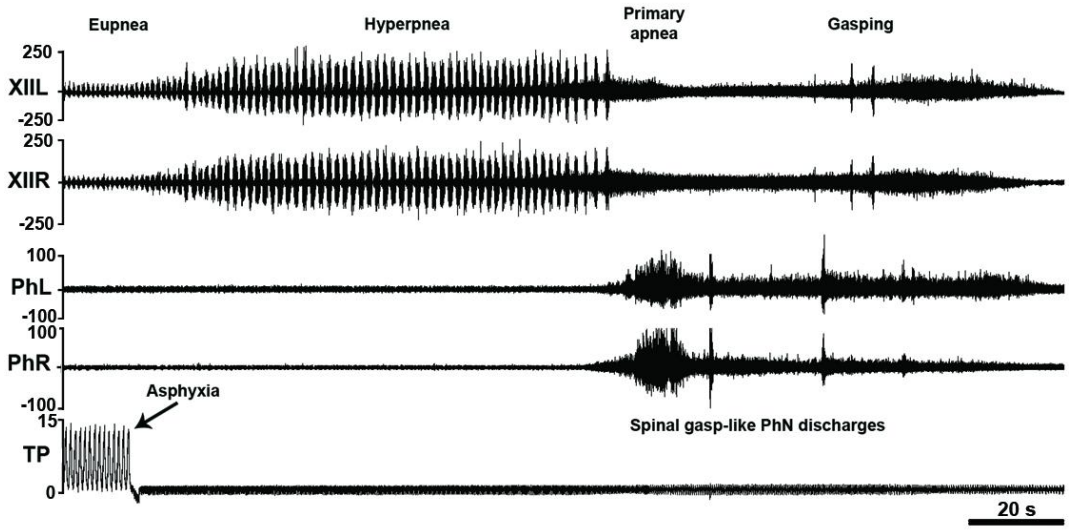

Figure 7. Asphyxia-induced phrenic nerve bursting in the C1-transected unanesthetized supracollicularly decerebrate rat. Out-of-phase asphyxia-induced phrenic and hypoglossal bursting in a C_1-transected unanesthetized supracollicularly decerebrate rat. Asphyxia elicits left-right synchronized medullogenic gasping in hypoglossal nerve (XII) discharge uncoupled from left-right synchronized myelogenic phrenic nerve bursting. Time scale bar 0.5 s. PhL, left phrenic nerve; PhR, right phrenic nerve; XIIL, left hypoglossal nerve; XIIR, right hypoglossal nerve; TP, tracheal pressure; CO_2, end-tidal carbon dioxide. Modified with permission from Ghali and Marchenko (2016a).

3. Zaki Ghali Marchenko approach: microsurgical pearls

3.1 Anesthesia and temperature

In our experimental experience, we have observed several general trends correlating with successful procedural outcome which may prove beneficial and instructive to the investigator seeking to optimize and adapt the technique of decerebration in neurophysiological experimentation (Table 2). We recommend induction and maintenance of animals using potent inhalational anesthetics during the general surgical preparation, since the distribution of fat-soluble agents including pentobarbital, urethane, or alpha-chloralose to adipose stores and biphasic elimination, comprised of replace with Greek letter alpha (a) (fast) and replace with Greek letter beta (b) (slow) phases, could render decerebrate models prepared using these agents, in effect, slightly anesthetized. We have critically observed that maintaining relative hypothermia, with a core body temperature of approximately 32.5-35.5 °C, during biparietal trephination, decerebrative encephalotomy, skull base hemostasis, and postprocedural recovery generates more stable animal preparations compared with normothermic ($>$ 36 °C) conditions. It may be that moderate hypothermia protects the neuronal and astrocytic elements constituting the brainstem during the neurogenic hypotension which immediately follows decerebrative transection (Shintani et al., 2010). Concurrent use of a heating blanket and the surgical lamp often proves sufficient in maintaining normothermia during the operation. Accordingly, during the initial surgical preparation, exclusive use of the surgical lamp *sans* heating blanket typically generates moderate neuroprotective hypothermia. Following decerebration, we utilize a servo-controlled heating blanket in order to maintain animal temperature within 37.0 $\pm$ 0.5 °C.

3.2 Cephalic fixation

Rigidity of head fixation occasionally correlates inversely with magnitude of the arterial pressure: tightening the head fixation reduces blood pressure and gently releasing it slightly systolic, and diastolic, arterial blood pressure. Accordingly, the animal's head should be fixed to an extent permitting craniotomies to be performed in a mechanically stable manner, though not excessively so such that animal systolic arterial pressure decreases below 90 mmHg nor diastolic arterial pressure decreases below 60 mmHg.

3.3 Permissive hypotension

Maintenance of lower levels of systolic arterial blood pressure (70 to 100 mmHg) during the interim period interposed between biparietal trephination through perioperative recovery may effectively reduce post-transection bleeding from the circle of Willis. However, we have typically observed greater degrees of systolic hypotension during the decerebration procedure consistently correlate with lower levels of blood pressure experienced by the animal during post-transection neurogenic shock. We accordingly believe the severity and duration of this transient hypotension could inversely correlate with animal longevity post-operatively, though certainly mitigated by the judicious use of neuroprotective hypothermia and isoflurane gas anesthesia.

3.4 Arterial inflow and venous outflow control

Bilateral ligation of the internal carotid arteries achieves excellent hemostasis and prevents intraoperative and postoperative blood loss (Ghali and Marchenko, 2015, 2016a,b; Ghali, 2015, 2019a,c; Hayashi, 2003; Marchenko et al., 2012; Sapru and Krieger, 1978). Our use of bilateral internal carotid artery ligation accordingly carries the risk of possible ischemogenic cerebral edema, which may be mitigated by reducing, to the extent permissibly feasible, the interval interposed between vascular ligation and decerebrative transective encephalotomy. Dobson and

Table 1. Decerebrative encephalotomy microsurgical technique and perioperative management.

Microsurgical maneuver	Purpose and comments
High bilateral ligation of internal carotid arteries above the level of pterygopalatine arteries	Preserve carotid sinus and carotid bodies
Animal spontaneously cooled to moderate hypothermia	Protects neural tissue
Animal placed in stereotaxic device	Prone
Cranial fixation with bars in external acoustic meatus	Excessive pressure results in hypotension
Head and neck ventroflexed to facilitate exposure to suboccipital zone and upper cervical region	Opens the posterior fossa and upper cervical cord
Midline rostrocaudal scalp incision	Scalpel or scissors
Bilateral lateral retraction of cutaneous subcutaneous flap	4-0 suture threads, two on each scalp flap, creates hexagonal shaped bay
Dissection of soft tissue overlying cranial convexity	Facilitates bone drilling
Biparietal craniectomies contained by coronal and lambdoid sutures	Placed parasagittally in order to prevent bleeding from superior sagittal sinus
Bregma and lambda adjacent bays	Allows securing of SSS in order to closely compress this venous structure against the overlying bone
Bilateral parietal durotomies	Facilitates placement of superior sagittal sinus ligatures
Ligation of superior sagittal sinus to overlying bone	Prevents bleeding during decerebration
Osteotomy of midline sagittal strip of bone	Permits ligation and transection of superior sagittal sinus
Double ligation and transection of superior sagittal sinus	Permits diencephalomesencephalic transection in a single motion
Diencephalomesencephalic transection 2-2.5 mm rostral to lambda	Between caudal thalamus and rostral mesencephalon
Removal of telencephalic and diencephalic structures	Prevents central transtentorial and transforaminal herniation from cerebral edema
Anterior and middle cranial fossae packed with cold thrombin soaked gelfoam sponges	Achieves hemostasis of the cranial base
Gradual weaning of isoflurane anesthesia	Allows recovery of medullary sympathetic oscillators
Animal loaded with and maintained on vecuronium	Permits neurophysiological recordings under stable conditions
Rearming to normothermia	Servocontrolled heating blanket

Table 2. Variants of decerebration.

Authors	Variant	Operative premise
Marchenko and Sapru (2003), Marchenko and Rogers (2006a), Marchenko and Rogers (2006b), Marchenko and Rogers (2007), Marchenko and Rogers (2009), Marchenko et al. (2012), Ghali and Marchenko (2015), Ghali and Marchenko (2015), Ghali and Marchenko (2016a), Ghali and Marchenko (2016b), Ghali (2019a), Ghali (2019c), Dobson and Harris (2012), Hayashi (2003),	Mechanical transection with removal of telencephalic and diencephalic structures	Supracollicular or midcollicular coronal transection with removal of cerebrum
Faber et al. (1982)	Mechanical transection with preservation of telencephalic and diencephalic structures	Supracollicular or midcollicular coronal transection with preservation of cerebrum
Pollock and Davis (1930), Bennett et al. (1998)	Ischemic decerebration via surgical ligation	Surgical ligation of internal carotid arteries bilaterally and basilar artery
Fouad and Bennett (1998)	Ischemic decerebration via embolization	Embolization of cranial base arteries
Faber et al. (1982)	Chronic decerebration	Supracollicular or midcollicular coronal section without removal of cerebrum

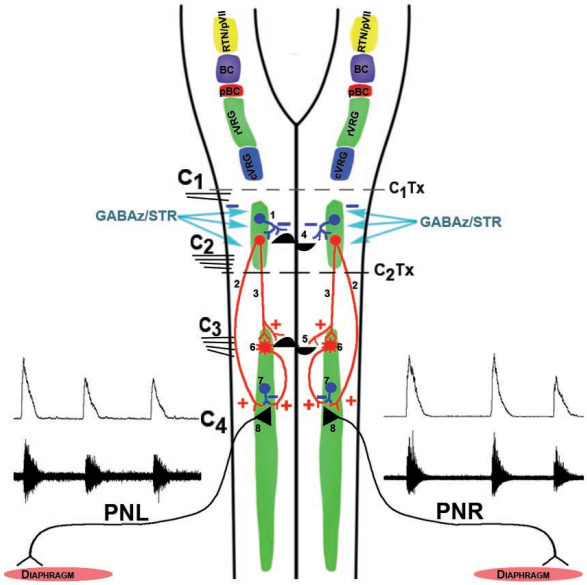

Figure 8. Conceptual models of brainstem and spinal generators underlying phasic activity in phrenic nerve discharge. Color traces indicate excitatory (+, red) and inhibitory (-, blue) synapses. Top: Medullary drive to the phrenic motor nucleus. The retrotrapezoid nucleus-parafacial respiratory group (RTN/pVII, yellow) consists of a group of Phox2b transcription factor expressing neurons. The retrotrapezoid nucleus is a central chemoreceptor region exquisitely sensitive to modifications of the hydrogen ion neural interstitial concentration (from the reaction of arterial CO_2 with H_2O) and provides tonic excitatory drive to Bötzinger complex decrementing glycinergic postinspiratory and augmenting expiratory neurons, pre-Bötzinger complex pre-inspiratory, pre-inspiratory inspiratory phase spanning, and decrementing early-inspiratory units, rostral ventral respiratory group augmenting and late inspiratory neurons , along with other elements in the medullary respiratory network. The parafacial respiratory group is comprised of a group of pre-inspiratory units interacting with or providing originate drive to pre-Bötzinger pre-inspiratory units. The Bötzinger (BC, violet) and pre-Bötzinger (pBC, dark red) complexes interact to generate the respiratory rhythm and control bulbospinal inspiratory neurons in the rostral ventral respiratory group (rVRG, green) and bulbospinal expiratory units in the caudal ventral respiratory group (cVRG, cyan). 1) Combined treatment of C_1-C_2 spinal neurons with the selective $GABA_A$ receptor antagonist gabazine (GABAz) and the selective glycine receptor antagonist strychnine (STR) removes inhibition of a generator (4) located among C_1-C_2 pre-phrenic interneurons which in turn provides phasic excitation (2) to PhMNs directly or via phrenic interneurons. In addition to cessation of phasic excitation, tonic inhibition contributes to burst termination. GABAz/STR may disinhibit C_1-C_2 pre-phrenic interneurons, which in turn provide tonic excitatory drive to a phrenic rhythm generator (5). GABAz/STR-disinhibited excitatory C_1-C_2 pre-phrenic interneurons activate PhMNs (8) directly (2) or indirectly (3) via C_3-C_5 pre-phrenic interneurons (6). PhMNs also receive tonic inhibition from intra-phreninuclear interneurons (7). In this model, the phrenic nucleus is the originator of phasic excitation and possesses tonic inhibitory elements which contribute to burst termination. In either model, the generator may function as a network oscillator or discharge by virtue of the presence of intrinsic bursting units (i.e., pacemaker-like cells). PhL, left phrenic nerve; PhR, right phrenic nerve; GABAz/STR, gabazine/strychnie. Modified with permission from modified with permission from Fig. 11 of Ghali and Marchenko (2016a).

Harris (2012) advocate the use of reversible temporary clipping of the common carotid arteries in order to protect the influence of carotid sinus baroreceptor stretch upon the activity of the sympathetic oscillators and cardiovagal premotoneurons residing within the brainstem and regulating the arterial blood pressure and sinoatrial period (Tang et al., 2010). In our experience, dissection and high ligation of the internal carotid arteries above the level of the pterygopalatine artery achieves these goals commensurately. In their technique performing decerebration in rabbits, Taylor et al. (1991) describe leaving one carotid artery intact in order to reduce the frequency of paroxysmal hypotensive episodes, which could putatively ensue from loss of hypothalamic neuronal inputs to rostral ventrolateral medullary presympathetic units. We accordingly suggest silk suture ligation of the internal carotid arteries above the level of the pterygopalatine artery bilaterally (Ghali and Marchenko, 2015, 2016a,b; Ghali, 2015, 2019a,c; Marchenko et al., 2012, 2015) or reversible temporary clipping of the internal carotid arteries to be performed in conjunction with packing of the skull base and cranial cavity with cold thrombin-soaked gelfoam packing without or with concurrent use of tissue adhesive represent equivalently viable alternatives to achieving reduction of cranial arterial inflow (Dobson and Harris, 2012). Though studies have occasionally anecdotally described arterial blood pressure dynamics prior to, and following, decerebration (Faber et al., 1982; Sapru and Krieger, 1978), no study has sought to characterize time variant recovery of hemodynamic variables during the interregnum. Sparing of the mesencephalic locomotor region constituted by the pedunculopontine and cuneiform nuclei by a supracollicularly placed transective encephalotomy permits animal locomotor activity in response to noxious or non-noxious cutaneovisceral stimuli. Parenteral intravenous administration of bolus and maintenance doses of neuromuscular type nicotinic acetylcholin-

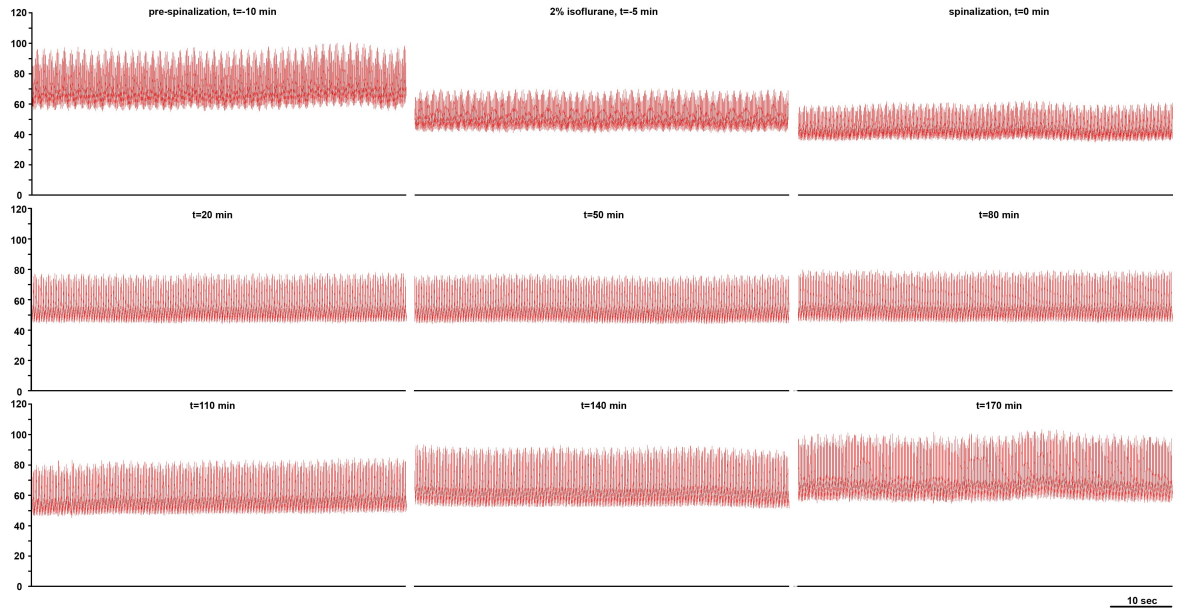

Figure 9. Acute recovery of dynamic arterial pressure magnitude (mmHg; vertical axis) to normotensive values following high cervical C_1 transection in the unanesthetized supracollicularly decerebrate rat. Timescale bar in lower right hand corner. Modified with permission from Fig. 2 of Ghali (2019a).

ergic antagonists prevents animal locomotor rhythmic activity, effectively permitting the neurophysiologist to successfully obtain stable supraspinal or spinal individual and/or multiunit neuronal and/or neural efferent recordings; (Marchenko et al., 2002). Light sedation renders muscle excursions sufficiently diminutive permitting the elegant conduct of electromyogram recordings. Superior sagittal sinus ligation successfully and preemptively achieves cerebral venous hemostasis effectively facilitating the execution of decerebrative encephalotomy in a single methodical transective motion using the microspatula and prevents cranial bleeding following diencephalomesencephalic transection.

3.5 Bilateral trephination of the parietal calvarial convexities

There exist a variety of approaches by which the cerebrum may be exposed in order to achieve access permissive of a decerebrative transection. Prior silk suture ligation or temporary clip occlusion of the internal carotid arteries effectively reduce decerebrative transection-related bleeding and are commonly requisite among all described methods (Figs. 25 and 26). We ligate the right and left internal carotid arteries above the level of the pterygopalatine arteries within minutes of each other and within the hour preceding scalp incision preparing the cranial surface for trephination and the cerebral hemispheric convexities for decerebration. Should the time lapse interposed between internal carotid artery ligation and diencephalomesencephalic decerebrative transection prove excessive, initial animal blood pressure decreases more profoundly and animals are less hemodynamically stable following the procedure. A blood flow steal phenomenon may arise in the circle of Willis, whereby the elimination of internal carotid artery blood flow preferentially diverts basilar artery blood flow from the parenchymal contents contained within the confines of the infratentorial fossa to the parenchymal contents contained within the confines of the supratentorial fossa, accordingly and predictably generating powerful reductions in brainstem perfusion. Studies have accordingly described a myriad of variations of trephination techniques utilized to achieve operative exposure of the cranial cavity to perform decerebrative transection. One may fashion a single craniotomy inclusive of, and extending across, the left and right parietal bony convexities, gently lifting the bone from the underlying superior sagittal sinus. Avulsion of the superior sagittal sinus when significantly adherent to endosteum significantly enhances the risk of iatrogenically precipitating hemodynamically-catastrophic bleeding, especially in older animals. Accordingly, we prefer to trephine the parietal convexities bilaterally, initially preserving a 1 mm-wide strip of bone overlying the superior sagittal sinus (SSS) from bregma to lambda (Fig. 1E-1H). We generally leave a segment of bone overlying the superior sagittal sinus significantly of significantly narrower width compared with investigators and drill osteotomy bays into the sagittal strip of bone overlying the superior sagittal sinus where the superior sagittal sinus will be silk suture ligated in order to achieve better purchase, securing, and compression of this venous structure against the bone. This operative step fundamentally distinguishes our approach from the experience of the majority of investigators. Thread ligation across a broad segment of midsagittal bone would only gently compress the ventral surface of the superior sagittal sinus upwards and consequently fails to adequately secure the venous channel given the relationship between the curvature of the midsagittal bone with respect to that of the superior sagittal sinus. Ensuring the width of the midline strip of bone overlying the sagittal suture remains narrow to the greatest extent reasonably feasible yields the greatest likelihood of effectively achieving a secure ligation.

3.6 Supracollicular decerebrative transective encephalotomy

The specific technique of decerebrative encephalotomy varies according to the type of trephination employed. When biparietal

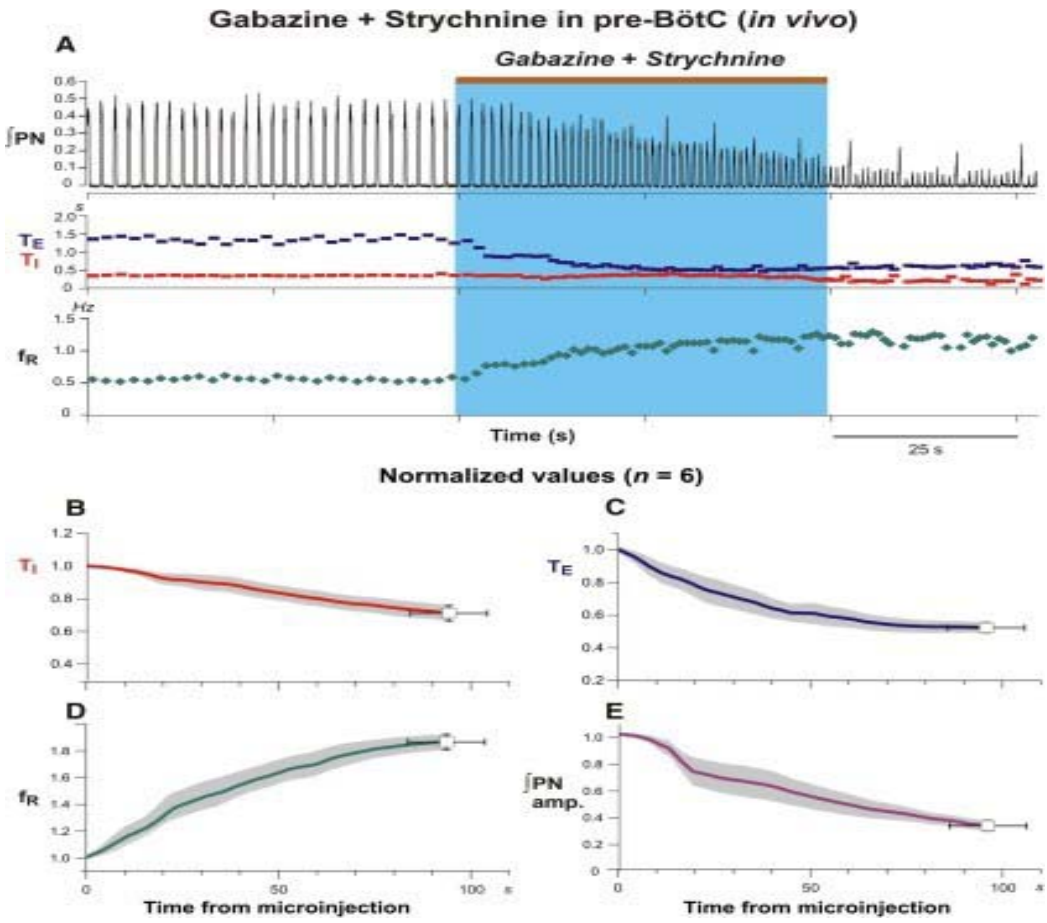

Figure 10. Microinjections of gabazine and strychnine in the pre-Bötzinger complex augments frequency and reduces amplitude of phrenic nerve discharge in the anesthetized adult rat. A: Contemporaneous bilateral microinjections of gabazine and strychnine in pre-BötC elicit augmentations of respiratory frequency and reductions in respiratory amplitude evident in integrated phrenic nerve (∫PN) activity in response to (both 30 mM; brown bar at top and blue rectangle indicate injection period). Gabazine and strychnine microinjections in pre-BötC generate profound reductions of inspiratory (TI, red; B) and expiratory (TE, blue; C) duration which collectively augment the respiratory frequency (fR, green; D) of bursting in phrenic nerve discharge duration. Microinjections of gabazine and strychnine paradoxically reduce the phrenic nerve amplitude. Coherent oscillatory synchrony amongst phrenic motoneurons neurons requires inhibitory mechanisms (Marchenko and Rogers, 2009). By extrapolative deduction, pharmacological reduction of inhibitory mechanisms effectively reduces neural power generated by the pre-Bötzinger complex. Modified with permission from Fig. 4 of Marchenko et al. (2016).

craniectomies with an intact intervening median segment of sagittal bone represent our cranial access, we advance the microspatula through one craniectomy window in a manner directed contralaterally to the deepest and furthest reaches of the posteroinferolateral middle cranial fossa perpendicular to a coronal plane bisecting the mesencephalodiencephalic junction 2.0 to 2.5 mm rostral to a vertical plane through lambda and perpendicular to a transverse plane through the external acoustic meati and advanced ipsilaterally to the ipsilateral posteroinferolateral reaches of the middle cranial fossa towards the side of the craniectomy window across the skull base and repeat the same motion through the contralateral craniectomy window in order to achieve supracollicular decerebrative encephalotomy. Should biparietal craniectomies fashioned on alternate sides of the superior sagittal sinus with an intact intervening segment of bone be subsequently removed or a single trans-sagittal craniotomy inclusive of right and left halves of the parieto-cranial calvarium and extending across the perisagittal suture segment of bone overlying the superior sagittal sinus represent our cranial access, only a single transective cut gently carried from the contralateral to the ipsilateral posteroinferolateral reaches of the middle cranial fossa and across the skull base proves necessary in order to effectively dissociate the telencephalic and diencephalic elements of the cerebral hemispheres from the bulb.

3.7 Skull base hemostasis

Following decerebrative transective encephalotomy, we rapidly pack the anterior and middle cranial fossae using cold thrombin-soaked gelfoam sponges. We avoid both underpacking, which may achieve inadequate hemostasis and yield a persistent low rate of bleeding, and overpacking, which may precipitate transforaminal herniation. Post-transective neurogenic hypotension typically resolves within approximately one hour, in parallel with animal bolusing with, and maintenance on, intravenously administered vecuronium, with isoflurane anesthesia concurrently, gradually, and judiciously weaned. Studies

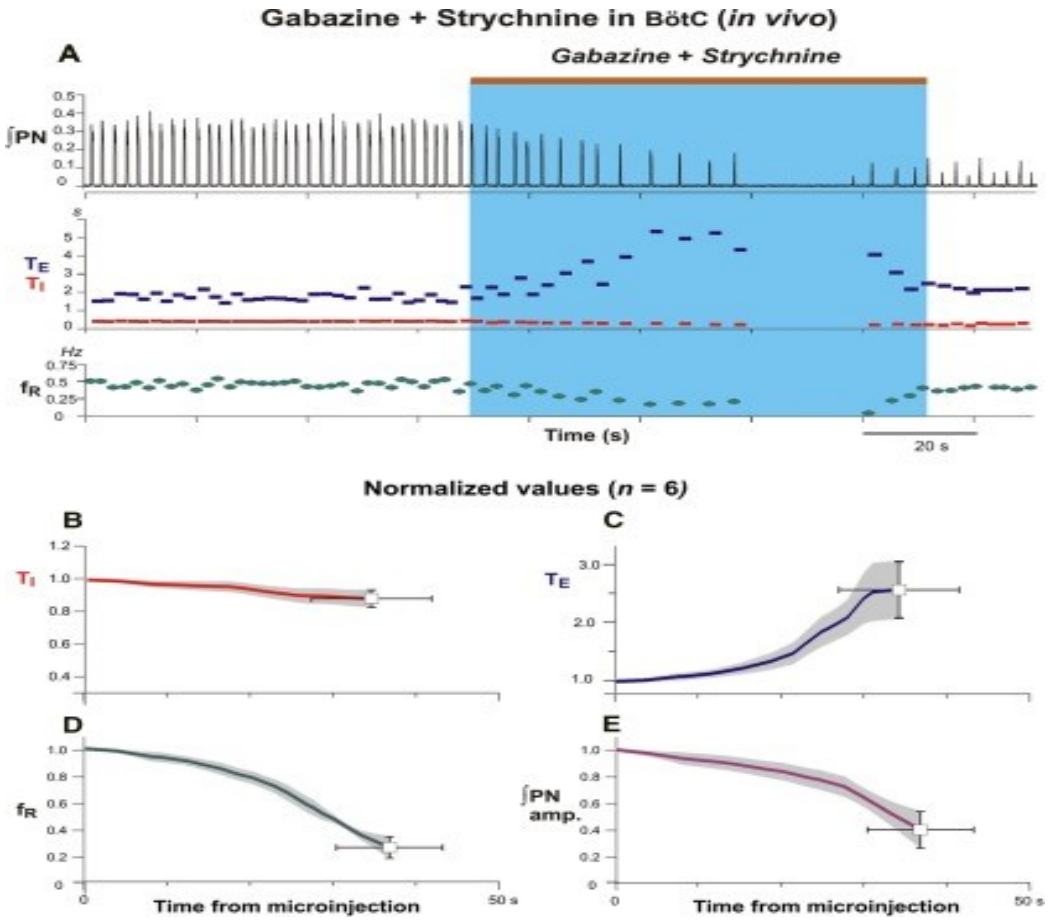

Figure 11. Microinjections of gabazine and strychnine in the Bötzinger complex reduces frequency and amplitude of phrenic nerve discharge in the anesthetized adult rat. A: Contemporaneous bilateral microinjections of gabazine and strychnine in BötC reduces respiratory frequency and amplitude in integrated phrenic nerve (∫PN) activity (both 30 mM; brown bar at top and blue rectangle indicate injection period). Gabazine and strychnine microinjections in BötC elicit no significant effects on inspiratory duration (TI, red; B), though generate profound increases of the expiratory duration (TE, blue; C) contributing to a significant attenuation of the respiratory frequency (fR, green; D). Microinjections of gabazine and strychnine expectedly reduce the phrenic nerve amplitude. Coherent oscillatory synchrony amongst phrenic motoneurons neurons requires inhibitory mechanisms (Marchenko and Rogers, 2009). By extrapolative deduction, pharmacological reduction of inhibitory mechanisms effectively reduces neural power generated by the pre-Bötzinger complex. Modified with permission from Fig. 7 of Marchenko et al. (2016).

have accordingly described or advocated the use of packing the cranial vault using gelatin sponges or cotton balls soaked in cold thrombin solution (de Almeida et al., 2010) and/or tissue adhesive (Dobson and Harris, 2012) in order to prevent blood loss and mechanically secure vessels transected at the base of the cranial cavity (Dobson and Harris, 2012). Some studies have accordingly relied significantly or exclusively on the use of cold thrombin-soaked gelfoam packing of the cranial fossae to achieve hemostasis. We use this technique as an auxiliary decorative measure, or icing on the cake in a manner of reference, and accordingly recommend this should not represent the principal method of achieving hemostasis. Secure and firm ligation of the internal carotid arteries bilaterally and superior sagittal sinus rostrally and caudally accordingly represent the most effective and sure methods of preventing peri-decerebrative bleeding. Thus, though some studies have described the utility of minimizing parenchymaml removal in reducing blood loss (Faber et al., 1982), we reiterate and emphasize properly securing the inflow and outflow vessels of the intracranium far outweighs any reasonably conceivable benefit derived from the collectively proposed adjunctive methods.

4. Empirical utility of decerebration

Decerebrative transective encephalotomy permits the investigator to ethically forego the use of anesthetics and accordingly conduct neural recordings and experimental maneuvers *sans* the confounding influence of anesthetics upon propriobulbar interneuronal microcircuits constituting neural networks and evaluate the mechanistic behavior of interacting arrays of neuronal ensembles behaving in the context of an intact network and natural sources of spatiotemporally dynamic tonic pseudo-tonic excitatory and inhibitory drive in animal preparations *in vivo* and *in situ* (Ghali and Marchenko, 2015, 2016a,b; Ghali, 2015, 2019a,c; Marchenko et al., 2012; Marchenko and Rogers, 2009, 2007, 2006a,b). Decerebrate preparations thus prove uniquely beneficial in subjecting the mechanistic underpinnings and neurophysiological prop-

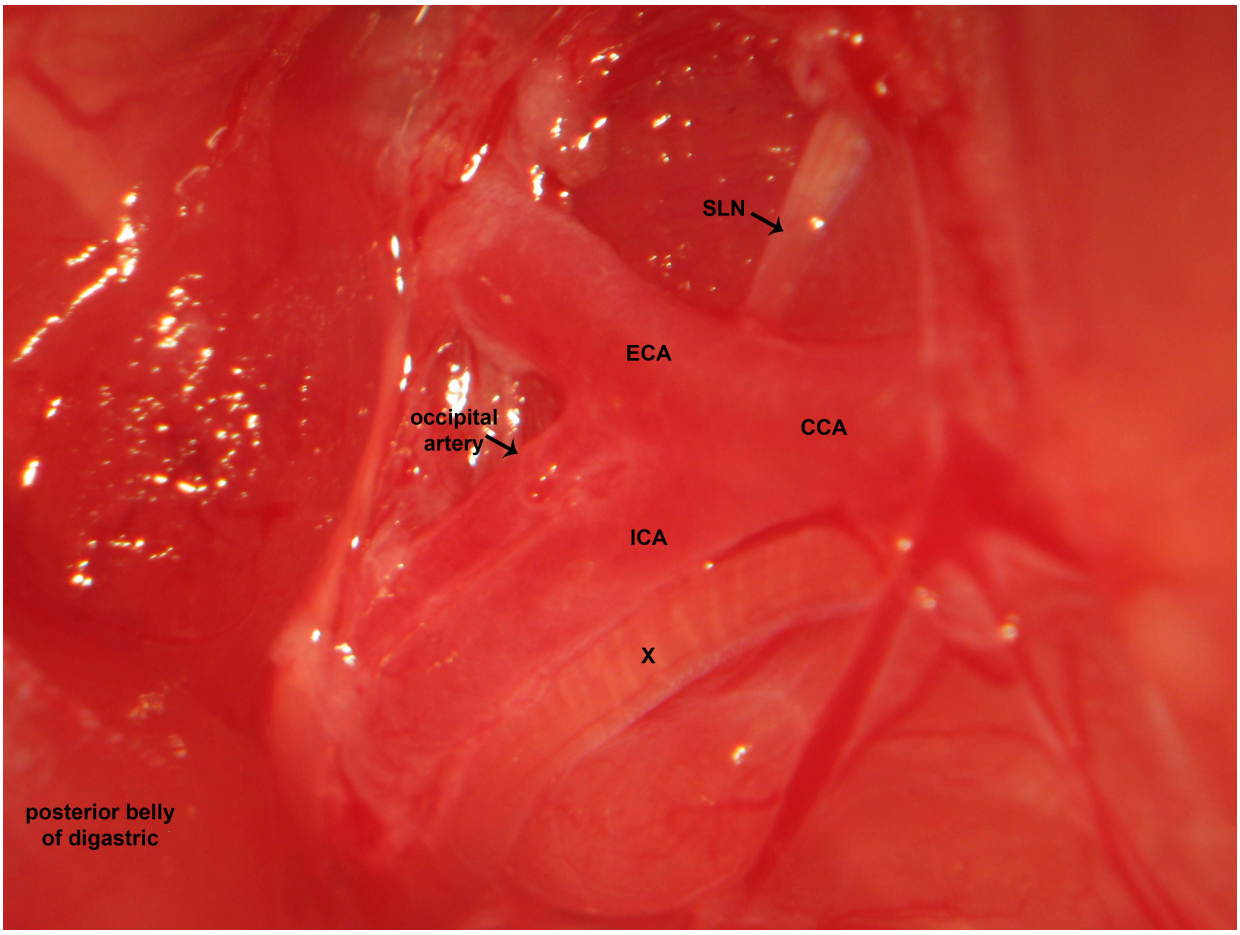

Figure 12. Carotid dissection. The carotid bifurcation is dissected in the high cervical region. The common carotid, external carotid, and internal carotid artery are identified. Fine sharp dissection gently clears soft tissue investing the high cervical neurovascular bundle. The microsurgical photograph demonstrates dissection of the right cervical region. The vagus nerve courses lateral to the common carotid artery, common carotid artery bifurcation, and internal carotid artery. The superior laryngeal nerve emanates from the vagus nerve and courses medially to supply the cricothyroid muscle

erties of neural networks generating the breathing rhythm and pattern (Ghali and Marchenko, 2015, 2016a,b; Ghali, 2015, 2019c; Marchenko et al., 2012; Marchenko and Rogers, 2009, 2007, 2006a,b), sympathetic oscillations, cardiovagal premotoneuronal outflow (Ghali, 2017a,b, 2019a), and patterned locomotor activity (Gerasimenko et al., 2005) to rigorous empirical interrogation. Extracellular neuronal recordings may be facilely performed (Marchenko et al., 2012) and intracellular recordings may be feasibly conducted in the unanesthetized decerebrate preparation (Lipski et al., 1996; Marchenko et al., 2012). Advantages offered through the use of the unanesthetized decerebrate animal preparations are legion, myriad, and principally derive from the eschewal of the confounding effects of intravenously administered and potent inhalational anesthetics upon the propagation of somatodendritic postsynaptic potentials and axonal conduction velocity in central neural networks (Sapru and Krieger, 1979). Coherent depolarization wavefronts propagate through neuronal microcircuits constituting dynamically and emergently synchronized neuronal ensembles sans the influence of anesthetics. The effects collectively reduce the interexperimental variance and enhance consistency of results obtained across individual animals, permitting the effective inclusion of significantly fewer subjects in order to achieve the desired 'a priori' level of statistical significance indicating results obtained reflect a true effect rather than a haphazard occurrence with a probability less than the 'a priori' determined alpha value. Decortication removes the cortex of the cerebrum sans transection, sparing and preserving the diencephalic substance. Accordingly, the use of decorticate animals could putatively represents a useful alternative to the use of decerebrate preparations in studies evaluating neuronal microcircuit generating the breathing rhythm and pattern, sympathetic oscillations, cardiovagal premotoneuronal outflow, and hypothalamic, thalamic, and hippocampal rhythms (Baccelli et al., 1965; Dasgupta and Hausler, 1956; Imig and Durham, 2005; Klosterhalfen and Klosterhalfen, 1985; Palisses et al., 1988, 1989).

5. Variants of microsurgical techniques utilized to achieve decerebration

Studies have conducted decerebrative encephalotomy across several species, including primates (Liu, 1979), cats (Christakos et al., 1991; Lombardi et al., 1990; Richardson and Mitchell, 1982; Sica and Gandhi, 1990), dogs (Tonkovic-Capin et al., 1998; Zu-

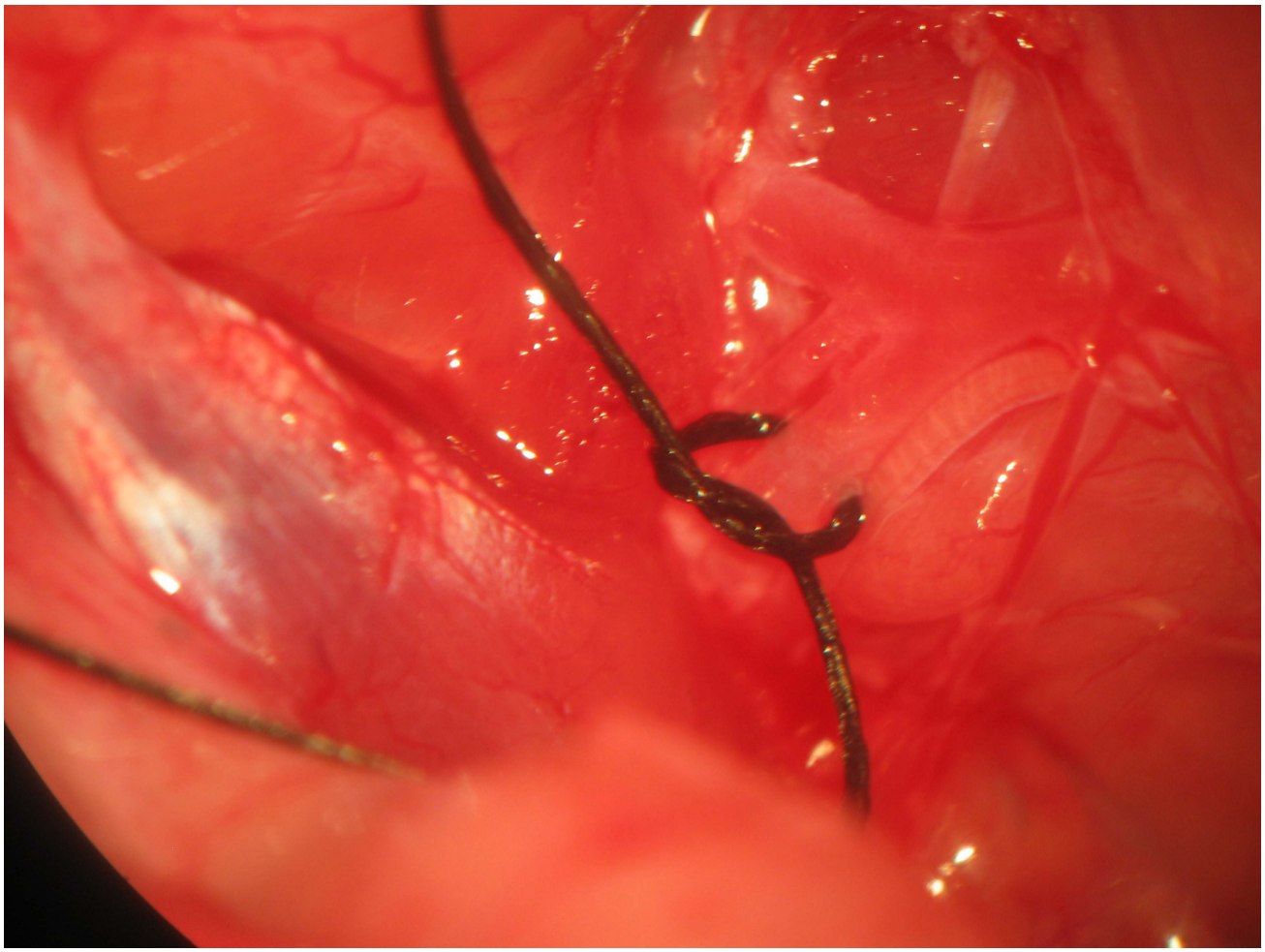

Figure 13. Internal carotid artery ligation. Identification of the occipital artery distinguished it from the internal carotid artery, which is ligated bilaterally sparing the carotid bodies and sinus.

perku et al., 2019), rabbits (Waites et al., 1996), rats (Ghali and Marchenko, 2015, 2016a,b; Ghali, 2015, 2019c; Marchenko et al., 2012; Woods, 1964), mice (Meehan et al., 2012), and birds (Sholomenko et al., 1991). These studies have accordingly described several variations of techniques and strategies utilized complete the decerebration procedure with varying success (Table 2; Bennett et al. (1998); Faber et al. (1982); Fouad and Bennett (1998); Hayashi (2003); Pollock and Davis (1930)). The available strategies include mechanical encephalotomy performed through a transverse plane above or below the level of the superior colliculi, with the transected cerebrum either left in place (Faber et al., 1982) or removed (Hayashi, 2003), and ischemogenic liquefactively infarctive decerebration, which may be achieved via internal carotid and high basilar vessel occlusion achieved microsurgically (Bennett et al., 1998; Pollock and Davis, 1930) or endovascularly by injecting embolisate (Fouad and Bennett, 1998). Soi-disant vascular decerebration proceeds via ligation of the basilar and internal carotid arteries *sans* trephination of the parietal calvarial convexity or mechanical decerebrative transection (Bennett et al., 1998; Fouad and Bennett, 1998; Pollock and Davis, 1930). Cerebral edema ensuing from parenchymal ischemia and consequent herniation and transgression of cerebral tissue upon the confines encasing the fine neural elements of the brainstem and spinal cord represent the principal set of impediments, and paradoxically endorsed advantages, presented by soi-disant "vascular decerebration.". Chronic decerebration involves coronal sectioning near the mesencephalic colliculi without removal of cerebral tissue located rostrally, with dorsally and laterally related tissue also preserved (Faber et al., 1982). Transective encephalotomy without removal of the forebrain could precipitate herniation of the supratentorial neural tissue through the tentorial incisura upon the brainstem and/or herniation of the brainstem through the foramen magnum (transforaminal) upon the spinal cord consequent to ischemogenic edema of cerebral parenchyma lacking a blood supply left in place within the confines of the cranial cavity. In the event of encephalotomy *sans* parenchymal removal, confirmation of diencephalomesencephalic transection, extent of cerebral edema, and the possible presence of herniation appropriately requires postoperative evaluation.

Dobson and Harris (2012) present an elegant method by which to effectively achieve transection, reporting an oversall 95% success rate, bearing resemblance to our approach, though exhibiting some variations distinguishing it from our set of strategies and techniques. Contrasted with our procedure, the authors catheter-

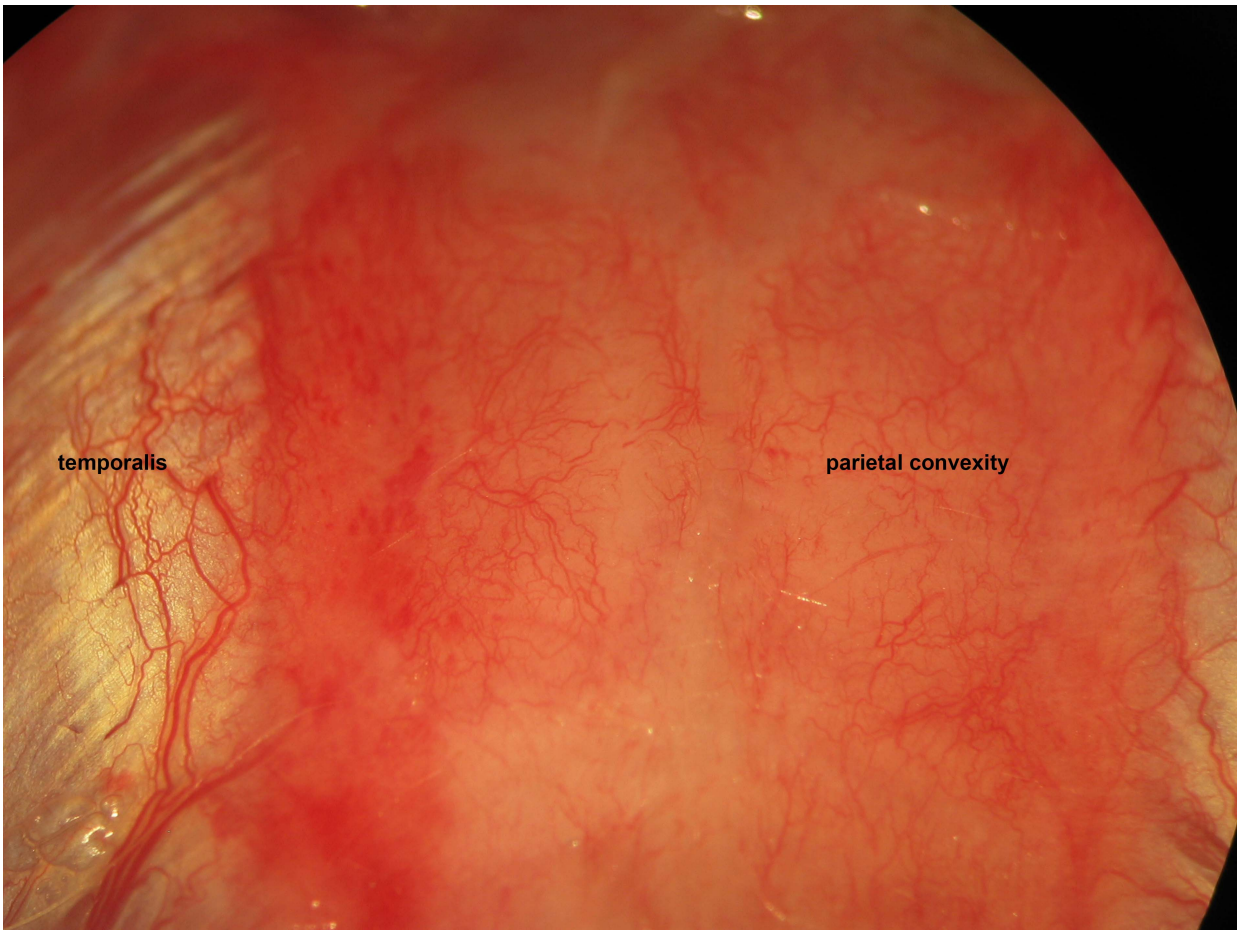

Figure 14. Cranial incision. Rostrocaudal cranial incision is made 5 mm caudal to lambda to 5 mm rostral to bregma. Epicranial soft tissue covers the parietal calvarium and extends in continuity to cover the frontal, occipital, and temporal calvarium.

ize the lumina of the left common carotid artery and internal jugular vein in order to obtain experimental measurements of arterial blood pressure and intravenously infuse continuous infusions of fluids and drugs, respectively. Temporary clipping of the right common carotid artery contralaterally effectively and preemptively ensures, secures, and achieves reduction of cranial inflow during the decerebration procedure. We prefer to cannulate the lumina of the femoral vessels in order to maintain the cervical inflow and outflow vessels irrigating and draining the intracranium, respectively, patent, thus sparing the normal physiological influences of baroreceptor stretch and chemoreceptor activation upon the neuronal ensembles incipiently initiating and centrifugally propagating emergently and dynamically synchronous waves organizing into regularly rhythmic activity within and amongst respiratory microcircuit oscillators constituting the respiratory central pattern generator and supraspinal sympathetic oscillators. We suggest ligating the internal carotid arteries bilaterally enhances reductions of blood flow conveyed through shunting diversion from the vertebrobasilar circulation to the cerebrum, essentially annihilating and abolishing the risk of bleeding following encephalotomy. Dobson and Harris (2012) indicate temporary occlusion of the non-cannulated internal carotid artery to represent a preferable approach by more effectively maintaining integrity of baroreceptors conveying oscillatory feedback inhibitory neurosynaptic influences upon neuronal ensembles constituting brainstem sympathetic oscillators and feedback excitatory synaptic influences upon neuronal ensembles constituting interneuronally coupled cardiovagal premotoneuronal oscillators. Conversely, we venture to assert ligating the internal carotid arteries superiorly with respect to the level of the pterygopalatine arteries effectively protects the arterial bifurcation, carotid sinus and bodies, thus preserving baroreceptor and chemoreceptor mediated modulation of the respiratory central pattern generator, sympathetic oscillators, and cardiovagal premotoneurons.

Dobson and Harris (2012) trephine the cranial convexity with burr holes initially placed in the parietal bones followed by centrifugal extension to a generous craniectomy, contrasted with our technique whereby we bilaterally trephine the parietal calvarium by carving trapezoid-shaped windows gently following and paralleling the contours of the coronal and lambdoid sutures and temporalis muscle insertions into the lateral margins of the parietal convexity utilizing a diamond drill bit. Thrombin-soaked gelfoam sponges firmly held against the skull base may effectively achieve hemostasis mechano-compressively the event of bleeding (Dobson and Harris, 2012). Conversely, a cursory, though thorough, visual inspection of the floors of the anterior and middle cranial fossae constituting the remnant expanse of the skull base in our experience never reveals brisk nor active bleeding. Though some oozing

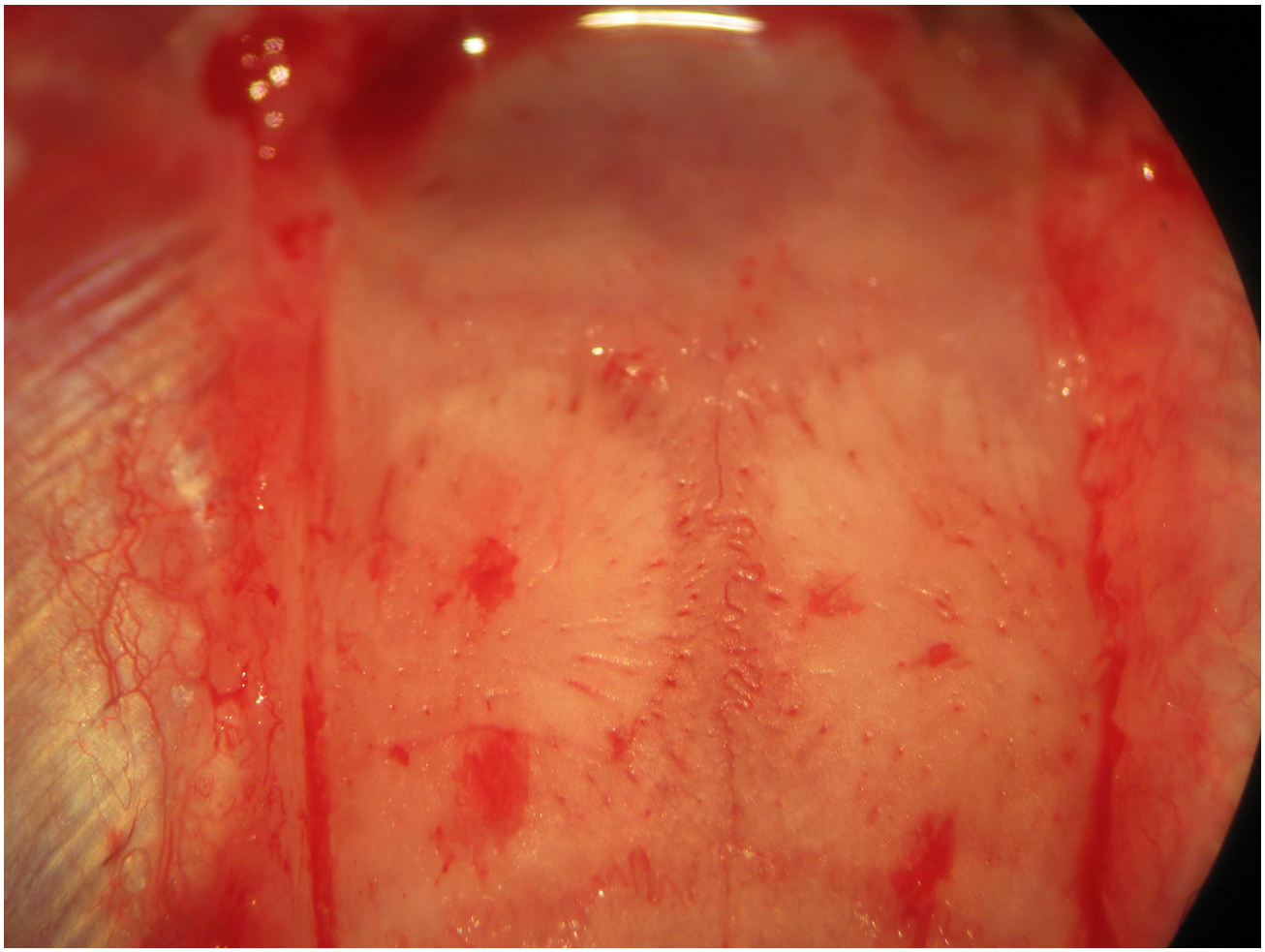

Figure 15. Epicranial soft tissue dissection. Galea aponeurotica, loose connective tissue, and pericranial periosteum rostrocaudally constitute epicranial soft tissue layers following incision through the epidermis, dermis, and subcutaneous fat. We incise then bluntly dissect the epicranial soft tissue remnant following skin incision. Biparietal craniectomies are performed taking exquisite care to spare the mid-sagittal stripe of bone associated with the sagittal suture and overlying the superior sagittal sinus. The proximal insertion of the temporalis muscles delineate the lateral extents of the craniectomy windows. The levels 0.5 mm caudal to the coronal suture and 0.5 mm rostral to the lambdoid suture delineate the rostral and caudal extents of the craniectomy windows, respectively.

may occur consequent to decerebrative transective encephalotomy, the major large caliber vessels are left untransected and no major egress of blood emerges from putative transection of smaller caliber vessels. Dobson and Harris (2012) ligate and secure the superior sagittal sinus to the overlying segment of bone bilaterally flanking the sagittal suture rostrally caudal to lambda and caudally rostral to bregma, a step initially developed by Sapru and Krieger (1978) and later improved, optimized, and refined by our efforts (Ghali and Marchenko, 2015, 2016a,b; Ghali, 2015, 2019a; Marchenko et al., 2012, 2015, 2002). Similar to the microsurgical technique employed in our operative approach, Dobson and Harris (2012) ensuantly resect the intervening segment of bone bilaterally flanking the sagittal suture and rostrally and caudally double ligate the superior sagittal sinus, effectively securing this large caliber high-flow venous conduit draining the cerebral hemispheres, though secure ligation of the superior sagittal sinus to the overlying segment of bone bilaterally flanking the sagittal suture performed exclusively effectively achieves cranial venous hemostasis.

After securing the superior sagittal sinus, Dobson and Harris (2012) remove the cerebral cortex in layers sufficient to visualize the mesencephalic colliculi constituting the tectal plate, followed by diencephalo-mesencephalic transection and removal of cerebral tissue rostral with respect to a transverse plane through the superior colliculi. Adequate mesencephalic collicular visualization achieved via layer-by-layer removal of cerebral cortex may provide investigators with significantly greater comfort. In contrast, we use the level 2.0 to 2.5 mm rostral to lambda indicate the approximate location of the neuroanatomic transverse plane separating the superior colliculi from the caudal thalamus in order to perform diencephalo-mesencephalic transection. Possible blood loss ensuing from rupture of the basilar artery has led researchers to indicate the transection should be kept rostrally placed. Dobson and Harris (2012) report observing moderate postoperative decreases of common carotid arterial pressure immediately following aspiration of supratentorial cerebral tissue lateral to the mesencephalic colliculi, though following neither initial cortical as-

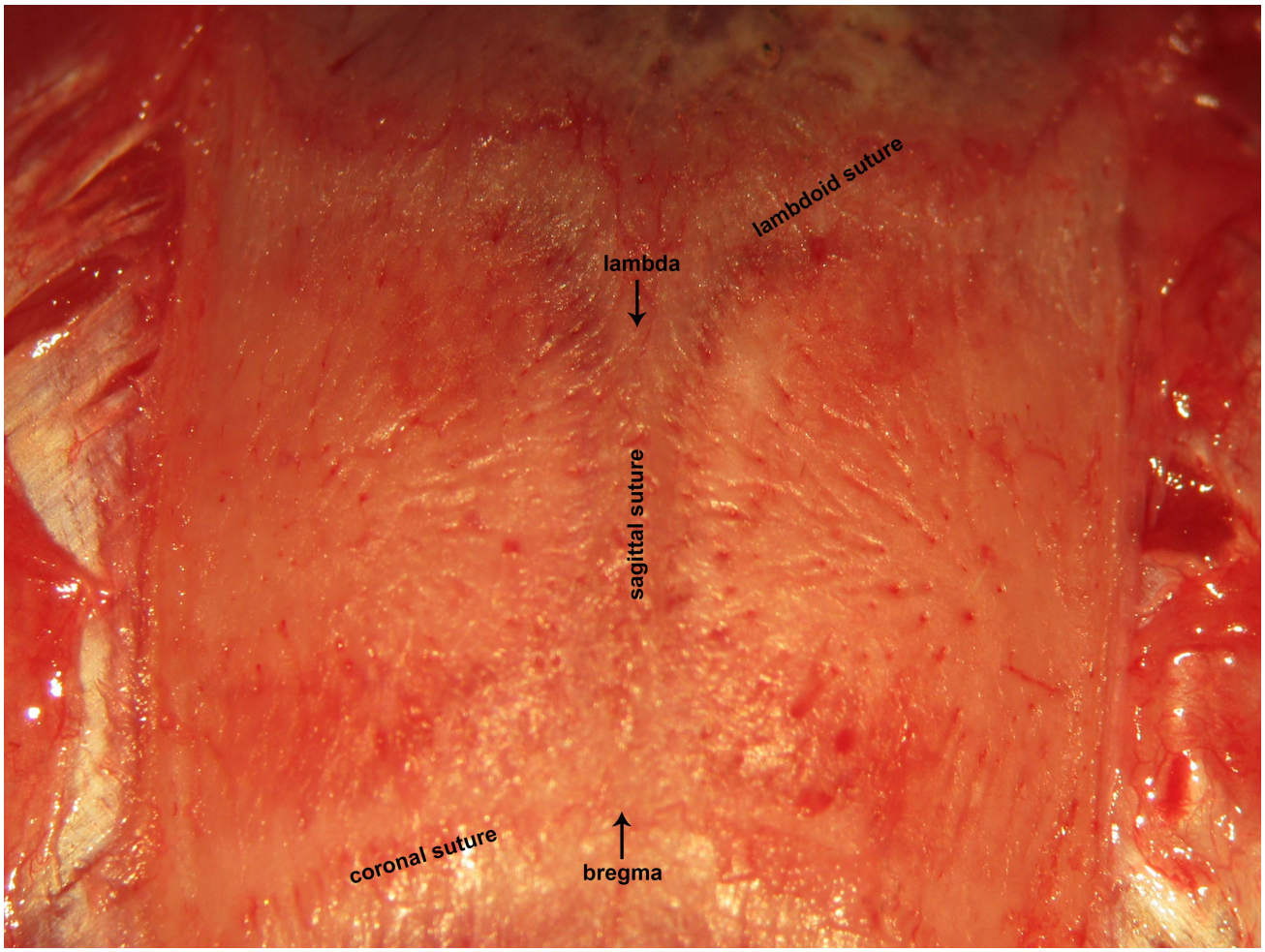

Figure 16. Craniocalvarial landmarks. The sagittal suture is interposed between bregma and lambda. These classic landmarks may be used to identify the location of critical neural structures in neurophysiological experiments. Bregma represents the junction between the sagittal suture with the coronal suture. Lambda represents the junction between the sagittal suture with the lambdoid suture.

piration, and diencephalo-mesencephalic transection. Iatrogenically injuring the transverse sinuses and interrupting descending hypothalamic angiotensinergic drive from paraventricular nucleus neurons to rostral ventrolateral medullary presympathetic units and intermediolateral cell column preganglionic sympathetic neurons could contribute to post-decerebrative hypotension and neurogenic distributing shock. We remove cerebral parenchyma located rostral to, and surrounding, the superior mesencephalic colliculi from the cranial cavity using vacuum aspiration and thoroughly visually inspect the floors of the anterior and middle cranial fossae under microscopic magnification in order to identify interventionable bleeding. However, this may occur in the form of extremely slow and rapidly self-terminating oozing from the transective lesioning proper, though no bleeding occurs from the major cranial inflow arteries or outflow venous sinuses or their tributaries. We subsequently pack the anterior and middle cranial fossae with cold thrombin-soaked gelfoam sponges in order to generate thrombin clots in the distal transected ends of any possibly iatrogenically ruptured vessels, coordinately achieving hemostasis and preemptive preventing delayed patterns of intracranial bleeding. Successful pretransective placement of appropriately applied silk suture ligatures securely and firmly constricting and occluding the lumina of the internal carotid arteries bilaterally and superior sagittal sinus rostrally and caudally halt acute, and prevent delayed, peri-decerebrative bleeding. We have never observed bleeding from the superior sagittal sinus, transverse sinuses, or any major vessel in our experiments while performing decerebrative transective encephalotomy. Bilateral supra-pterygopalatin arterial ligation of the internal carotid arteries and meticulously securing of the superior sagittal sinus optimize intraoperative and postoperative skull base hemostasis.

6. Perioperative management

An interregnum of neurogenic shock intervenes between decerebrative transective encephalotomy and recovery of propriobulbar neuronal ensembles constituting sympathetic oscillators sufficient to generate arterioconstriction, venoconstriction, and arterial pressure levels permissive of neurophysiological recordings and experimental interrogation. Our perioperative management paradigm and resuscitation strategy likely contribute prominently to generating hemodynamically stable decerebrate preparations. Dobson and Harris (2012) describe the development of moderate reductions of systolic arterial pressure by approximately 30% shortly

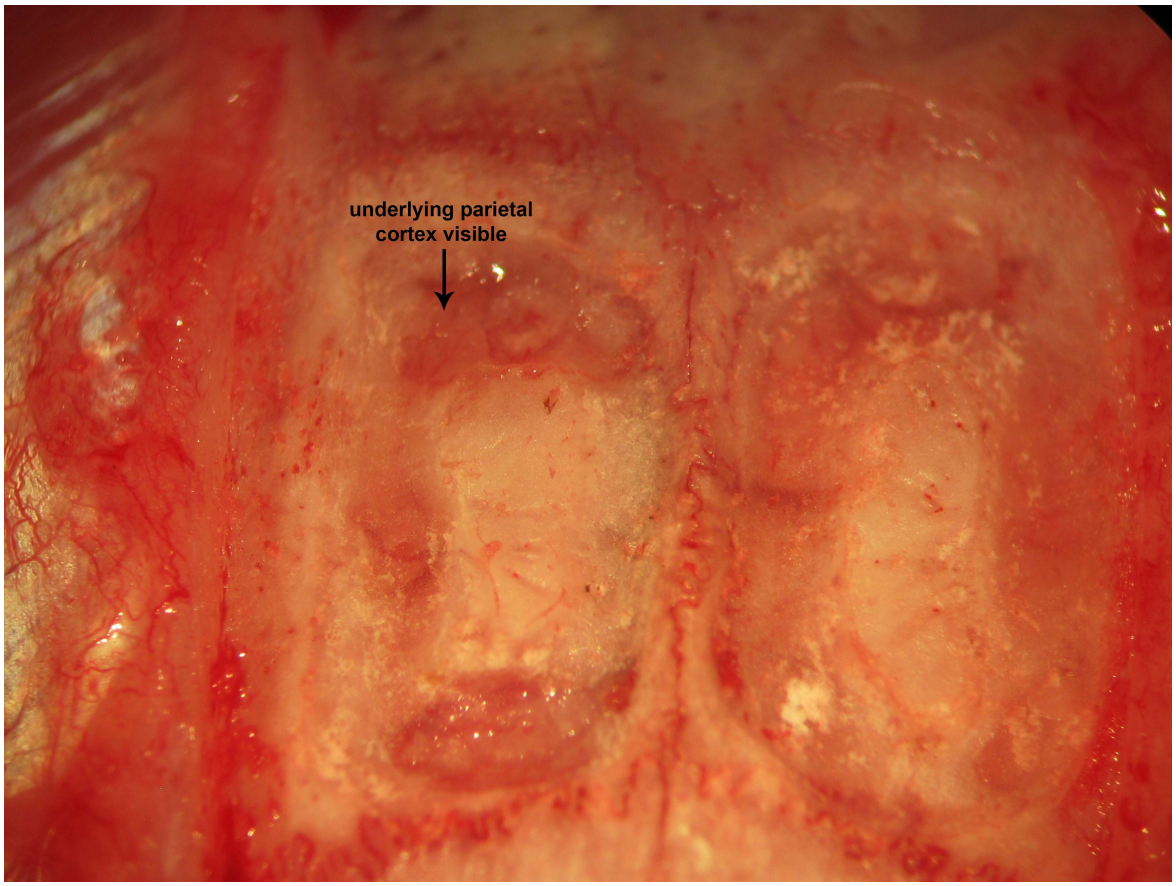

Figure 17. Biparietal trephination. Drilling of the parietal convexities visualizes the the parietal cortex and overlying vessels through the drilling paths.

following removal of cerebral parenchyma lateral to the mesencephalic colliculi, potentially consequent to transverse sinus injury and venous bleeding. We characteristically observe profound reductions of the arterial blood pressure seemingly catastrophic to the unseasoned and uninitiated investigator immediately following decerebrative transective encephalotomy. This likely results from the composite influences of neurogenic shock and high levels of anesthetic concentration throughout the procedure in order to ensure protection of the neural elements. Perioperative management strategy following decerebration critically dictates preparation stability and signal-to-noise ratio of neurophysiological recordings (Ghali and Marchenko, 2015, 2016a,b; Ghali, 2015, 2019a,c; Marchenko et al., 2012). We accordingly assert the most prudent strategy to mitigate the potentially untoward and deleterious effects deriving from neurogenic distributive vasodilatory shock upon neurons and astrocytes and to prevent the development of tissue hypoperfusion in the setting of arterial pressures correlating with levels which would otherwise precipitate neurogenic distributive vasodilatory shock under normothermic and unanesthetized conditions following decerebrative transection involves coordinately reducing the neural metabolic rate of oxygen consumption through the judicious use of moderate hypothermia and isoflurane gas anesthesia, effectively permitting the activity of propriospinal interneuronal microcircuit oscillators constituting brainstem sympathetic subnetworks to recover spontaneously and sufficiently to generate sympathetic tone and dynamic arterial pressure sufficiently robust to self-sustain perfusion and flow meeting the brainstem and cerebellar metabolic demands of oxygen consumption exacted during normothermic unanesthetized conditions. Our use of potent inhalational anesthetics and moderate hypothermia permits arterial pressure to decline to lower levels *sans* neural injury.

Decrements of arterial pressure to levels corresponding with neurogenic distributive vasodilatory shock following decerebrative transective encephalotomy thus likely ensues from interruption of hypothalamic neuronal excitatory synaptic drive to rostral ventrolateral medullary presympathetic cells and intermediolateral cell column preganglionic sympathetic neurons (Bains and Ferguson, 1995; Ghali, 2017a,b). Accordingly, the decerebration procedure in essence removes suprabulbar descending spatiotemporally dynamic excitatory drive provided to metencephalic and myelencephalic sympathetic oscillators (Antal, 1984; Ogundele et al., 2017). Integrity of the mesencephalic tonic excitatory axonodendritic and axonosomatic synaptic conveyed to neurons constituting these neural networks, deriving principally from the collicular plate and periaqueductal gray matter following cerebrectomy, may also be functionally compromised by a wave of descending peri-transective neural interstitial. Neuroprotection of the mesencephalic, metencephalic, and myelencephalic neuronal and astrocytis elements constituting and forming supramyelic sympathetic oscillators conveying presympathetic axonodendritic and axonosomatic synaptic drive to intermediolateral preganglionic sym-

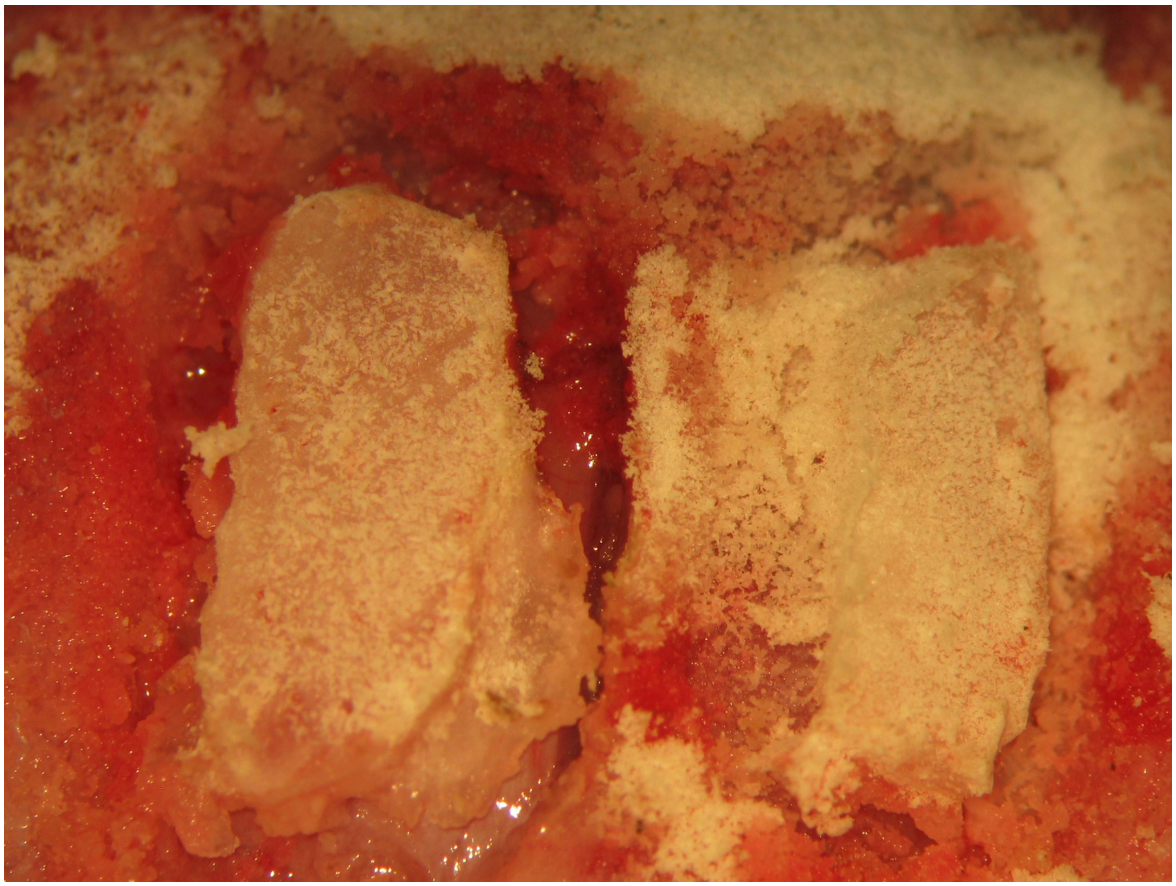

Figure 18. Biparietal craniectomy. The craniectomy sites are intermittently cleaned of bone dust. gently lifting bone from thinned osseous attachments completes the craniectomy.

pathetic neurons synergistically contributes to the synergistic re-emergence and recovery of coherent and correlated sympathetic oscillator discharge generating normotensive, and frequently hypertensive, preparations.

Corticobulbar projections may putatively contribute to the tonic excitatory support and/or inhibitory modulation of metencephalic and myelencephalic sympathetic oscillators (Antal, 1984). The activity membrane voltage of propriospinal interneuronal microcircuit oscillators constituting neuronal ensembles residing within the medullary lateral tegmental field and rostral ventrolateral medulla may also be indirectly supported through the provision of synaptic inputs from surrounding propriobulbar and reticulobulbar interneuronal clusters receiving excitatory synaptic drive from the descending axons of corticobulbar (Antal, 1984) and diencephalobulbar neurons (Ogundele et al., 2017). We suggest neuronal somata extant within the paraventricular nucleus and conveying descending axonal inputs to brainstem sympathetic oscillators may represent the most, critical suprabulbar presympathetic zone. Angiotensinergic paraventricular nucleus cells contemporaneously provide excitatory synaptic drive to rostral ventrolateral medullary presympathetic units and intermediolateral cell column preganglionic sympathetic neurons. Rhodamine B+ amine microinjections in rostral ventrolateral medulla extensively retrogradely labels regions spanning the extent of the paraventricular nucleus, lateral zona incerta, and median reuniens subnuclei of the thalamus (Ogundele et al., 2017).

Rostral ventrolateral medullary presympathetic bulbospinal neurons are justifiably widely believed and regarded to convey and provide the principal excitatory synaptic drive to sympathetic preganglionic neurons located in the intermediolateral cell column of the spinal cord through direct neurochemical synaptic contacts and interneuronal relays (Ghali, 2017a,b; Guyenet et al., 2018; Mueller et al., 2019). Neurons diffusely distributed throughout the extent and expanse of the diencephalon and brainstem residing within the hypothalamic paraventricular nucleus, ventrolateral metencephalic tegmentum (Nam and Kerman, 2016; Stornetta et al., 2002), caudal raphé (Larsen et al., 2000), and medullocervical pressor area (Goodchild and Moon, 2009; Seyedabadi et al., 2006) also convey presympathetic synaptic drive to thoracic intermediolateral cell column preganglionic sympathetic neurons. The sympathetic oscillations proper most likely originate and arise from the coherent and correlated rhythmic discharge of, and interactions amongst and between, propriobulbar neuronal ensembles constituting neural network arrays residing within the medullary lateral tegmental field and rostral ventrolateral medulla (Barman, 2019; Ghali, 2017a,b). We consequently believe hypotension and neurogenic shock following decerebration chiefly reflects loss of descending tonic excitatory propriobulbar drive supplied to neuronal elements residing within the medullary lateral tegmental field (Dempesy et al., 1995, 2000; Ghali, 2017a,b; Guyenet, 2006; Guyenet et al., 2018; Marchenko and Sapru, 2003; Mueller et al., 2019), rostral ventrolateral medulla (Barman, 2019; Guyenet et al.,

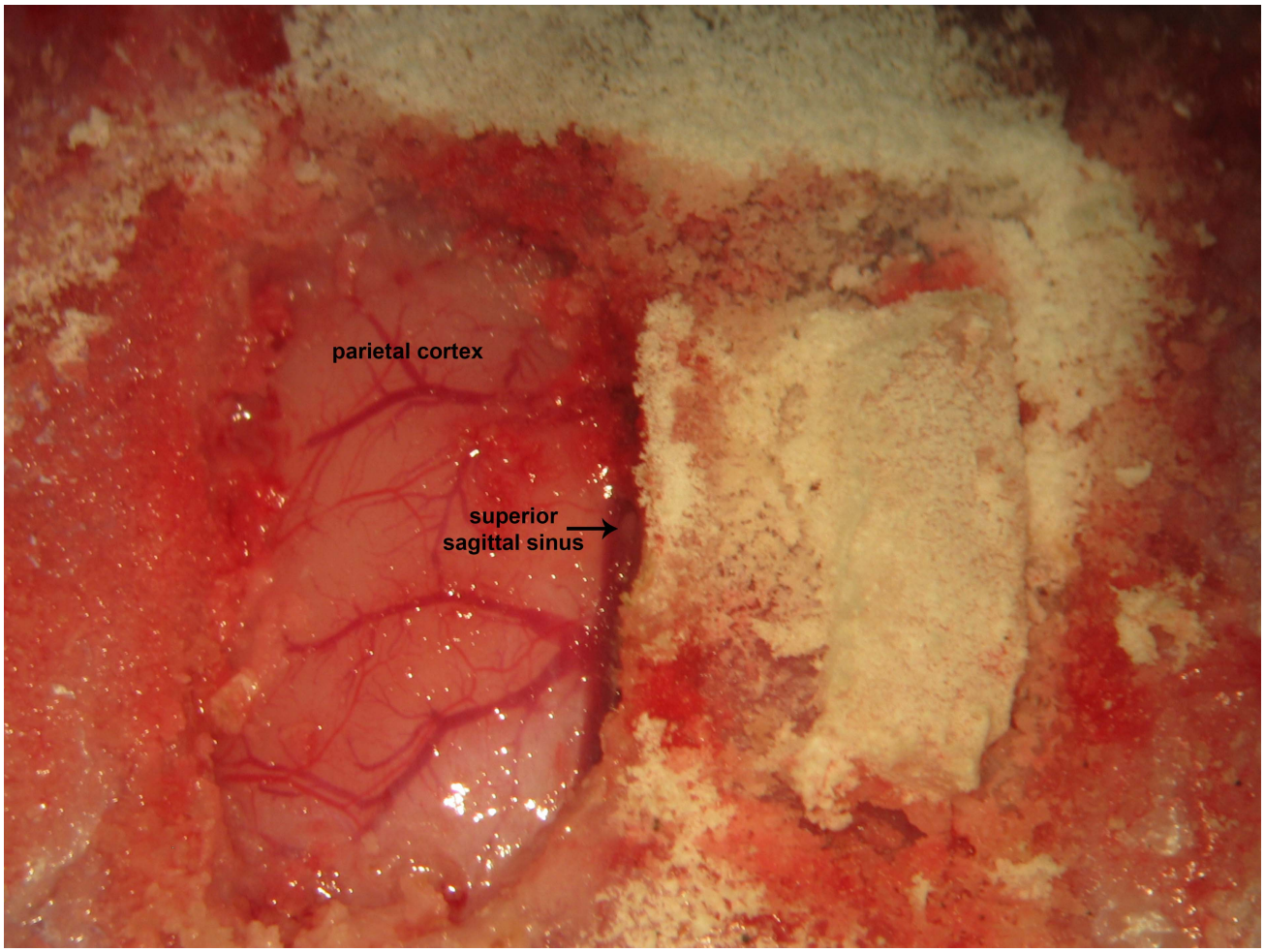

Figure 19. Biparietal cranial windows. Gently lifting and avulsion of the contralateral parietal bone from its osseous attachments following right parietal trephination.

2018; Mueller et al., 2019; Schreihofer and Guyenet, 1997; Sun et al., 1988) and intermediolateral cell column (Accorsi-Mendonça et al., 2016; Ghali, 2017a,b; Guyenet, 2006; Lipski et al., 1996; Schreihofer and Guyenet, 1997; Stornetta, 2009).

Decerebration generates an evaluable set of experimental neurophysiological recordings *sans* anesthesia. Critically, we venture to propose immediate withdrawal of anesthesia effectively removes a critical neuroprotectant in the context of neural circuitry yet to recover from the mechano-disruptive effects of supracollicular transection. Thus, contrasted with the experience of studies recommending the immediate withdrawal of anesthesia, putative with the goal of in order to disinhibiting brainstem and spinal sympathetic microcircuit oscillators and hasten the recovery of arterial pressure to normotensive values (Dobson and Harris, 2012), we accordingly prefer to maintain potent inhalational anesthesia and core animal temperature moderately hypothermic following decerebrative encephalotomy in order to ensure neuroprotection while permitting restitution of the sympathetic oscillators from neurogenic shock ensuant from the removal of corticobulbar and hypothalamobulbar tonic excitatory axonodendritic and axonosomatic synaptic. Accordingly, gradual reduction of anesthetic concentration allows natural restitution of tonic excitatory synaptic drive conveyed to sympathetic oscillators in the brainstem and spinal cord from surrounding propriobulbar networks in order to substitute lost inputs deriving from descending supramesencephalic tonic fast excitatory glutamatergic inputs. We typically gently administer a modest bolus dose of normal saline, Ringer-Locke solution, or artificial cerebrospinal fluid solution immediately following decerebrative transection and aspiration of the cerebral hemispheres and small volume boli throughout the resuscitation period. Femoral arterial pressure generally starts to recover spontaneously towards normal values, contemporaneously with which we gradually wean potent inhalational anesthesia and intravenously administer boli and maintenance infusions of the neuromuscular antagonist vecuronium. Coordinate weaning of isoflurane anesthesia in parallel with gradual incremental administration of the neuromuscular type nicotinic acetylcholinergic antagonist vecuronium significantly reduces oxygen consumption by skeletal myocyte and, we surmise, allows the animal to tolerate transient periods of slight decreases of dynamic arterial pressure magnitude pending recovery to normotensive and slightly hypertensive values. Our microsurgical technique and perioperative management of anesthetic concentration and animal optimizes and ensures neural tissue perfusion and viability.

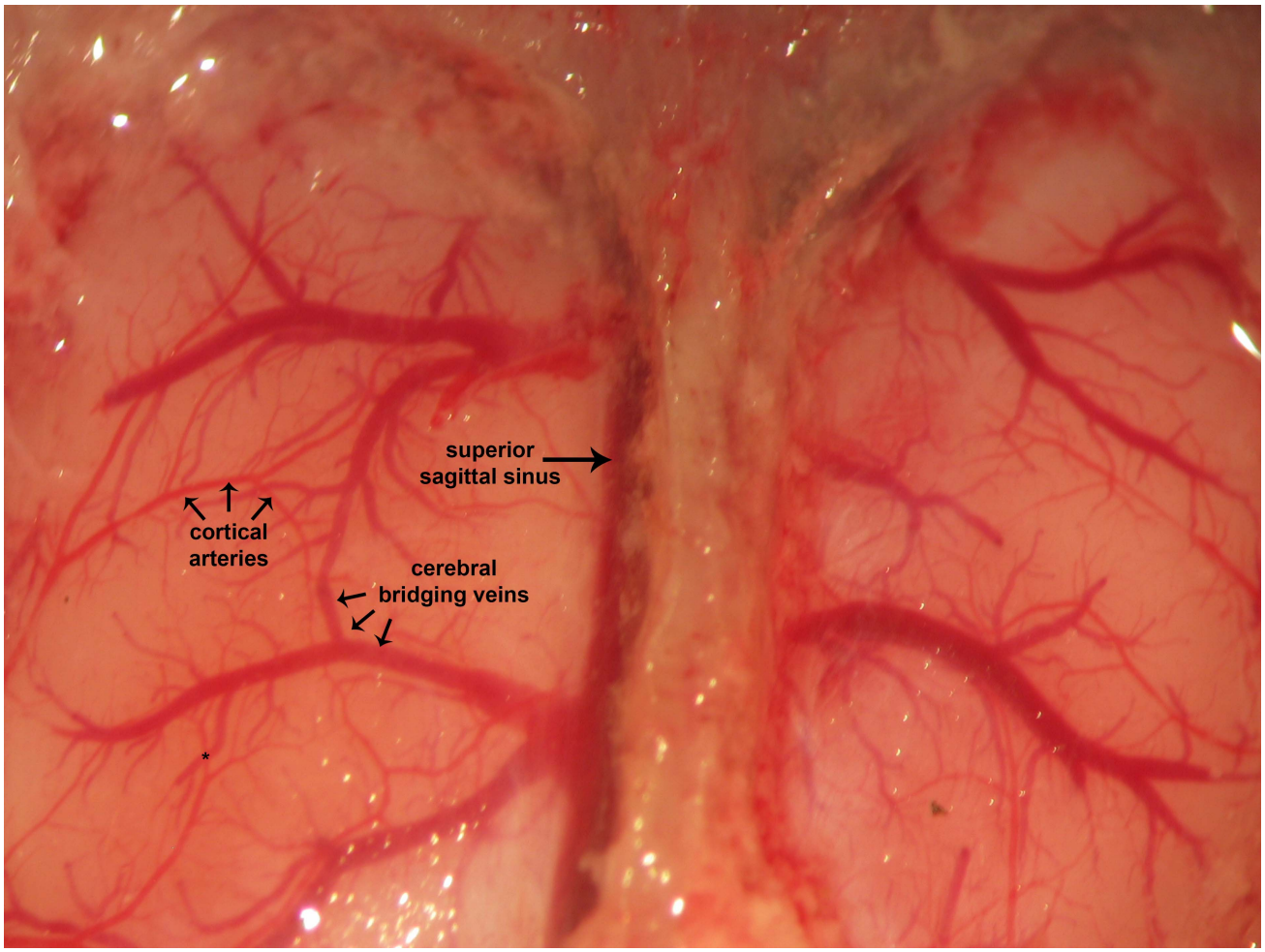

Figure 20. Dural and cerebral vessels. Dura invests and covers the brain. Visualized vascular elements are intact. Cerebral edema arises consequent to pre-craniotomy ligature occlusion of the ICA. The superior sagittal sinus may often be found located parasagitally immediately to the right of the midline sagittal suture. This ontogenically recapitulates the human neurovascular anatomy, where the superior sagittal sinus may be found located approximately 11 mm to the right of midline. Cortical arteries are red whereas cerebral bridging veins are purple. This reflects differential saturation of hemoglobin heme moieties with molecular oxygen (O2) of the arterial blood (~99-100%) relative to the venous blood (~70-75%).

7. Advantages of the Zaki Ghali Marchenko approach

The investigator stringently adhering to our presented set of microsurgical techniques and perioperative management strategies will consistently generate normotensive to slightly hypertensive decerebrate animal preparations. Bilateral ligation of the internal carotid arteries above the level of the pterygopalatine arteries reduces cranial inflow. Proximal and distal double ligation of the superior sagittal sinus effectively mitigates or eliminates venous blood loss during decerebrative transective encephalotomy. The cerebrum may become edematous during the interregnum interposed between bilateral ligation of the internal carotid arteries and decerebrative transection consequent to neuronal and astrocytic ischemia compromising sodium potassium adenosine triphosphatase pump mediated electrogenic and osmogenic efflux of monovalent sodium cations and influx of monovalent potassium cations in a ratio of 3:2. Neurons experiencing ischemia develop elevated cytosolic concentrations of calcium, enhancing the allosteric activation of cytosolic and nuclear degradative phospholipases, proteases, and endonucleases, and elaborate cytochrome c from the inner mitochondrial matrix into the cytosol, activating apoptotic cascades. Minimizing the duration interposed between internal carotid artery ligation and decerebrative transective encephalotomy likely mitigates the severity and extent of ensuant cerebral edema and contributes to optimizing preparation stability. Superior sagittal sinus ligation to the overlying narrowing segment of bone flanking the sagittal suture secures cerebral venous drainage to the torcular herophili and, in conjunction with bilateral ligation of the internal carotid arteries, completely eliminates blood loss ensuant from decerebrative transective encephalotomy. Superior sagittal sinus occlusion may cause cerebral venous congestion, exacerbation of cerebral edema, and cerebral herniation. Performing decerebrative transection immediately following ligature securing of the superior sagittal sinus prevents the development of herniation. Cold thrombin soaked gelfoam sponge packing of the cranial cavity proves hemostatic and may generate

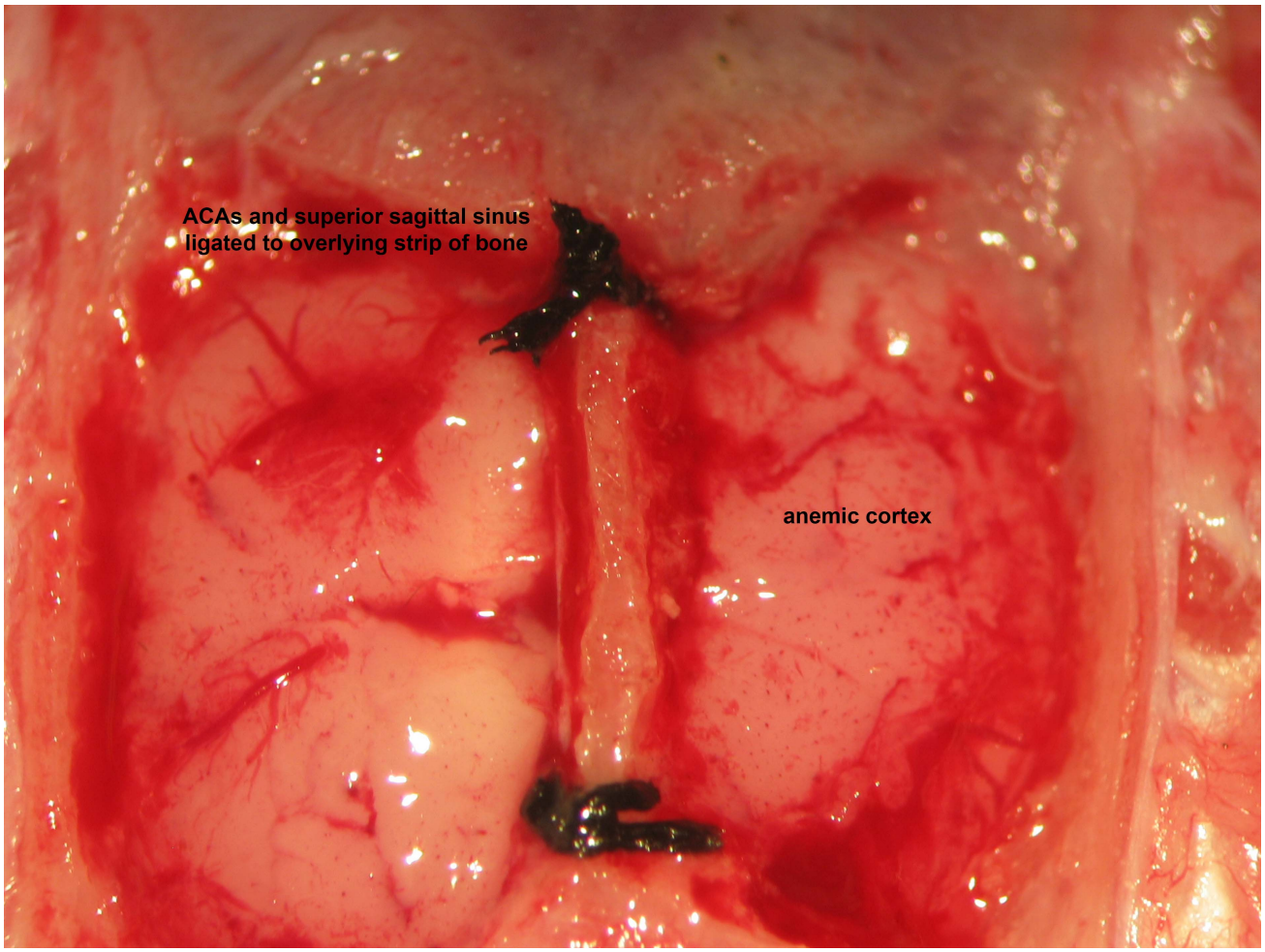

Figure 21. Securing of the superior sagittal sinus. Ligation of the superior sagittal sinus to overlying bone follows thinning of the mid-sagittal strip of bone at its proximal and distal aspects to create a tract through which the superior sagittal sinus may be firmly secured to the overlying bone. Wide bilateral dural opening offers generous exposure and access to the telencephalic cerebral hemispheric surfaces. Collective ligation of the anterior cerebral arteries , superior sagittal sinus, and overlying strip of bone follows insertion of a needle with attached 4-0 silk suture through one parietal craniocalvarial window below the anterior cerebral arteries and retrieval from the contralateral parietal craniocalvarial window, performed rostral to lambda then caudal to bregma.

thrombi effectively occluding the transected ends of narrow caliber skull base vessels. Suction aspiration of the cerebrum immediately following decerebrative transection effectively eliminates the risk of iatrogenic herniation and transgression of the posterior cranial fossa contents upon the upper cervical spinal cord through the foramen magnum.

Our set of microsurgical techniques thus effectively reduces the duration necessary to perform supracollicular decerebrative encephalotomy to only a few seconds. Profound reduction of the arterial pressure observed across all animals following microsurgical removal of the cerebrum represents the principal disadvantage of the technique. Importantly, the development of critically severe hypotension should not alarm the experimental surgeon, since, if properly instituted, the judicious perioperative management of anesthetics and animal temperature strikes a delicate balance between cytoprotection of eloquent neural parenchyma and recovery of brainstem and spinal sympathetic oscillators, arterial pressure, and neural networks generating the breathing rhythm and pattern. The described set of techniques and strategies universally generates recovery of animal dynamic arterial pressure magnitude to normotensive, and often hypertensive, values, powerfully indicative of the recovery of oscillatory synchrony amongst propriobulbar interneuronal networks constituting sympathetic microcircuit oscillators and generators. Phrenic neural activity initially recovers with a bradypneic regular rhythm constituted by bell-shaped bursts. Rate and amplitude of fictive neural breathing gradually increases in parallel with elevations of animal core body temperature and metabolic production of CO_2 by neural parenchyma, vessels, and extra-neuraxial viscera. Spatiotemporally dynamic burst profile of the phrenic burst gradually transforms from bell-shaped to augmenting in parallel with the weaning of isoflurane anesthesia, indicating integrity of neuronal and glial elements constituting the respiratory rhythm and pattern generating neural networks.

Our set of microsurgical techniques accomplishing decerebration bears some resemblance with the description offered by previous investigators, though its unique and consistent success hinges

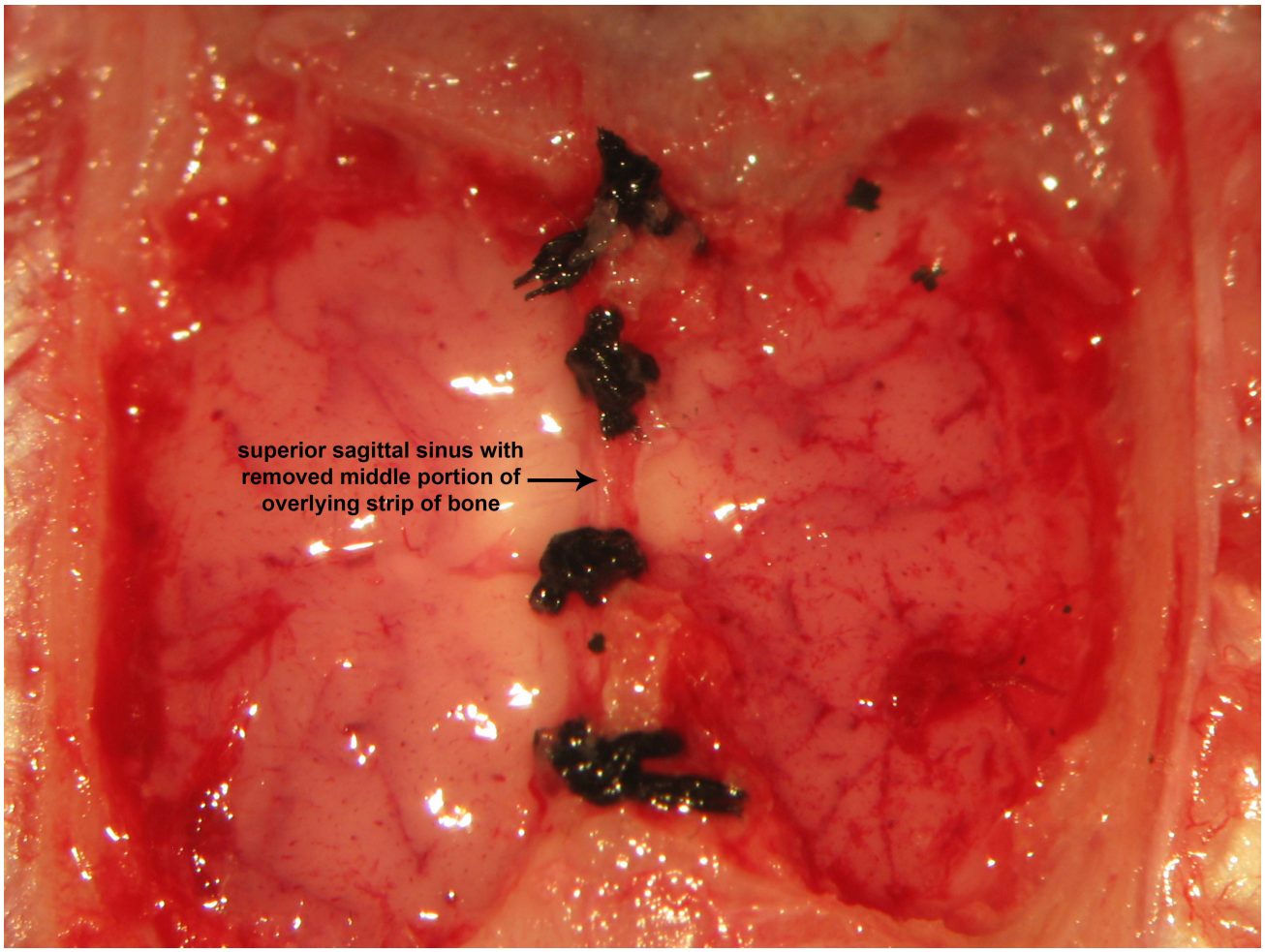

Figure 22. Double ligation and transection of the superior sagittal sinusRostral and caudal double ligation and transection of the superior sagittal sinus follows safe removal of the middle half of the mid-sagittal strip of bone using a variable surgical drill. Iridectomy scissors successfully achieve transective division of the superior sagittal sinus between bregma and lambda.

critically upon successfully performing several nuanced critical maneuvers with incredible precision. These operative steps include complete elimination of the cervical internal carotid arterial inflow provided to the contents housed within confines of the intracranium and securing of the superior sagittal sinus to the overlying narrow segment of bone flanking the sagittal suture bilaterally. The extents of the cervical internal carotid arteries must be distinguished from the proximal extents of the occipital arteries emanating from the proximal extent of the external carotid artery. We accordingly suggest conflating the occipital artery with the proximal extent of the internal carotid artery immediately following the bifurcation of the common carotid artery may conceivably represent a common error unfortunately committed by novices during their early and incipient endeavors seeking to successfully perform the technique. The cervical internal carotid artery should be ligated high above the origins of the pterygopalatine arteries in order to preserve baroreceptor stretch and chemoreceptor activation mediated modulation of neuronal ensembles generating the breathing rhythm and pattern, sympathetic oscillations, and cardiovagal premotoneuronal outflow. Simply ligating the superior sagittal sinus to a wide segment of peri-sagittal suture bone may not completely secure this venous structure, given continued presence of a paravenous angle preventing the suture thread from collapsing the sinus. Thus, drilling bays into the peri-sagittal sutural bone may sufficiently narrow this segment to allow the microsurgeon to achieve effective purchase and properly secure this vessel. Suction aspiration of the cerebral tissue immediately follows decerebrative encephalotomy through a coronal plane interposed between the rostral surface of the crura cerebri, red nuclei, midbrain reticular formation, periaqueductal gray matter, and superior colliculi, reducing operative time. We permit postoperative reductions in blood pressure *sans* aggressive weaning of anesthesia in order to effectively achieve neuroprotection by coordinately decreasing the brainstem and spinal cord metabolic consumption of oxygen and mitigating the effects of glutamatergic excitotoxicty upon neurons. Meticulous, careful, gentle, fast, and judicious microsurgical technique proves requisite and critical in eliminating or minimizing intraoperative blood loss and optimizing animal condition. Intraoperative monitoring of femoral arterial blood pressure guides the perioperative titration of potent inhalational anesthetic concentration and animal temperature. Normobaric hyperoxygenation using hyperoxia may contribute slightly to increasing dissolved ar-

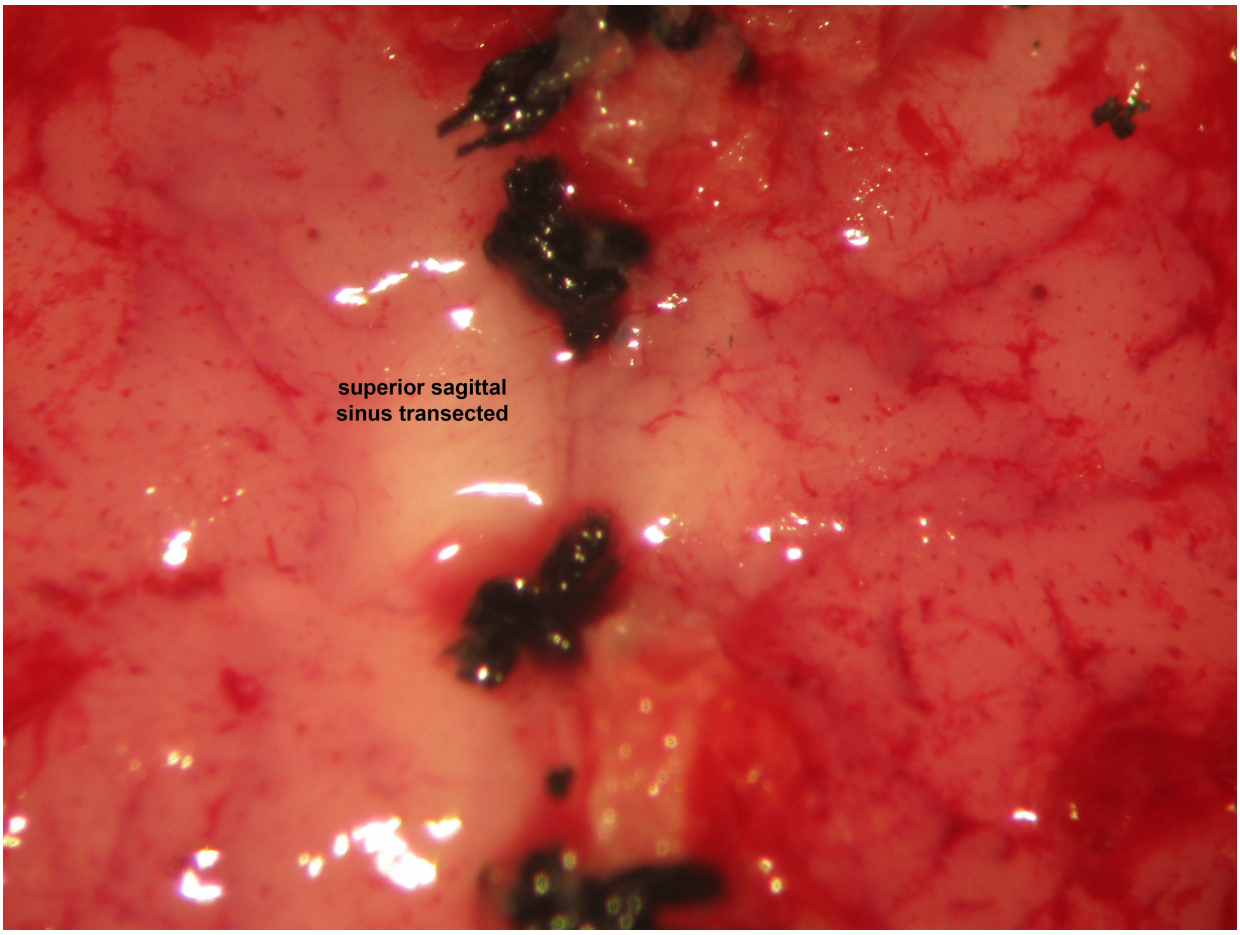

Figure 23. Decerebrative transective encephalotomy. We perform decerebrative transective encephalotomy through a supracollicular transverse plane 2-2.5 mm rostral to lambda using a microspatula. Removal of the cerebrum using suction proceeds accordingly: parietal cortex, parietal and frontal lobe, diencephalon, occipital lobe, and temporal lobe.

terial oxygen levels and enhancing tissue oxygenation, though the resultant incremental augmentation of the arterial oxygen tension generates a modest, though non-negligible, contribution to oxygen carrying capacity, content, and delivery.

Consistent recovery of arterial pressure to normotensive and slightly hypertensive values and dynamic emergent generation of triphasic eupnea exhibiting a robust augmenting spatiotemporally dynamic profile of burst shape visually in the phrenic electroneurogram and high (often exceeding 220 Hz), medium, and low frequency oscillations in phrenic nerve spectra (Ghali and Marchenko, 2013; Marchenko et al., 2012; Marchenko and Rogers, 2009, 2007, 2006a,b) clearly provides evidence indicating the success of our procedure at preserving and protecting neuronal ensembles constituting the respiratory rhythm and pattern generators. Restitution of high frequency oscillations in phrenic nerve spectra represent exquisitely sensitive and specific neurophysiological markers indicating integrity of the brainstem neural circuitry generating breathing, sympathetic activity, and cardiovagal premotoneuronal outflow, proving testament to the fidelity and precision of our set of microsurgical techniques achieving decerebration. The slightest injury compromising the neuronal circuitry generating these rhythms and oscillations and dynamically emergent rhythms would significantly attenuate the augmenting pattern of phrenic nerve bursting, and peak neuronal firing rate, and spectral power of high frequency oscillations. Recovery of dynamic arterial pressure magnitude to normotensive, or hypertensive, values commensurately indicates the neuronal ensembles constituting the neural network arrays comprising the brainstem oscillators generating sympathetic activity are exquisitely well-preserved and protected. Our set of microsurgical techniques and perioperative strategies managing anesthesia and core animal temperature accordingly generates consistently hemodynamically stable decerebrate preparations with an extraordinarily high success rate. We have yet to observe appreciable bleeding in our experiments resulting from decerebrative transective encephalotomy. Our decerebrate animal preparations accordingly remain hemodynamically stable indefinitely, permitting electromechanically stable neuronal and neural efferent recordings, contrasted with classically cited survival times experienced by unanesthetized decerebrate animal preparations occurring on the typical order of a few hours. We have accordingly utilized this preparation successfully to perform neuronal and neural efferent recordings in excess of fourteen hours.

8. Challenges of decerebration

Attendant massive exsanguination and posthemorrhagic hypotension resulting from the decerebration procedure have accord-

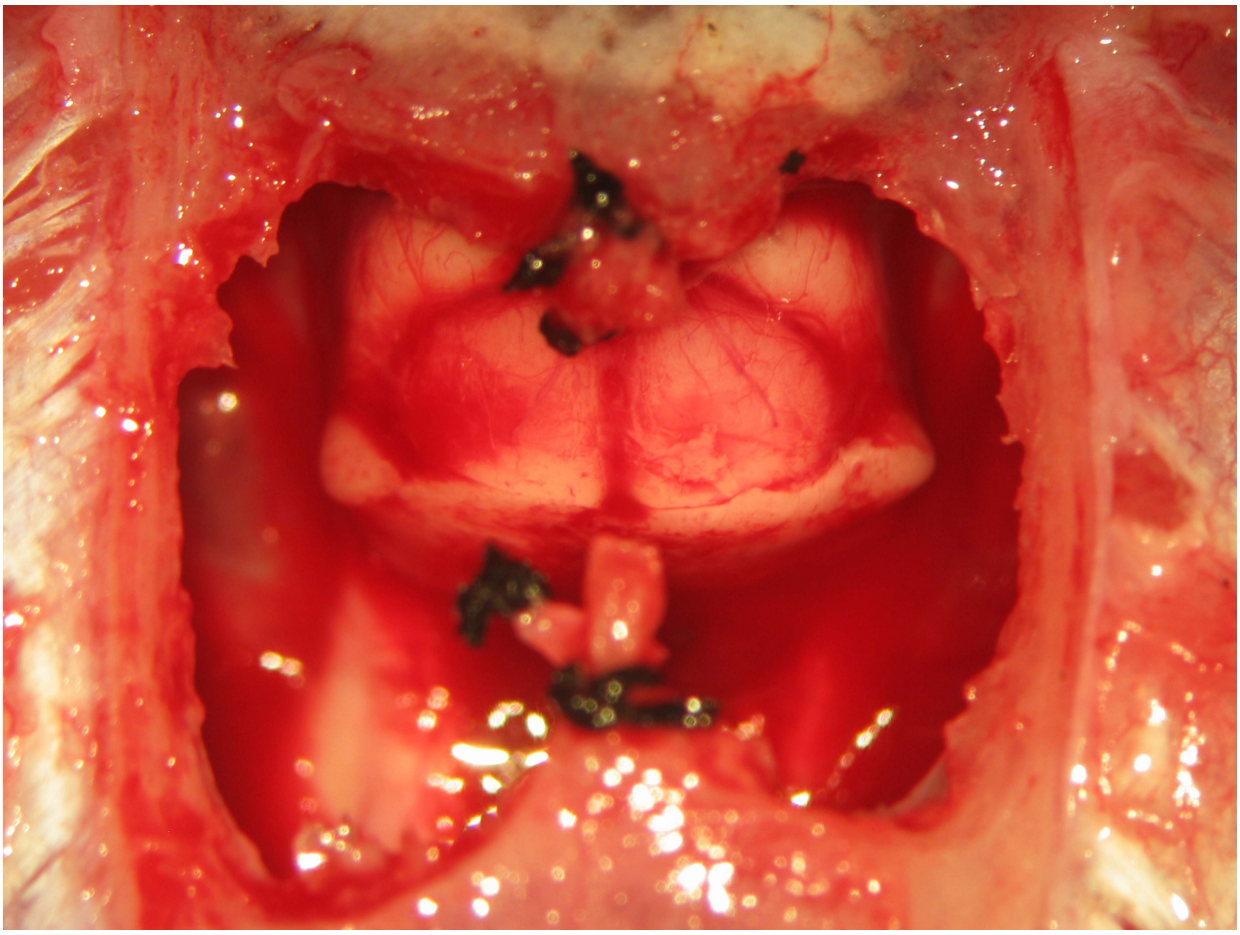

Figure 24. Completion of supracollicular decerebration. The superior colliculus may be visualized following an appropriately placed encephalotomy.

ingly prevented the consistent and facile generation of stable decerebrate animals permissive of neurophysiological interrogation accordingly to the experience of many investigators (Woolf, 1984). Conversely, we assert precise and judicious microsurgical technique, pre-decerebrative bilateral ligation of the internal carotid arteries above the origins of the pterygopalatine arteries, safely securing the superior sagittal sinus, post-encephalotomy packing of the cranial vault with cold thrombin-soaked gelfoam sponges, and perioperative hypothermic and potent inhalational anesthetic neuroprotection generate stable decerebrate preparations capable of lasting significant durations. Preparations of unanesthetized decerebrate animals *in vivo* continue to generate motion artifact through the rhythmic expansion and collapse of the thoracic cavity and mechanical pulsations deriving from the arterial blood pressure preclusive of high fidelity intracellular neuronal recordings. Bilateral pneumothoracotomy significantly attenuates the chest wall excursions generated by the alternating expansion and collapse of the lungs in mechanically-ventilated animals. However, arterial pressure oscillations and the ventricular impulse continue to generate rhombomyelic and cerebellar interstitial tissue vibrations, significantly modifying the electromechanical stability of intracellular, and to some extent, extracellular, neuronal recordings. Fortuitously, use of the *in situ* arterially-perfused preparation of the unanesthetized decerebrate juvenile rat allows the investigator to conduct extraordinarily stable intracellular neuronal recordings, given elimination of motion artifact coordinately and synergistically generated by chest wall excursions and arterial pressure pulsations (Marchenko et al., 2016; Pickering and Paton, 2006) (personal communication, Emeritus Professor Dr. V. Marchenko). Though empirical interrogation of the neural networks *sans* the confounding influence of potent inhalational or intravenous anesthetics represents the principal advantage of employing the decerebration technique, the paradoxically necessary use of parenterally intravenously administered vecuronium to achieve neuromuscular antagonism sufficiently to generate electromechanically stable recordings of individual neuronal activity, may putatively influence the activity of, and oscillatory synchrony amongst, brainstem, cerebellar, and spinal neural networks. Importantly, removal of cortical (Antal, 1984) and thalamic structures (Ogundele et al., 2017) may effectively eliminate critical modulatory influences of the cerebral hemispheres exerted upon the activity of propriobulbar, bulbospinal, propriospinal, and spinobulbar neuronal ensembles constituting dynamic emergent rhombomyelic networks generating the respiratory rhythm and pattern, sympathetic oscillations, and cardiovagal premotoneuronal outflow. Decorticate models may accordingly represent a viable alternative when seeking to investigate thalamic and hypothalamic neurophysiology and oscillations.

9. Validation of empirical power

9.1 Phrenic motoneurons and fast synchronous oscillations

We will accordingly provide a few examples in order to highlight and underscore the preferability of employing unanesthetized decerebrate preparations compared with the use of anesthetized animals (Ghali and Marchenko, 2015, 2016a,b; Ghali, 2015, 2019a,c; Marchenko et al., 2012; Marchenko and Rogers, 2009, 2007, 2006a,b). Prior to our work, the highest firing rate of phrenic motoneurons recorded was shown to correspond with discharge frequencies exhibited by the medium frequency spectral band of oscillations (Christakos et al., 1991), thus leading various investigators to suggest the high frequency band of synchronized oscillatory activity extant within respiratory related neural spectra may be generated by an epiphenomenological mechanism whereby cycle skipping and summation of the medium frequency band of activity summates to higher frequencies of activity (van Brederode and Berger, 2008). Studies accordingly generated smoothed pseudo Wigner-Ville distribution (SPWVD) time frequency representations of coherence (de Souza Neto et al., 2001; Djebbari and Bereksi-Reguig, 2013; Rajshekhar et al., 2009) between semicosine wave transformed unitary discharge of phrenic motoneurons and whole phrenic nerve discharge (Marchenko et al., 2012). We segregated phrenic motoneurons segregating into high, medium, and low frequency groups (Marchenko et al., 2012) correlated with the high, medium and low frequency oscillations in phrenic nerve discharge (Lebedev and Nelson, 1996) using K-means cluster analysis. Accordingly, using the unanesthetized decerebrate adult rat, we provided the first citable evidence of phrenic motoneurons discharging at rates corresponding with peak frequencies attained by high frequency oscillations in the phrenic neurogram (Fig. 1) (Marchenko et al., 2012). Our results powerfully support the hypothesis and derivative conjectures that the synchronous discharge of motoneurons at analogous frequency bands generates high frequency oscillations in phrenic nerve and respiratory related neurogram discharge (Marchenko et al., 2012). Definitively and incontrovertibly establishing this hypothesis would accordingly require contemporaneous recordings of multiple phrenic motoneurons within the phrenic motoneuron pool and demonstrating unit-to-unit and unit-to-nerve coherence at the corresponding phrenic spectral bands (personal communication V. Marchenko and R. Rogers).

9.2 Hypoglossal nerve pre-inspiratory and inspiratory activities and phrenic nerve inspiratory activity: crossmodal modulation by vagal influences and hypercapnia

Use of the unanesthetized decerebrate preparation of the adult rat has also allowed us to precisely interrogate vagal and hypercarbic modulation of brainstem neural networks generating preinspiratory activity evident in the hypoglossal nerve discharge (Fig. 2) (Ghali and Marchenko, 2016b; Ghali, 2015). Specifically, we demonstrated the presence of hypoglossal preinspiratory discharge in the vagus intact condition in the unanesthetized decerebrate preparation of the adult rat (Ghali, 2015), controverting the findings of Fukuda in the anesthetized preparation of the adult rat, and vagal accentuation of the activity (Ghali and Marchenko, 2016b; Ghali, 2015). We demonstrated potent crossmodal modulation of hypoglossal preinspiratory and inspiratory responses to hypercapnia by intactness of the vagal nerve. Accordingly, we observed greater accentuations of both the preinspiratory and inspiratory components of the respiratory neuromotor output in response to hypercarbia in the vagotomized compared with the vagus intact state (Ghali and Marchenko, 2016b).

9.3 Crossed phrenic phenomenon: dynamics and recovery of spontaneous crossed phrenic nerve activity following high cervical C_1 hemisection

Supraphrenic hemisection classically completely abolishes activity in the phrenic nerve discharge ipsilateral to the lesion with variable rapidity of recovery (Ghali, 2017d). Porter (1895) initially demonstrated cessation of ipsilateral diaphragmatic chest wall movements following high cervical hemisection above the level of the phrenic nucleus in morphine anesthetized preparations of a dog and several anesthetized rabbits as. Transective division of the phrenic nerve contralateral to the side of spinal cord hemisection effectively resurrected diaphragmatic and intercostal activity ipsilateral to spinal cord lesioning, evidenced by the reemergence of chest wall movements (Porter, 1895). Studies have accordingly termed and designated this pattern of recovery the soi-disant crossed phrenic phenomenon, whereby a stressor provoking the accentuation of neural discharge by propriobulbar neuronal circuitry constituting the respiatory central pattern generator elicits reemergence of respiratory related neural activity evident in neurogram, electromyogram, or chest wall movements, ipsilateral to a supraphrenic hemisection of the spinal cord (Ghali and Marchenko, 2015; Ghali, 2017d). Investigators would later demonstrate the same phenomenon of reemergence of the phrenic motoneuronal population activity, as demonstrated by diaphragmatic electromyography (Goshgarian, 1979, 1981; Gransee et al., 2017; Martínez-Gálvez et al., 2016) and phrenic electroneurography (Fuller et al., 2008, 2006; Golder et al., 2003; Golder and Mitchell, 2005; O'Hara and Goshgarian, 1991; Polentes et al., 2004; Zimmer and Goshgarian, 2007) in response to hypercapnia, hypoxia, or contralateral phrenicotomy. Studies have also since successfully demonstrated spontaneous recovery of activity in the phrenic nerve discharge ipsilateral to the site of lesioning, with earlier recovery observed when utilizing phrenic electroneurographic (Fuller et al., 2006; Golder and Mitchell, 2005; Zimmer and Goshgarian, 2005, 2006, 2007), compared with diaphragmatic electromyographic (Goshgarian, 1981; Martínez-Gálvez et al., 2016), evaluation of the phrenic motoneuronal population activity. Studies mechanistically attributed the observed patterns of recovery following cervical spinal cord hemisective injury to reemergence of latent descending crossed phrenic pathways decussating below the level of the lesion or the ingrowth of axons to the contralateral phrenic motor nucleus (Ghali and Marchenko, 2015; Ghali, 2017a). Since the use of anesthesia attenuates neural respiratory outputs, we hypothesized more rapid recovery of spontaneous crossed phrenic nerve activity would be revealed through the use of unanesthetized models. We successfully identified spontaneous recovery of crossed activity in the phrenic nerve discharge ipsilateral to a C_1 hemisection in the unanesthetized preparation of the supracollicularly decerebrate adult rat commencing within minutes and progressing during the course of hours (Fig. 3), summarily controverting and overturning the findings of Porter (1895) and his successors (see Tables. 1 and 2 of Ghali (2017a)). Read-

ministration of isoflurane anesthesia in the decerebrate condition effectively annihilated recovery in phrenic nerve discharge ipsilateral to C_1 hemisection (Fig. 4), supporting our hypothesis crossed polysynaptic bulbophrenic pathways may be constitutively active and preferentially suppressed by anesthesia and spinal shock.

9.4 Myelogenic respiratory rhythm generation and pattern formation: dynamics and recovery of phrenic nerve discharge following high cervical C_1 transection

Studies have provided robust evidence across a variety of species and animal models indicating the spinal cord may be capable of generating rhythmic activity distributing to respiratory related neural outputs (Aoki et al., 1980; Palisses et al., 1988, 1989; Reinoso et al., 1996; Viala et al., 1979). Spontaneous recovery of respiratory related neural activity was previously demonstrated to occur in cats (Aoki et al., 1980) and dogs (Reinoso et al., 1996). The works of Viala and colleagues identified pharmacologically induced respiratory-locomotor rhythmic activity across several studies performed in various preparations of the rabbit (Corio et al., 1993; Dubayle and Viala, 1996; Palisses et al., 1988, 1989). Utilizing the unanesthetized decerebrate preparation of the Sprague-Dawley adult rat, we demonstrated spontaneous, pharmacologically-generated, and asphyxia induced patterns of bilaterally synchronized rhythmic bursting activity in phrenic nerve discharge following bulbospinal interruption achieved via a transective injury through a plane between the brainstem and cervical cord at the C_1 spinal level (Ghali and Marchenko, 2016a). Patterns of spontaneous activity following C_1 transection included pseudoregular rhythmic bursting (Fig. 5) and slow synchronous oscillations (Ghali and Marchenko, 2016a), with oscillatory frequency variably consistent with that of the vasogenic autorhythmicity. Chemical disinhibition of upper cervical (C_1 to C_2) phrenic interneurons using topical application of a cocktail containing a mixture of gabazine (4 mM) and strychnine (4 mM) generated bilaterally synchronized decrementing bursts of variable duration exhibiting maximal peak of discharge during onset, bearing striking resemblance to prolonged gasps evident in bulbospinal intact preparations (Fig. 6) (Ghali and Marchenko, 2016a). Asphyxic challenge generated bilaterally synchronized decrementing rhythmic bursting evident in phrenic nerve discharge in C_1 transected unanesthetized decerebrate rats (Fig. 7) (Ghali and Marchenko, 2016a), suggesting the existence of propriospinal circuitry constituting a spinal gasping generator localizing to the upper cervical spinal cord (Fig. 8).

9.5 Myelogenic sympathogenesis: dynamics and recovery of arterial pressure following high cervical C_1 transection

In the 19^{th} century, Dittmar (1873) demonstrated precipitous declines of the arterial pressure following cervical transection dissociating the bulb from spinal cord preganglionic sympathetic neurons. Investigators have extensively and consistently demonstrated profound reductions of the arterial pressure following high cervical transection followed by variable recovery to near normal values occurring between several days to weeks following injury, a demonstration seminally made by Sherrington (1906) and replicated by the experience of subsequent studies (Burke, 2007; Dittmar, 1873; Goltz, 1874; Sherrington, 1906). Using the unanesthetized decerebrate preparation of the rat, we demonstrated rapid acute recovery of arterial pressure following C_1 transection occurring during the course of several hours (Fig. 9) (Ghali, 2019a). We accordingly believe the use of an unanesthetized decerebrate preparation of the adult rat will continue to be revelatory of critical neuronal network dynamics, not otherwise demonstrable utilizing anesthetized preparations by eschewing the confounding effects of anesthesia upon neuronal ensembles and their oscillatory synchrony (Ghali and Marchenko, 2015, 2016a,b; Ghali, 2015; Marchenko et al., 2012).

10. Promise of utilizing decerebrate preparations in unveiling and illumining mechanisms generating neural oscillations and mysteries of neurobiological networks

10.1 Supraspinal and spinal respiratory rhythmogenesis and pattern formation

Burgeoning evidence continues to accrue precisely detailing the mechanisms by which brainstem neuronal ensembles and propriobulbar circuitry elegantly generate the respiratory rhythm and pattern, though these mechanisms have remained in controversy since the discovery of the pre-Bötzinger complex in 1991 as the kernel for inspiratory rhythm generation by the seminal serial transection studies of Smith et al. (1991) using the *in vitro* preparation of the neonatal rat. *In vitro* brainstem slices containing the preBötzinger complex consistently and reproducibly generate a regular respiratory rhythm with reduced natural sources of tonic drive (Gray et al., 2010; Morgado Valle and Beltran Parrazal, 2017), initially leading several researchers to propose fast inhibitory synaptic neurotransmission may not be critical to form the rhythm proper. Moreover, respiratory rhythmic activity evident in neurons and hypoglossal neural efferent activity of brainstem derived slice preparations containing the preBötzinger complex classically and characteristically persist in the presence of GABAergic and/or glycinergic antagonists. Studies have consequently interpreted these findings to indicate pacemaker mechanisms may be capable of independently generating respiratory rhythmic activity (Gray et al., 2010; Molkov et al., 2017; Morgado Valle et al., 2010; Smith et al., 1991). However, rhythmic phasic discharge manifest in neuronal and neural efferent output in brainstem slice preparations *in vitro* may arise consequent to transmembrane voltage depolarization from high concentrations of potassium used to augment natural sources of tonic drive, an assertion theoretically proposed by, and corroborated by modeling studies (Rybak et al., 2014). The use of high concentrations of potassium *in vitro* according represents a critical confound which invokes the necessity of utilizing *in vivo* studies in order to determine the necessity of fast inhibitory synaptic neurotransmission to generate triphasic eupnea characterizing the normal breathing rhythm and pattern (Marchenko et al., 2016).

Several studies have accordingly investigated breathing rhythm generation and pattern formation in anesthetized preparations *in vivo*. In a study conducted by Jancewzski, microinjections of the $GABA_A$ergic antagonist bicuculline and the glycinergic antagonist strychnine in Bötzinger and preBötzinger complexes in spontaneously breathing anesthetized rats powerfully modulated the Hering Breuer reflex in the vagal intact condition, though

respiratory rhythmic activity persisted and was unaltered by microinjections of these compounds in the medulla in the vagotomized condition. The researchers interpreted the results to collectively indicate the core respiratory rhythm and pattern generating circuitry organizing eupnea may operate independently of fast inhibitory neurosynaptic transmission. Conversely, several years prior, microinjections of pharmacological agonists and antagonists of GABAergic and glycinergic neurotransmission in Bötzinger and preBötzinger complex Bongianni were demonstrated to variably perturb the respiratory rhythm and pattern, evidencing a critical role of fast inhibitory neurosynaptic transmission in generating the breathing rhythm and pattern in anesthetized rabbits *in vivo*.

Marchenko et al. (2016) corroboratively and commensurately demonstrated microinjections of gabazine and strychnine in pre-Bötzinger (Fig. 25) and Bötzinger (Fig. 26) complexes significantly compromised respiratory rhythmic activity and often abolished the eupneic pattern altogether in the *in situ* unanesthetized preparation of the decerebrate juvenile rat and anesthetized preparation of the adult rat. Accordingly, the pacemaker currents generating intrinsic bursting behavior of preBötzinger complex characterizing pre-inspiratory, pre-inspiratory inspiratory, and decrementing early-inspiratory neurons exhibiting lower threshold for native spontaneous depolarization may prove capable of generating respiratory rhythmic activity in reduced preparations with a reduction of natural sources of tonic drive and during hypoxic conditions compromising the integrity and functionality of inhibitory network elements (Ghali, 2019c), though fast inhibitory synaptic neurotransmission and network mechanisms may be critically required in order to generate triphasic eupneic discharge during non-hypoxic normocapnic conditions at rest (Ghali, 2019c). Specifically, we believe and accordingly venture to propose microinjections of antagonists of persistent sodium (riluzole) and/or calcium activated cationic (cadmium) pacemaker currents and voltage-gated calcium channels (Ω-conotoxin) and specific pharmacological agonists and antagonists of GABAergic (e.g., gabazine) and glycinergic (e.g., strychnine) signaling in an unanesthetized preparation of the decerebrate rat will significantly and precisely elucidate the role of pacemaker currents and fast inhibitory synaptic neurotransmission in respiratory rhythmogenesis and pattern formation in the *in vivo* condition with the full complement network connectivity. We also seek to replicate and extend the seminal serial transection studies conducted by Smith identifying the pre-Bötzinger complex as the principal kernel of inspiratory rhythm generation using *in vitro* brainstem slices of the neonatal rat to the *in vivo* unanesthetized decerebrate adult rat commencing at the pontomesencephalic border and progressing caudally towards and through the cervical cord in order to identify putative novel oscillators generating rhythmic activity in respiratory related neural discharges residing within the brainstem and spinal cord (Ghali and Marchenko, 2016a). We will accordingly electrophysiologically interrogate oscillator locations identified by the serial transection studies by performing individual extracellular unit recordings. This set of experiments conducted properly in an unanesthetized decerebrate preparation of the rat will contribute to elucidating types of breathing rhythmicity generable by brainstem and/or spinal cord in the presence of pharmacological antagonism of pacemaker activity and/or fast inhibitory synaptic neurotransmission and coordinately identify novel pacemakers.

10.2 Supraspinal sympathogenesis

Sympathetic-mediated accentuation of the arteriolar tone augments afterload and of venous tone augments right and left ventricular preload and force of myocardial contraction via Frank-Starling mechanisms, collectively increasing the magnitude of the arterial blood pressure; withdrawal of sympathetic drive generates reciprocal effects (Ghali, 2017a,b). Beyond a general consensus that supraspinal brainstem oscillators generate the resting sympathetic tone converging on maintaining arteriolar and venous tone within a physiological range and supporting sinoatrial chronotropy, atrioventricular dromotropy, and myocardial inotropy in the bulbospinal intact condition, there exists only controversy (Ghali, 2017a,b). Also, whether brainstem sympathetic oscillators principally utilize pacemaker (Sun et al., 1988) versus network (Lipski et al., 1996) mechanisms to generate coherent and correlated rhythmic activity remains in question. The concept of a critical zone residing within the brainstem generating and maintaining the resting vasomotor tone was initially proposed when Dittmar (1873) demonstrated that destruction of parts of the rostral ventrolateral medulla (RVLM) elicited precipitous declines in the arterial pressure. Investigators would later demonstrate that specific electrolytic lesioning of the RVLM reduces arterial blood pressure (ABP) to levels similar to those of observed following spinalization in anesthetized cats , rabbits, and rats Recovery of blood pressure in RVLM-lesioned rats to normal values following resuscitation from the influences of anesthesia (Cochrane and Nathan, 1989) provided evidence indicating other brainstem regions may contain presympathetic units and coordinately provide bulbospinal drive to spinal cord preganglionic sympathetic neurons and compensate for compromise of presympathetic drive provided by the RVLM.

Accordingly, one set of hypotheses proposes presympathetic neurons of the RVLM, rostral ventromedial medulla, caudal raphé, ventrolateral metencephalic tegmentum, and paraventricular nucleus generate coherent and correlated activity natively. hypothalamic and brainstem loci containing nuclearly arranged presympathetic units may receive tonic excitatory drive from other areas distributed throughout the neuraxis. The works of Barman and Gebber (Barman, 2019) and Dempesy et al. (1995) have extensively characterized the role of the medullary lateral tegmental field, a once mysterious, poorly-characterized, and ill-defined zones, in generating and modulating the activity of the rostral ventrolateral medullary presympathetic units and thus intermediolateral cell column preganglionic sympathetic neurons (Barman, 2019; Ghali, 2017a). LTF lesioning reduces arterial blood pressure and attenuates RVLM stimulation-induced pressor responses. Combined lesioning of RVLM and LTF precipitate catastrophic reductions in both ABP and heart rate. Accordingly, a few studies have astutely ventured to propose LTF may represent the originate source of basal sympathetic tone. Neurons extant throughout the expanse of the medullary division of the lateral tegmental field (LTF), an exclusively propriobulbar entity (c.f. pre-Bötzinger complex -- the propriobulbar kernel of inspiratory rhythm generation), discharge prior and project to presympathetic units within the RVLM and caudal raphé and exhibit activity correlated with

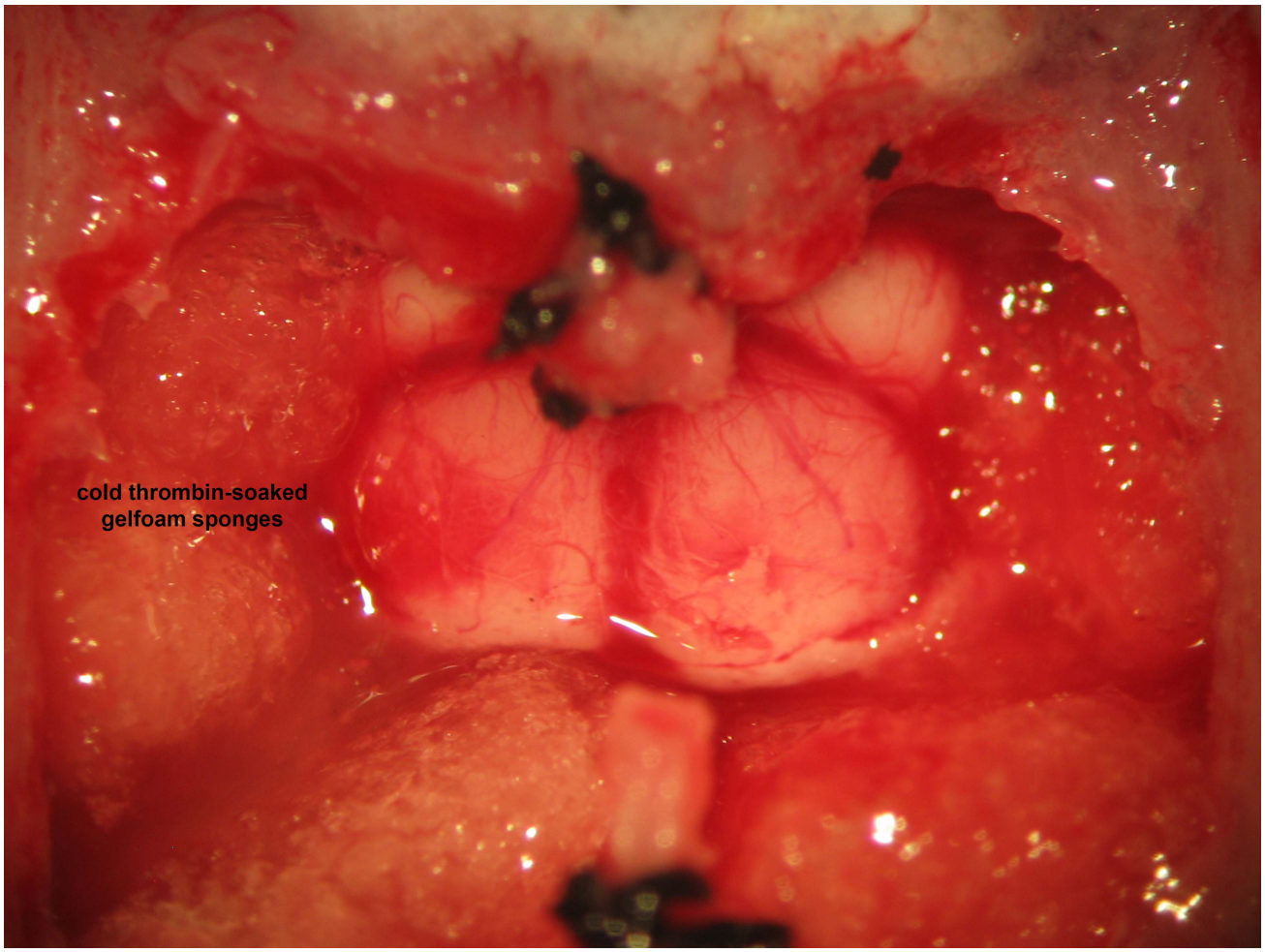

Figure 25. Cranial base hemostasis. Packing of the cranial vault with cold thrombin-soaked gelfoam sponges achieves hemostasis of skull base vessels. The microsurgeon should avoid overpacking in order to preventdownward herniation of the brainstem.

the cardiac-related rhythm in sympathetic nerve discharge. We interpret these data to collectively indicate the LTF originates basal sympathoexcitation. The medullary LTF also coordinates a variety of reflexes (i.e., baroreflex, Bezold-Jarisch reflex) (Barman et al., 2005; Jarisch and Henze, 1937; Von Bezold and Hirt, 1867). Convergence of a panoply of descending afferents deriving from the infralimbic cortex, associated limbic structures, and vestibular inputs upon the medullary LTF suggests a critical role of this zone in the sympathetic responses to fear and coordinating the sympathetic response with emesis proper (Yates et al., 1995). The medullary LTF appears to play an indispensable and integrative role by crossmodally modulating the respiratory impulse and arterial blood pressure in response to a host of descending and peripheral stimuli. We seek to determine the effects of microinjections of pharmacological antagonists of persistent sodium and calcium activated nonselective cationic currents and pharmacological agonists and antagonists of GABAergic and glycinergic in medullary lateral tegmental field and rostral ventrolateral medulla upon the arterial pressure and sympathetic output in unanesthetized decerebrate rats.

10.3 Medullocervical pressor area

Distinct though overlapping neuronal ensembles residing within the caudal medulla and upper cervical spinal cord contribute to generating accentuations of sympathetic activity, pressor responses, and augmentation of cerebral blood flow (Golanov et al., 2001; Goodchild and Moon, 2009; Seyedabadi et al., 2006). Medullocervical pressor area neuronal somata convey efferent axons supplying thoracolumbar intermediolateral cell column preganglionic sympathetic neurons. glutamate microstimulation of which evokes marked sympathetic pressor responses natively and in the presence of muscimol chemical inhibition of rostral ventrolateral medullary neurons in anesthetized rats (Seyedabadi et al., 2006), indicating the medullocervical pressor area (MCPA) mediates pressor responses independently of the rostral ventrolateral medulla. Vesicular glutamate transporter types 1 (VGlut1) and 2 (VGlut2) messenger ribonucleic acid (mRNA) positivity indicates a glutamatergic chemical phenotype of these units. (Goodchild and Moon, 2009; Seyedabadi et al., 2006). Activation of hypoxia sensitive rostral ventrolateral medullary reticulospinal units amplifies cerebral blood flow through the sequential activation of the medullary vasodilator area and subthalamic vasodilator area (Golanov et al., 2001). We seek to extend and further

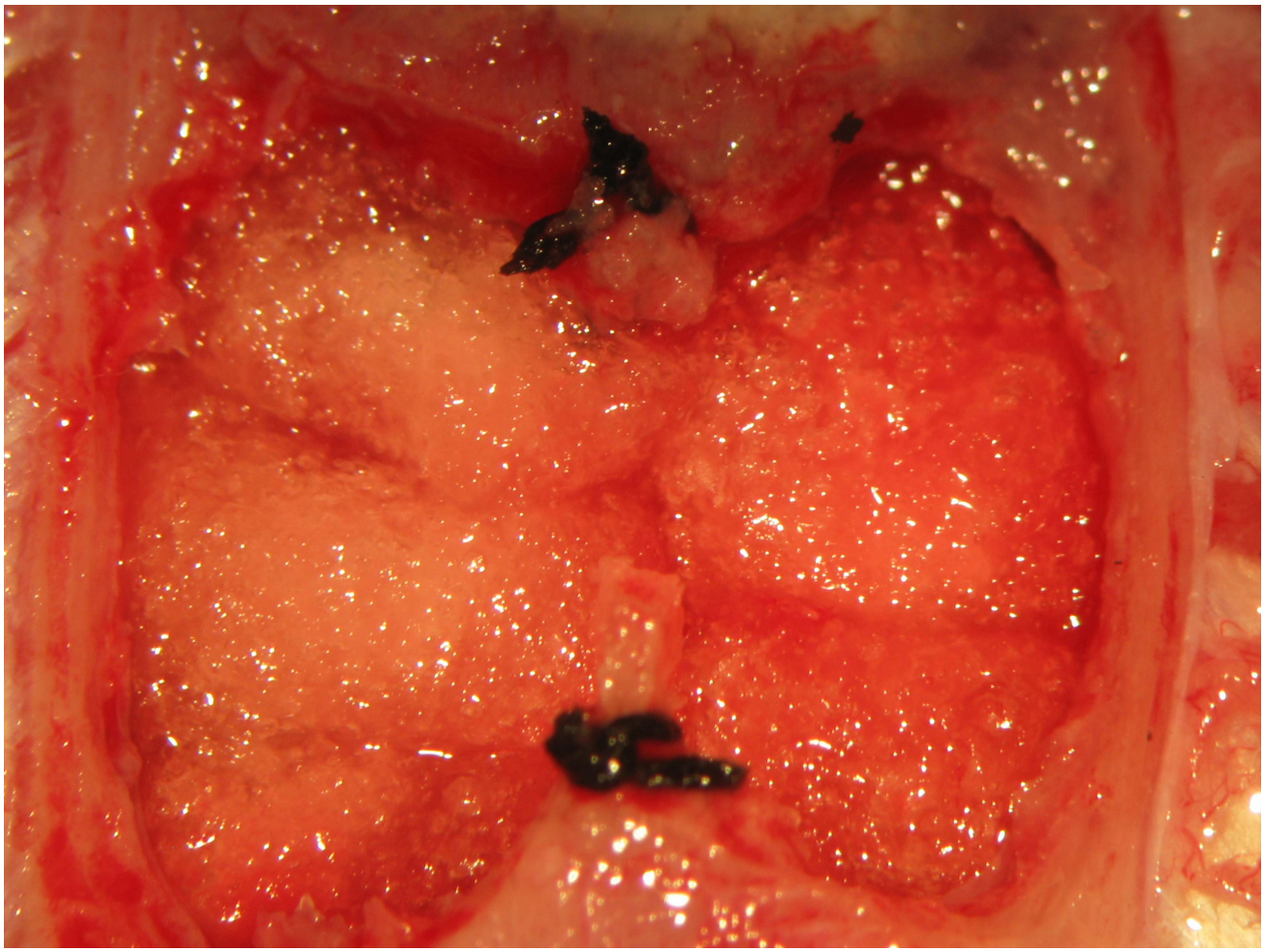

Figure 26. Packing of the cranial fossae. Cold thrombin-soaked gelfoam sponges are gently placed above the mesencephalic tectal surface.

dissect the implications of these findings by conducting a similar set of investigations in unanesthetized decerebrate animals absent the confounding influences of anesthesia seeking to determine responses of cerebral blood flow, sympathetic activity, and phrenic nerve discharge to microinjections of glutamate and pharmacological agonists and antagonists of GABAergic and glycinergic signaling in in these zones. Therapeutic electrical or chemical microstimulation of the medullocervical pressor area (Goodchild and Moon, 2009; Seyedabadi et al., 2006) may be used to augment arterial pressure during the acute phase of spinal shock following spinal cord injury and of the medullary and subthalamic vasodilator zones (Golanov et al., 2001) may be used to enhance collateral blood flow to cerebral parenchyma rendered ischemic by thromboembolic or dissective large vessel occlusion, subarachnoid hemorrhage-related vasospasm, microcirculatory dysfunction, or global hypoxia from intracranial hypertension and amplifying blood flows to ischemic zones of gliomas, accordingly rendering these lesions more responsive to the cytotoxic effects of chemotherapeutic agents and stereotactic radiosurgery.

10.4 Spinal sympathogenesis

Experimental transection of the spinal cord most commonly precipitously reduces mammalian systolic arterial pressure to approximately 40 to 50 mmHg chiefly consequent to the annihilative interruption of descending brainstem presympathetic bulbospinal excitatory drive provided to preganglionic sympathetic fibers residing within the intermediolateral cell column of the thoracolumbar spinal cord. Spinal transection exerts variable effects on the arterial blood pressure and sympathetic nerve activity. Some investigators observe precipitous declines and others report only minimal decrements below normal values (Ghali, 2019a; Sherrington, 1906). Studies have accordingly reported arterial blood pressure recovers with varying kinetics. According to the reported experience of some studies, recovery of arterial blood pressure occurs within several days following transective interruption of bulbar neuronal inputs to spinal cord preganglionic sympathetic neurons. In other studies, the recovery occurs within weeks to months following spinal cord injury. We have previously demonstrated recovery of arterial pressure towards near normal and normal values following cervicomedullary transection in the unanesthetized preparation of the decerebrate rat occurring on the order of hours following injury. These studies accordingly provide evidence indicating a powerful capacity of neuronal ensembles constituting propriospinal interneuronal networks to generate sympathetic tone independently of supraspinal inputs contributing to the recovery of arterial blood pressure (Ghali, 2019a). Recovery of arterial blood pressure to near normal values following bulbospinal dis-

sociation indicates networks residing within the myelic substance must endogenously generate coherent and correlated neuronal activity distributing to sympathetic neural efferent activity, though researchers have yet to specifically neuroanatomically and neurophysiologically characterize and interrogate these networks. Evidently, the thorough elucidation of mechanisms generating and modulating spinal sympathetic output following bulbospinal dissociation require further studies. We accordingly seek to systematically evaluate the contribution of the medullocervical pressor area and spinal sympathetic oscillators, intermediolateral cell column preganglionic sympathetic neurons, and dorsal root afferents to recovery of arterial blood pressure following cervicomedullary transection prior to and following dorsal rhizotomy in the unanesthetized decerebrate rat. We also seek to elucidate whether spinal oscillators chiefly utilize pacemaker versus network mechanisms to generate sympathetic activity. We will achieve these goals by microinjecting pharmacological agonists and antagonists of glutamatergic and $GABA_A$ergic and glycinergic signaling, and by downregulating identified persistent sodium and calcium activated nonselective cationic currents and/or voltage-gated calcium channels gated via microinjections of either or riluzole, cadmium, and/or Ω-conotoxin.

10.5 Mayer waves

Studies have extensively interrogated and attempted to describe the mechanisms contributing to the generation of oscillatory variability in sympathetic neuronal, sympathetic neural efferent, and cardiovascular hemodynamic spectra. The existence of these variabilities in cardiovascular and autonomic neural outflow spectra has inspired a multitude of fruitful investigations. The sympathetic discharge contains nested fast sympathetic rhythms discharging with central tendencies approximating 10 Hz (present exclusively in unanesthetized decerebrate animals) and 2-6 Hz and coherent and correlated with spectral peaks in cardiac sympathetic nerve discharge and arterial blood pressure and much slower sympathetic rhythms (Ghali, 2017a). These slow oscillations are collectively comprised of variably defined very low (< 0.1 Hz, varies according to study), low (~0.1-0.4 Hz, varies according to species), and high frequency (~0.25-0.4 Hz, varies according to respiratory frequency) bands of variability manifesting in the arterial pressure waveform, cardiac interval, and sympathetic and parasympathetic neuronal and neural efferent spectra. Respiratory sinus arrhythmia generates the high frequency band of sympathetic neural and hemodynamic spectral variability reflecting sinoatrial acceleration inspiratory related inhibition of cardiovagal premotoneuronal discharge. Mayer waves constitute the low frequency of variability generated by a complex interplay among and between central and peripheral mechanisms. The rhythmic contraction and relaxation of vascular smooth muscle, accordingly termed vasogenic autorhythmicity, generates very low frequency oscillations.

Studies have alternatively demonstrated abolition or persistence with spectral power reduction of Mayer wave oscillations following sinoaortic denervation mediated interruption of the baroreflex arc. Montano demonstrated the presence of Mayer waves in spectra of medullary lateral tegmental field, rostral ventrolateral medulla, caudal ventrolateral medulla, and caudal raphe neurons in unanesthetized decerebrate and pentobarbital anesthetized cats. Montano later demonstrated persistence of Mayer waves in arterial pressure following high cervical transection in unanesthetized vagotomized midcollicularly (i.e., intercollicularly; through a transverse plane bisecting the superior and inferior colliculi) decerebrate cats. We have interpreted the data and our anecdotal observations to collectively indicate Mayer waves are chiefly generated by supraspinal and spinal oscillators and are modulated and synchronized by baroreflex influences upon neuronal ensembles. We accordingly propose autochthonous oscillations of the arterioles may be mechanotransduced through the neural interstitium and generate oscillations of somatodendritic and axonal neurolemmal membranes and biophysical properties of the neurons at correspondent frequencies and at Mayer wave frequencies through the out-of-phase summation of lower frequency rhythms. We accordingly seek to evaluate the effects of baroloading, barounloading, sinoaortic denervation, chemoreceptor activation (e.g., phenylbiguanide, hypercapnia, hypoxia), pulmonary stretch receptor loading and unloading, and high cervical transection on the peak frequency, spectral band power, and coherence of Mayer wave oscillations amongst and between central sympathetic and nonsympathetic neurons, sympathetic neural efferent activity (e.g., cervical sympathetic nerve, thoracic splanchnic sympathetic nerve, renal sympathetic nerve), and arterial blood pressure. We also seek to determine coherence amongst and between neurons of supraspinal and spinal sympathetic oscillators at the Mayer wave frequency band and the attendant effects of glutamate microstimulation and muscimol chemical inhibition. brainstem zones generating Mayer wave oscillations. Our studies will accordingly determine the origins of Mayer wave genesis using carefully conducted experiments in the unanesthetized decerebrate preparation of the adult rat. The implications of this rhythmic behavior and the mechanisms of its generation are extensive and profound.

10.6 Brainstem reticular formation

The most useful scheme considers the brainstem to be organized into discrete nuclear zones diffusely distributed throughout non-discretely organized reticular networks (Brownstone and Chopek, 2018; Marlinskii, 1992; Opris et al., 2019; Takakusaki et al., 2016; Yasargil and Sandri, 1990). Brainstem nuclei are empirically interrogable and experimentally tenable. It proves a simple matter to perform individual or multiunit recordings of, and determine the effects of microinjections of pharmacological agonists and antagonists of different neurochemical signaling pathways upon, neurons in these zones (Marchenko et al., 2016). The brainstem nuclei are visually demonstrable in histologic specimens, discretely bounded by a variable transition zone from reticularly or loosely-organized cells (Dobbins and Feldman, 1994). Consequently, the majority of neurophysiologists seeking to illuminatively interrogate the mechanistic underpinnings of network interactions amongst neurons of the bulb, and those in hopes of generating a successful set of experiments sustaining a continuous influx of government or research foundation issued grant funding, preferentially subject discretely arranged nuclear zones to experimental interrogation. The role of reticular zones in modulating central pattern generation of breathing, sympathetic oscillations, and locomotor discharge, escaping the precision of certainty, remains largely unexplored. We may parsimoniously conceive of the brainstem reticulospinal network to be organized in nodal architecture, with nodes variably or alternatively excitatory or inhibitory.

Brainstem reticulospinal units convey excitatory and inhibitory modulatory synaptic drives shaping phasic and tonic discharge of motoneurons supplying upper and lower extremity and thoracic, abdominal, and pelvic musculature. Accordingly, a close and considerate evaluation of the literature readily reveals this most mystical of Nature's creations to tacitly conceal the mechanisms by which to effectively alleviate a substantial fraction of the most severe and catastrophic of the human morbidity burden ensuing from ischemia to the cerebrum.

We have extensively characterized the architectural organization of the brainstem reticular formation and generally determined the course, laterality, and neurochemical character of reticulospinal tracts and pathways conveying excitatory and inhibitory synaptic drives modulating phasic and tonic activities of motoneurons (Brownstone and Chopek, 2018). Approximately 85% of reticulospinal axons extant within the substance of the bulb coordinately provide synaptic drives to motoneurons of the cervical and lumbar enlargements. Cervically projecting brainstem reticulospinal units often provide both ipsilateral and contralateral synaptic drives to spinal pre-motoneuronal interneurons and motoneurons. The pedunculopontine (PPN) and cuneiform (CnF) nuclei collectively comprise the mesencephalic locomotor region of the mesencephalic reticular formation (Opris et al., 2019). These nuclei variably and specifically project to zones containing heterogeneously semi-compactly organized neuronal ensembles constituting the medullary reticular formation (the experimental stimulation of which may independently generate locomotion). Target efferents of the mesencephalic locomotor region include the nucleus gigantocellularis (CnF, PPN), nucleus gigantocellularis pars alpha (CnF, PPN), nucleus gigantocellularis pars ventralis (CnF, PPN), lateral nucleus paragigantocellularis (CnF, PPN), dorsal paragigantocellularis (PPN), the caudal extension of the nucleus gigantocellularis (PPN), and the ventral division of the caudal medial medullary reticular formation (PPN). The metencephalic reticular formation may be conceptually divided into a medial zone, comprised of the nucleus reticularis pontis oralis rostrally and the nucleus reticularis pontis caudalis caudally, the neurons of which project to lateral spinal cord motoneurons innervating appendicular hindlimb musculature and a lateral zone, the neurons of which project to medially located spinal cord motoneurons innervating the axial muscles supporting posture. The medial metencephalic reticular formation extends caudally into the medullary reticular formation dorsal to the nucleus gigantocellularis. The dorsally related pontine tegmental field may be conceptually divided into ventral, dorsal, and lateral zones. Pontine reticulospinal units span the rostrocaudal extent of the metencephalon, with neurons projecting ipsilaterally in greater abundance compared with those projecting contralaterally. Contralaterally projecting reticulospinal units are preferentially located within the caudal pons (Sivertsen et al., 2016).

Median, medial, and lateral divisions constitute the medullary reticular formation. Median midline raphe serotonergic reticulospinal neurons facilitate spinal motoneuronal discharge (Brownstone and Chopek, 2018). The nucleus gigantocellularis, nucleus gigantocellularis pars alpha, and nucleus gigantocellularis ventralis, the caudal extension of which may be divided into ventral and dorsal components, effectively constitute the medial medullary reticular formation (Sivertsen et al., 2016). The lateral paragigantocellularis, dorsal paragigantocellularis, and the dorsolateral parvocellular reticular formation collectively constitute the lateral medullary reticular formation. The intermediate division of the medullary reticular formation may be found interposed between the nucleus gigantocellularis ventrally and the dorsolateral parvocellular reticular formation and the ventral and dorsal divisions of the caudal extension of the nucleus gigantocellularis dorsally. Medullary reticulospinal neuronal somatodendritic membranes receive excitatory synaptic drive from axons of neurons of the contralateral cerebellar nuclei and the ipsilateral subthalamic locomotor region. The axons of medullary reticulospinal units course within the ventrolateral funicular division of the myelic substance en *route* to making synaptic contacts with ipsilateral or contralateral neurolemmal somatodendritic membranes of spinal cord motoneurons and pre-motoneuronal commissural interneurons circumscribing the central spinal canal providing inhibitory synaptic drive to ventral horn motoneurons. [Nota Bene: The majority of spinal cord commissural interneurons expressing the 65 and 67 kilodalton isoforms of glutamate decarboxylase and thus utilize GABAergic fast inhibitory neurotransmission, and likely represent a critical mechanism providing inhibitory modulation of patterned motor output (Yasargil and Sandri, 1990)]. Experimental stimulation of stereotactically identified zones corresponding with brainstem reticulospinal neurons alternatively generates excitatory, inhibitory, or biphasic postsynaptic potentials of premotoneuronal interneurons and motoneurons innervating flexor or extensor skeletal myocytes of the head, face, neck, and upper and lower extremities via ipsilateral and/or contralateral monosynaptic and/or polysynaptic relays (Brownstone and Chopek, 2018) and may generate movements across multiple joints. The firing of reticulospinal neurons with somata extant within the medial medullary reticular formation drives, and modulates endogenous spinally generated, patterned locomotor discharge (Marlinskii, 1992), though recruitment of lateral paragigantocellularis reticulospinal neurons may prove requisite in order to generate higher velocity locomotor activity. A proportion of gigantocellularis nucleus reticulospinal neurons convey an inhibitory modulation via glycinergic signaling upon target efferent interneurons and motoneurons.

We have thus provided a cursory, though concise and pointed discourse discussing the general architectural organization of brainstem reticulospinal tracts and pathways conveying excitatory and inhibitory synaptic drives modulating phasic and tonic activities of motoneurons. We accordingly propose studies employing retrograde transsynaptic labeling (e.g., using pseudorabies virus) techniques will thoroughly characterize the architectonic organization of the brainstem reticulospinal network (see Dobbins and Feldman (1994); Lane et al. (2008, 2009a,b)). The neurochemical identity of brainstem reticulospinal units may be determined by immunohistochemically labeling transverse slices sectioned from brainstem specimens using secondary fluorescent anti-immunoglobulin (amplification technique) targeting primary non-fluorescent anti-enzyme (e.g., 65 and 67 kilodalton isoforms of glutamate decarboxylase [GAD65/67]) or anti-cell surface transmembrane protein (e.g., glycine transporter type 2 [GLYT2]) antibody (molecular identification technique) (see

Marchenko et al. (2015)). Stimulation of brainstem zones corresponding with, and containing an abundance of, spinally projecting reticular neurons possessing a GABAergic or glycinergic phenotype (e.g., medullary nucleus gigantocellularis, gigantocellular depressor area) coordinately performed with electrophysiological recordings of individual motoneuronal units, motoneuronal population activity (motor nucleus multiunit records or neurogram), or muscle discharge in unanesthetized decerebrate preparations will thoroughly characterize the electrophysiological behavior of the bulboreticulospinal network and thus characterize the nature of bulboreticular modulation of the brainstem and spinal motoneurons (Brownstone and Chopek, 2018). Intracellular neuronal recordings will determine locoregional heterogeneity of response patterns and dynamics of excitatory and inhibitory postsynaptic potentials in response to electrical or chemical microstimulation of zones disparately distributed throughout the brainstem reticular network.

We venture to propose reduced brainstem reticulospinal GABAergic and glycinergic synaptic drives conveyed to brainstem and spinal motor networks attenuates fast synchronous oscillatory coherence amongst, and signal to noise ratio between phasic and tonic discharge of, motoneurons, representing the principal pathogenic mechanisms generating spastic paresis (Marchenko et al., 2015). Accordingly, determining the amplitude of, and ratio between, phasic and tonic components of individual and population motoneuronal activity and elucidating properties and spatiotemporal dynamics of the responses of phasic and tonic components of motoneuronal discharge to electrical or chemical microstimulation or inhibition of nodes disparately distributed throughout the brainstem reticular network individually or in unison in the setting of various motor disorders (compared with the normal physiological condition) will enhance our capacity to more precisely interrogate the specific neurobiological mechanisms giving rise to neurogenic muscle spasticity. Selectively augmenting GABAergic and glycinergic synaptic drive to motoneurons via electrical or chemical microstimulation of brainstem reticular network zones generates effects electrophysiologically distinct from parenteral administration of a pharmacological GABAergic agonist (e.g., baclofen, benzodiazepines, cyclobenzaprine), the current medical standard of care in the treatment of spasticity, which will coordinately augment phasic and tonic inhibitory drive to excitatory and inhibitory interneurons. While medical spasmolytics will certainly reduce the tonic background, activity generated by motoneurons, the use of these agents may coordinately excessively reduce the phasic discharge of motoneurons and generate sedative effects reducing the wakeful period and motivation to move. We suggest neural efferent outputs innervating limb and torso musculature may represent standardized metrics of evaluating power and smoothness of movement and postural output. Well-conducted, these studies should expectedly contribute to evolving an experimentally interrogable conceptualization of brainstem reticular modulation of motor output coordinately with developing and forming an understanding of the nature and character of supraspinal modulatory influences upon brainstem and spinal motor neuronal ensembles deriving from neural network arrays of the deep basal nuclei, supplementary, premotor, and motor cortices, cerebellar cortex and deep nuclei, ventral anterior, ventral thalamic, and centromedian nuclei, and brainstem zones in health and disease. These findings will collectively guide the rational development of therapies aimed at ameliorating motor disorders and shape our understanding of the benefit expectedly derived from these strategies.

We accordingly propose the following set of empirically evaluable therapeutic strategies designed to judiciously modify the firing behavior of bulbar reticulospinal units predicated and theoretically premised upon the described framework and presented conceptualization of brainstem reticular network structure and function may enhance and optimize the power, smoothness, and coordination of muscle contractions in individuals suffering from various motor disorders (see Marchenko et al. (2015)). Architectonic and electrophysiological characterization of GABAergic and glycinergic inhibitory reticulospinal neurons will effectively identify candidate zones which may be therapeutically stimulated in order to liberate smooth fluidity of skeletal muscle movement through the diminution of interregnum background erratic tonic activity interposed between purposeful contractions (Brownstone and Chopek, 2018). Augmenting the activity of these cells may effectively enhance resolution and ratio between phasic and tonic components of motoneuronal activity by amplifying coherent oscillatory synchrony amongst and between the individual motoneurons and by conveying a descending inhibitory modulation upon hyperactive spinal myotatic stretch reflex arcs. Stimulation of zones corresponding with nucleus gigantocellularis glycinergic units will provide a parallel inhibitory modulation of spinal motoneurons synergistic with the activity of Renshaw cells. Attenuating tonic background activity of brainstem and spinal motoneurons will amplify cellular responsivity to descending phasic synaptic drives by reducing the haphazard metabolic consumption of high energy phosphates (creatine phosphate) and phospho-phosphate esters (e.g., adenosine triphosphate, guanosine triphosphate) by uncoordinated fasciculations of skeletal muscle diminutively generative of appreciable displacements of the limb in space and of work against the gravitational force.

Neurosurgeons have extensively and variably utilized transcranial magnetic and deep brain stimulation of the motor cortex (Pagni et al., 2008), internal capsule (Franzini et al., 2008), thalamus (Yang et al., 2020), globus pallidus internus (Tan et al., 2016), subthalamic nucleus (Lin et al., 2020a; Tan et al., 2016; Vassal et al., 2019), pedunculopontine nucleus (Lin et al., 2020b), and cerebellum (Bologna and Beradrelli, 2018; França et al., 2018; Okromelidze et al., 2020; Rezaee et al., 2020) to ameliorate Parkinsonian tremor, rigidity, and bradykinesia (Lin et al., 2020a; Pagni et al., 2008; Tan et al., 2016; Vassal et al., 2019), essential tremor (Blaabjerg et al., 2020), and dystonia (Okromelidze et al., 2020; Pagni et al., 2008). Studies suggest, by extrapolative deduction, the putative efficacy of such techniques in relieving spasticity (Franzini et al., 2008; Pagni et al., 2008; Rezaee et al., 2020; Vassal et al., 2019). We may therapeutically enhance and amplify the activity and discharge of brainstem GABAergic and glycinergic reticulospinal neurons in human patients through electrical stimulation or by administering pharmacological agonists of specific receptor subtypes parenterally, epidurally, intraventricularly (via a surgically placed Ommaya reservoir), or locally microiontophoretically. High frequency electrical stimulation of brainstem zones

containing GABAergic or glycinergic reticulospinal units or regions conveying excitatory modulatory inputs to these regions via transcranial magnetic or deep brain stimulation could effectively augment brainstem inhibitory drive conveyed to brainstem and spinal motor networks. A modest reduction in tonic background motoneuronal activity may significantly enhance motor efficiency Local implantation of neural stem cells in specific zones of the brainstem reticular network in the presence of neuronal growth factors driving differentiation towards a neuronal lineage may therapeutically and specifically repopulate brainstem reticular regions with GABAergic and glycinergic reticulospinal neurons conveying descending inhibitory synaptic drives to brainstem and spinal motoneurons. In the setting of brainstem reticular neural stem cell implantation, high frequency stimulation may be synergistically used to promote local cell specific neurogenesis and amplify the extent of distal axodendritic synapse formation with motoneurons and interneurons constituting brainstem and spinal motor networks and improve electrochemical neural transduction efficiency. Conducting terminal neurophysiological experiments on unanesthetized decerebrate animals will permit the precise interrogation of the specific effects of electrically or chemically microstimulating brainstem zones corresponding with the location of GABAergic and glycinergic reticulospinal neurons and the complement of empirical therapeutic strategies upon the phasic and tonic components of motoneuronal discharge absent the confounding influences of anesthetic mediated potentiation of fast inhibitory synaptic neurotransmission in acute and chronic models of spasticity.

Classic microsurgical approaches may facilitate the placement of stimulatory electrodes or microcatheters designed to deliver therapeutic compounds within brainstem zones corresponding with the location of GABAergic and glycinergic reticulospinal neurons (Rhoton, 2000a,b; Spetzler et al., 2015). Microsurgical exposure of the brainstem ventrally may be achieved via transoral transpharyngeal transclival or transmaxillary routes, ventrolaterally via suboccipital trephination, C_1 laminectomy, and far lateral approach, and dorsally via suboccipital craniectomy with transvermian or transtelovelar approach in order to gain access to therapeutically modifiable brainstem reticulospinal neurons (Rhoton, 2000a,b; Spetzler et al., 2015). We accordingly indicate the critical need to generate electrophysiological and microiontophoretic dose response curves in order to establish threshold and lowest effect levels, optimal stimulation parameters, and toxicity levels in preclinical animal models and human patients. High frequency stimulation or glutamate microstimulation of suprabulbar and rhomebencephalic zones providing synaptic drives to reticulospinal units may generate NMDA dependent synaptic plasticity and long term synaptic potentiation (Kandel, 1979; Kandel et al., 2000); lower frequencies of stimulation could inadvertently cause long term synaptic depression and reduce the efficiency and fidelity of neurosynaptic conduction (Kandel, 1979; Kandel et al., 2000). Accordingly, differential kinetics of cytosolic calcium rates of rise represent the principal determinant of whether a postsynaptic dendrite experiences enhancement or attenuation of neurosynaptic transduction efficiency. The described set of strategies may be therapeutically exploited in order to enhance the activity of brainstem reticulospinal cells and indirectly excite a plethora of spinal commissural GABAergic and glycinergic interneurons conveying inhibitory modulation of contralateral ventral horn motoneuronal transmembrane potential.

11. Conclusions

We extensively discuss and detail critical and nuanced microsurgical techniques and perioperative strategies through which to optimize the generation of stable decerebrate animal preparations and accordingly present several methodological modifications annihilating or minimizing perioperative blood loss, hastening recovery of the neural elements comprising the brainstem oscillators generating the breathing rhythm and sympathetic tone driving the arterial blood pressure, and generating consistently stable decerebrate animal preparations (Ghali and Marchenko, 2015, 2016a,b; Ghali, 2015, 2019c; Marchenko et al., 2012; Marchenko and Rogers, 2009, 2007, 2006a,b). Optimizing microsurgical techniques and judiciously managing periprocedural anesthesia and animal temperature prove critical in achieving neuroprotection and generating stable long lasting preparations with robust sympathetic tone and an augmenting pattern of phrenic nerve discharge. Our methods and techniques optimize a model obviating the use of anesthesia and allowing the neurophysiologist to perform neural recordings in the native unanesthetized condition. The unanesthetized decerebrate preparation has accordingly revealed fundamental properties of neurobiological networks and interactions amongst neuronal ensembles otherwise not evident in anesthetized animals. We have accordingly taken the liberty of discoursing upon some mysteries of neurophysiology which may prove amenable to a more rigorous and precise interrogation using the unanesthetized decerebrate rat and suggest a few specific experiments which may prove revelatory of the mechanistic underpinnings of historically enigmatic processes. Specifically, we have discussed for the purposes of excogitation, pontification, and exposition the controversies continuing to surround the role of fast inhibitory synaptic transmission in respiratory rhythmogenesis and pattern formation in adults (Ghali, 2019c; Marchenko et al., 2016) and neonates (Ghali and Beshay, 2019), mechanisms generating supraspinal and spinal sympathetic oscillations (Ghali, 2017a), the origins of Mayer waves, and brainstem reticular formation modulation of brainstem and spinal motor networks which have evaded the collective deductive logical reasoning efforts of neuroscientists and physiologists across a variety of subdisciplines. The proper use of this underutilized model will continue to illumine the mysteries and mechanistic underpinnings of the behavior of complexly organized neural network arrays.

List of abbreviations

AAALAC, Association for Assessment and Accreditation of Laboratory Animal Care; BötC, Bötzinger complex; CnF, cuneiform nucleus; CO_2, carbon dioxide; EKG, electrocardiogram; fR, frequency of respiration; GABA, g-aminobutyric acid; $GABA_A$, g-aminobutyric acid A subtype (of receptor or signaling); GABAz, gabazine; GAD65/67, 65 and 67 kilodalton isoforms of glutamate decarboxylase; GLYT2, glycine transporter type 2; h, hours; HF, high frequency; HF+BG, high frequency with background; Hz, hertz; Kg, kilograms; LF, low frequency; LTF, lateral tegmental field; MCPA, medullocervical pressor area; MF, medium frequency; mg, milligrams; mL, milliliters; mmHg, mil-

limeters of mercury; mRNA, messenger ribonucleic acid; mV, millivolts; NMDA, N-methyl-$_D$-aspartate; O_2, oxygen; ∫PhNL, integrated left phrenic nerve activity; ∫PhNR, integrated right phrenic nerve activity; ∫PN, integrated phrenic nerve activity; ∫PNR, integrated right phrenic nerve activity; PhMN, phrenic motoneuron; PhN, phrenic nerve; PNR, right phrenic nerve; PPN, pedunculopontine nucleus; pre-BötC, pre-Bötzinger complex; RVLM, rostral ventrolateral medulla; SSS, superior sagittal sinus; STR, strychnine; TE, expiratory duration; TFR, time frequency representation; TI, inspiratory duration; VGlut1, vesicular glutamate transporter type 1; VGlut2, vesicular glutamate transporter type 2; ∫XIIR, integrated right hypoglossal nerve activity; XII, hypoglossal nerve; XIIR, right hypoglossal nerve.

Ethics approval and consent to participate

All procedures performed were in accordance with the ethical standards of the Drexel University Institutional Animal Care and Use Committee, national research committee, and with the 1964 Helsinki Declaration and its later amendments or comparable ethical standards. All animal housing and experiments were conducted in strict accordance with the Drexel University Institutional Animal Care and Use Committee Institutional Guidelines for Care and Use of Laboratory Animals and the Animal Welfare Act passed by the Esteemed and Distinguished United States Congress in 1966.

Conflict of Interest

No conflicts of interest to disclose.

Submitted: August 14, 2019
Accepted: January 28, 2020
Published: March 30, 2020

References

Accorsi-Mendonça, D., da Silva, M. P., Souza, G. M., Lima-Silveira, L., Karlen-Amarante, M., Amorim, M. R., Almado, C. E., Moraes, D. J. and Machado, B. H. (2016) Pacemaking property of RVLM presympathetic neurons. *Frontiers in Physiology* **7**, 424.

Amemiya, M. and Yamaguchi, T. (1984) Fictive locomotion of the forelimb evoked by stimulation of the mesencephalic locomotor region in the decerebrate cat. *Neuroscience Letters* **50**, 91-96.

Antal, M. (1984) Termination areas of corticobulbar and corticospinal fibres in the rat. *Journal für Hirnforschung* **25**, 647-659.

Aoki, M., Mori, S., Kawahara, K., Watanabe, H. and Ebata, N. (1980) Generation of spontaneous respiratory rhythm in high spinal cats. *Brain Research* **202**, 51-63.

Baccelli, G., Guazzi, M., Libretti, A. and Zanchetti, A. (1965) Pressoceptive and chemoreceptive aortic reflexes in decorticate and in decerebrate cats. *American Journal of Physiology* **208**, 708-714.

Bains, J. S. and Ferguson, A. V. (1995) Paraventricular nucleus neurons projecting to the spinal cord receive excitatory input from the subfornical organ. *American Journal of Physiology* **268**, R625-R633.

Barman, S. M. (2019) Ludwig Lecture: Rhythms in sympathetic nerve activity are a key to understanding neural control of the cardiovascular system. *American Journal of Physiology - Regulatory Integrative Comparative Physiology* **318**, R191-R205.

Barman, S. M., Phillips, S. W., Gebber, G. L., (2005) Medullary lateral tegmental field mediates the cardiovascular but not respiratory component of the Bezold-Jarisch reflex in the cat. *American Journal of Physiology* **289**, R1693-R1702.

Bennett, D. J., Hultborn, H., Fedirchuk, B. and Gorassini, M. (1998) Synaptic activation of plateaus in hindlimb motoneurons of decerebrate cats. *Journal of Neurophysiology* **80**, 2023-2037.

Bezdudnaya, T., Lane, M. A. and Marchenko, V. (2018) Paced breathing and phrenic nerve responses evoked by epidural stimulation following complete high cervical spinal cord injury in rats. *Journal of Applied Physiology* **125**, 687-696.

Blaabjerg, M., Pedersen, C. B., Andersen, M. S., Grønhøj, M. H., Krone, W., Bode, M. and Poulsen, F. R. (2020) [MR-guided focused ultrasound for treatment of essential tremor]. *Ugeskrift for Laeger* **182**. pii: V09190533.

Bologna, M. and Beradrelli, A. (2018) The Cerebellum and Dystonia. *Handbook of Clinical Neurology* **155**, 259-272.

Burke R. E. (2007) Sir Charles Sherrington's The integrative action of the nervous system: a centenary appreciation. *Brain* **130**, 887-894.

Brownstone, R.M. and Chopek, J.W. (2018) Reticulospinal Systems for Tuning Motor Commands. *Frontiers in Neural Circuits* **12**, 30.

Christakos, C. N., Cohen, M. I., Barnhardt, R. and Shaw, C. F. (1991) Fast rhythms in phrenic motoneuron and nerve discharges. *Journal of Neurophysiology* **66**, 674-687.

Clarke, R. W., Ford, T. W. and Taylor, J. S. (1988) Adrenergic and opioidergic modulation of a spinal reflex in the decerebrated rabbit. *Journal of Physiology* **404**, 407-417.

Cochrane, K. L. and Nathan, M. A. (1989) Normotension in conscious rats after placement of bilateral electrolytic lesions in the rostral ventrolateral medulla. *Journal of the Autonomic Nervous System* **26**, 199-211.

Cohen, M. I. (1975) Phrenic and recurrent laryngeal discharge patterns and the Hering-Breuer reflex. *American Journal of Physiology* **228**, 1489-1496.

Cohen, M. I. (1971) Switching of the respiratory phases and evoked phrenic responses produced by rostral pontine electrical stimulation. *Journal of Physiology* **217**, 133-158.

Corio, M., Palisses, R. and Viala, D. (1993) Origin of the central entrainment of respiration by locomotion facilitated by MK 801 in the decerebrate rabbit. *Experimental Brain Research* **95**, 84-90.

Darling, R. A. and Ritter, S. (2009). 2-Deoxy-D-glucose, but not mercaptoacetate, increases food intake in decerebrate rats. *American Journal of Physiology - Regulatory Integrative and Comparative Physiology* **297**, R382-R386.

Dasgupta, S. R. and Hausler, H. F. (1956) Respiratory changes in decorticate cats following transverse sections through the hypothalamus. *Experientia* **12**, 64.

de Almeida, A. T., Al-Izki, S., Denton, M. E. and Kirkwood, P. A. (2010) Patterns of expiratory and inspiratory activation for thoracic motoneurones in the anaesthetized and the decerebrate rat. *Journal of Physiology* **588**, 2707-2729.

de Souza Neto, E. P., Custaud, M. A., Frutoso, J., Somody, L., Gharib, C. and Fortrat, J. O. (2001) Smoothed pseudo Wigner-Ville distribution as an alternative to Fourier transform in rats. *Autonomic Neuroscience* **87**, 258-267.

Decima, E. E. and von Euler, C. (1969) Intercostal and cerebellar influences on efferent phrenic activity in the decerebrate cat. *Acta Physiologica Scandinavica* **76**, 148-158.

Dempesy, C. W., Richardson, D. E. and Fontana, C. J. (1995) Sympathetically-mediated cardiovascular responses induced by neurochemical microinjection in the brainstem lateral tegmental field of cat. *Brain Research* **704**, 141-144.

Dempesy, C. W., Richardson, D. E., Kocsis, B., Fontana, C. J. and Song, J. H. (2000) Lateral tegmental field neurons with activity correlated to the 10-Hz rhythm in sympathetic nerve discharge. *Brain Research* **852**, 213-216.

Dempesy, B., Le, S., Turner, A., Bokiniec, P., Ramadas, R., Bjaalie, J. G., Menuet, C., Neve, R., Allen, A. M., Goodchild, A. K. and McMullan, S. (2017) Mapping and analysis of the connectome of sympathetic premotor neurons in the rostral ventrolateral medulla of the rat using a volumetric brain atlas. *Frontiers in Neural Circuits* **11**, 9.

Destefino, V. J., Reighard, D. A., Sugiyama, Y., Suzuki, T., Cotter, L. A., Larson, M. G., Gandhi, N. J., Barman, S. M. and Yates, B. J. (2011) Responses of neurons in the rostral ventrolateral medulla to whole body rotations: comparisons in decerebrate and conscious cats. *Journal of Applied Physiology (1985)* **110**, 1699-1707.

DiMarco, A. F., von Euler, C., Romaniuk, J. R. and Yamamoto, Y. (1981) Positive feedback facilitation of external intercostal and phrenic inspiratory activity by pulmonary stretch receptors. *Acta Physiologica Scandinavica* **113**, 375-386.

Dittmar, C. (1873) Über die Lage des sogenannten Gefässcentrums in der Medulla oblongata. *Berlin Verhage Sächsische Akademie der Wissenschaften zu Leipzig Mathematisch-Physische Klasse* **25**, 449-469.

Djebbari, A. and Bereksi-Reguig, F. (2013) Detection of the valvular split within the second heart sound using the reassigned smoothed pseudo Wigner-Ville distribution. *BioMedical Engineering Online* 1**2**, 37.

Dobbins, E. G. and Feldman, J. L. (1994) Brainstem network controlling descending drive to phrenic motoneurons in rat. *Journal of Comparative Neurology* **347**, 64–86.

Dobson, K. L. and Harris, J. (2012) A detailed surgical method for mechanical decerebration of the rat. *Experimental Physiology* **97**, 693-698.

Dubayle, D. and Viala, D. (1996) Localization of the spinal respiratory rhythm generator by an *in vitro* electrophysiological approach. *Neuroreport* **7**, 1175-1180.

Faber, J. E., Harris, P. D. and Wiegman, D. L. (1982) Anesthetic depression of microcirculation, central hemodynamics, and respiration in decerebrate rats. *American Journal of Physiology - Heart and Circulatory Physiology* **243**, H837-H843.

França, C., de Andrade, D. C., Teixeira, M. J. and Cury, R. G. (2018) Cerebellum as a Possible Target for Neuromodulation After Stroke. *Brain Stimulation* **11**, 1175-1176.

Fouad, K. and Bennett, D. J. (1998) Decerebration by global ischemic stroke in rats. *Journal of Neuroscience Methods* **84**, 131-137.

Franzini, A., Cordella, R., Nazzi, V. and Broggi, G. (2008) Long-term chronic stimulation of internal capsule in poststroke pain and spasticity. Case report, long-term results and review of the literature. *Stereotactic Functional Neurosurgery* **86**, 179-183.

Fuller, D. D., Doperalski, N. J., Dougherty, B. J., Sandhu, M. S., Bolser, D. C. and Reier, P. J. (2008) Modest spontaneous recovery of ventilation following chronic high cervical hemisection in rats. *Experimental Neurology* **211**, 97-106.

Fuller, D. D., Golder, F. J., Olson Jr., E. B. and Mitchell, G. S. (2006) Recovery of phrenic activity and ventilation after cervical spinal hemisection in rats. *Journal of Applied Physiology* **100**, 800-806.

Gerasimenko, Y. P., Lavrov, I. A., Bogacheva, I. N., Shcherbakova, N. A., Kucher, V. I. and Musienko, P. E. (2005) Formation of locomotor patterns in decerebrate cats in conditions of epidural stimulation of the spinal cord. *Neuroscience and Behavioral Physiology* **35**, 291-298.

Ghali, M. G. Z. and Marchenko, V. (2013) Fast oscillations during gasping and other non-eupneic respiratory behaviors: clues to central pattern generation. *Respiratory Physiology and Neurobiology* **187**, 176-182.

Ghali, M. G. and Marchenko, V. (2015) Dynamic changes in phrenic motor output following high cervical hemisection in the decerebrate rat. *Experimental Neurology* **271**, 379-389.

Ghali, M. G. and Marchenko, V. (2016a) Patterns of phrenic nerve discharge after complete high cervical spinal cord injury in the decerebrate rat. *Journal of Neurotrauma* **33**, 1115-1127.

Ghali, M. G. and Marchenko, V. (2016b) Effects of vagotomy on hypoglossal and phrenic responses to hypercapnia in the decerebrate rat. *Respiratory Physiology and Neurobiology* **232**, 13-21.

Ghali, M. G. (2017a) Role of the medullary lateral tegmental field in sympathetic control. *Journal of Integrative Neuroscience* **16**, 189-208.

Ghali, M. G. (2017b) The brainstem network controlling blood pressure: an important role for pressor sites in the caudal medulla and cervical cord. *Journal of Hypertension* **35**, 1938-1947.

Ghali, M. G. Z. (2017c) The bulbospinal network controlling the phrenic motor system: laterality and course of descending projections. *Neuroscience Research* **121**, 7-17.

Ghali, M. G. (2017d) The crossed phrenic phenomenon. *Neural Regeneration Research* **12**, 845-864.

Ghali, M. G. (2015) Vagal modulation of pre-inspiratory activity in hypoglossal discharge in the decerebrate rat. *Respiratory Physiology and Neurobiology* **215**, 47-50.

Ghali, M. G. Z. (2018) Phrenic motoneurons: output elements of highly organized intraspinal network. *Journal of Neurophysiology* **119**, 1057-1070.

Ghali, M. G. Z. (2019a) Dynamic changes in arterial pressure following high cervical transection in the decerebrate rat. *The Journal of Spinal Cord Medicine* **16**, 1-12.

Ghali, M. G. Z. (2019b) Rubral modulation of breathing. *Experimental Physiology* **104**, 1595-1604.

Ghali, M. G. Z. (2019c) Mechanisms contributing to the genesis of hypoglossal preinspiratory discharge. *Journal of Integrative Neuroscience* **18**, 313-325.

Ghali, M. G. Z. and Beshay, S. (2019) Role of fast inhibitory synaptic transmission in neonatal respiratory rhythmogenesis and pattern formation. *Molecular and Cellular Neuroscience* **100**, 103400.

Ghali, M. G., Britz, G. and Lee, K. Z. (2019) Pre-phrenic interneurons: characterization and role in phrenic pattern formation and respiratory recovery following spinal cord injury. *Respiratory Physiology and Neurobiology* **265**, 24-31.

Golanov, E. V., Christensen, J. R., Reis, D. J. (2001) Neurons of a limited subthalamic area mediate elevations in cortical cerebral blood flow evoked by hypoxia and excitation of neurons of the rostral ventrolateral medulla. *Journal of Neuroscience* **21**, 4032-4041.

Golder, F. J., Fuller, D. D., Davenport, P. W., Johnson, R. D., Reier, P. J. and Bolser, D. C. (2003) Respiratory motor recovery after unilateral spinal cord injury: eliminating crossed phrenic activity decreases tidal volume and increases contralateral respiratory motor output. *Journal of Neuroscience* **23**, 2494-2501.

Golder, F. J. and Mitchell, G. S. (2005) Spinal synaptic enhancement with acute intermittent hypoxia improves respiratory function after chronic cervical spinal cord injury. *Journal of Neuroscience* **25**, 2925-2932.

Golder, F. J., Reier, P. J. and Bolser, D. C. (2001a) Altered respiratory motor drive after spinal cord injury: supraspinal and bilateral effects of a unilateral lesion. *Journal of Neuroscience* **21**, 8680-8689.

Golder, F. J., Reier, P. J., Davenport, P. W. and Bolser, D. C. (2001b) Cervical spinal cord injury alters the pattern of breathing in anesthetized rats. *Journal of Applied Physiology* **91**, 2451-2458.

Goltz, F. (1874) Ueber die funktionen des lendenmarks des hundes. pfluegers arch. gesamte physiol. *Menschen Tiere* **8**, 460-498.

Goodchild, A. K. and Moon, E. A. (2009) Maps of cardiovascular and respiratory regions of rat ventral medulla: focus on the caudal medulla. *Journal of Chemical Neuroanatomy* **38**, 209-221.

Goodchild, A. K., van Deurzen, B. T., Hildreth, C. M. and Pilowsky, P. M. (2008) Control of sympathetic, respiratory and somatomotor outflow by an intraspinal pattern generator. *Clinical Experimental Pharmacology and Physiology* **35**, 447-453.

Goshgarian, H. G. (1979) Developmental plasticity in the respiratory pathway of the adult rat. *Experimental Neurology* **66**, 547-555.

Goshgarian, H. G. (1981) The role of cervical afferent nerve fiber inhibition of the crossed phrenic phenomenon. *Experimental Neurology* **72**, 211-225.

Gould, D. J. and Goshgarian, H. G. (1997) Glial changes in the phrenic nucleus following superimposed cervical spinal cord hemisection and peripheral chronic phrenicotomy injuries in adult rats. *Experimental Neurology* **148**, 1-9.

Gould, D. J. and Goshgarian, H. G. (1999) The effects of mitotic inhibition on the spinal cord response to the superimposed injuries of spinal cord hemisection and peripheral axotomy. *Experimental Neurology* **158**, 394-402.

Gransee, H. M., Gonzalez Porras, M. A., Zhan, W. Z., Sieck, G. C. and Mantilla, C. B. (2017) Motoneuron glutamatergic receptor expression following recovery from cervical spinal hemisection. *Journal of Comparative Neurology* **525**, 1192-1205.

Gray, P. A., Hayes, J. A., Ling, G. Y., Llona, I., Tupal, S., Picardo, M. C., Ross, S. E., Hirata, T., Corbin, J. G., Eugenín, J. and Del Negro, C. A. (2010) Developmental origin of preBötzinger complex respiratory neurons. *Journal of Neuroscience* **30**, 14883-14895.

Grélot, L., Milano, S., Portillo, F., Miller, A. D. and Bianchi, A. L. (1992) Membrane potential changes of phrenic motoneurons during fictive vomiting, coughing, and swallowing in the decerebrate cat. *Journal of Neurophysiology* **68**, 2110-2119.

Guyenet, P. G. (2006) The sympathetic control of blood pressure. *Nature Reviews Neuroscience* **7**, 335-346.

Guyenet, P. G., Stornetta, R. L., Abbott, S. B., Depuy, S. D., Fortuna, M. G. and Kanbar, R. (2010) Central CO2 chemoreception and integrated neural mechanisms of cardiovascular and respiratory control. *Journal of Applied Physiology (1985)* **108**, 995-1002.

Guyenet, P. G., Stornetta, R. L., Holloway, B. B., Souza, G. M. P. R. and Abbott, S. B. G. (2018) Rostral ventrolateral medulla and hypertension. *Hypertension* **72**, 559-566.

Hayashi, N (2003). Exercise pressor reflex in decerebrate and anesthetized rats. *American Journal of Physiology - Heart and Circulatory Physiology* **284**, H2026-H2033.

Head, H. and Riddoch, G. (1917) The automatic bladder, excessive sweating and some other reflex conditions, in gross injuries of the spinal cord. *Brain* **40**, 188-263.

Imig, T. J. and Durham, D. (2005) Effect of unilateral noise exposure on the tonotopic distribution of spontaneous activity in the cochlear nucleus and inferior colliculus in the cortically intact and decorticate rat. *Journal of Comparative Neurology* **490**, 391-413.

Israely, S. and Leisman, G. (2019) Can neuromodulation techniques optimally exploit cerebello-thalamo-cortical circuit properties to enhance motor learning post-stroke? *Reviews in the Neuroscience* **30** 821-837.

Iwakiri, H., Oka, T., Takakusaki, K. and Mori, S. (1995) Stimulus effects of the medial pontine reticular formation and the mesencephalic locomotor region upon medullary reticulospinal neurons in acute decerebrate cats. *Neuroscience Research* **23**, 47-53.

Iwamura, Y., Uchino, Y., Ozawa, S. and Torii, S. (1969) Spontaneous and reflex discharge of a sympathetic nerve during "para-sleep" in decerebrate cat. *Brain Research* **16**, 359-367.

Jarisch, A. and Henze, C. (1937) Über Blutdrucksenkung durch chemische Erregung depressorischer Nerven. *Archiv für Experimentelle Pathologie und Pharmakologie* **187**, 706–730.

Kandel, E. R. (1979) Cellular insights into behavior and learning. *Harvey Lecture* **73**, 19-92.

Kandel, E. R., Schwartz, J. H. and Jessell T. M (2000) Principles of Neural Science 4/e. New York, NY, USA: McGraw Hill.

Kawahara, K., Yoshioka, T., Yamauchi, Y. and Niizeki K. (1993) Heart beat fluctuation during fictive locomotion in decerebrate cats: locomotor-cardiac coupling of central origin. *Neuroscience Letters* **150**, 200-202.

Kim, J. H., Wang, J. J. and Ebner, T. J. (1988) Alterations in simple spike activity and locomotor behavior associated with climbing fiber input to Purkinje cells in a decerebrate walking cat. *Neuroscience* **25**, 475-489.

Klosterhalfen, W. and Klosterhalfen, S. (1985) Habituation of heart rate in functionally decorticate rats. *Behavioral Neuroscience* **99**, 555-563.

Kotani, N. and Akaike, N. (2013) The effects of volatile anesthetics on synaptic and extrasynaptic GABA-induced neurotransmission. *Brain Research Bulletin* **93**, 69-79.

Lane, M. A., White, T. E., Coutts, M. A., Jones, A. L., Sandhu, M. S., Bloom, D. C., Bolser, D. C., Yates, B. J., Fuller, D. D. and Reier, P. J. (2008) Cervical prephrenic interneurons in the normal and lesioned spinal cord of adult rat. *Journal of Comparative Neurology* **511**, 692-709.

Lane, M. A., Jones, A. L., O'Steen, B. E., Hunsaker, F. L., Vavrousek, J., Salazar, K., Fuller, D. D. and Reier, P. J. (2009a) Pre-phrenic interneurons as an anatomical substrate for plasticity following cervical spinal cord injury (SCI) in the adult rat. *The FASEB Journal* **23**, 5.

Lane, M. A., Lee, K. Z., Fuller, D. D. and Reier, P. J. (2009b) Spinal circuitry and respiratory recovery following spinal cord injury. *Respiratory Physiology and Neurobiology* **169**, 123-132.

Larsen, P. D., Zhong, S., Gebber, G. L. and Barman, S. M. (2000) Differential pattern of spinal sympathetic outflow in response to stimulation of the caudal medullary raphe. *American Journal of Physiology - Regulatory Integrative Comparative Physiology* **279**, R210-R221.

Lebedev, M. A. and Nelson, R. J. (1996) High-frequency vibratory sensitive neurons in monkey primary somatosensory cortex: entrained and nonentrained responses to vibration during the performance of vibratory-cued hand movements. *Experimental Brain Research* **111**, 313-325.

Lin, H., Na, P., Zhang, D., Liu, J., Cai, X. and Li, W. (2020a) Brain connectivity markers for the identification of effective contacts in subthalamic nucleus deep brain stimulation. *Human Brain Mapping* doi: 10.1002/hbm.24927. [Epub ahead of print]

Lin, F., Wu, D., Lin, C., Cai, H., Chen, L., Cai, G., Ye, Q. and Cai, G. (2020b) Pedunculopontine Nucleus Deep Brain Stimulation Improves Gait Disorder in Parkinson's Disease: A Systematic Review and Meta-analysis. *Neurochemical Research* doi: 10.1007/s11064-020-02962-y. [Epub ahead of print]

Lipski, J., Kanjhan, R., Kruszewska, B. and Rong, W. (1996) Properties of presympathetic neurones in the rostral ventrolateral medulla in the rat: an intracellular study '*in vivo*'. *Journal of Physiology* **490**, 729-744.

Liu, J. C. (1979) Tonic inhibition of thermoregulation in the decerebrate monkey (Saimiri sciureus). *Experimental Neurology* **64**, 632-648.

Lombardi, F., Montano, N., Finocchiaro, M. L., Ruscone, T. G., Baselli, G., Cerutti, S. and Malliani, A. (1990) Spectral analysis of sympathetic discharge in decerebrate cats. *Journal of the Autonomic Nervous System* **30**, S97-S99.

Malheiros Lima, M. R., Totola, L. T., Lana, M. V. G., Strauss, B. E., Takakura, A. C. and Moreira, T. S. (2018) Breathing responses produced by optogenetic stimulation of adrenergic C1 neurons are dependent on the connection with preBötzinger complex in rats. *Pflügers Archiv* **470**, 1659-1672.

Marchenko, V., Ghali, M. G. and Rogers, R. F. (2012) Motoneuron firing patterns underlying fast oscillations in phrenic nerve discharge in the rat. *Journal of Neurophysiology* **108**, 2134-2143.

Marchenko, V., Ghali, M. G. and Rogers, R. F. (2015) The role of spinal GABAergic circuits in the control of phrenic nerve motor output. *American Journal of Physiology - Regulatory Integrative Comparative Physiology* **308**, R916-R926.

Marchenko, V., Granata, A. R. and Cohen, M. I. (2002) Respiratory cycle timing and fast inspiratory discharge rhythms in the adult decerebrate rat. *American Journal of Physiology - Regulatory Integrative Comparative Physiology* **283**, R931-R940.

Marchenko, V., Koizumi, H., Mosher, B., Koshiya, N., Tariq, M. F., Bezdudnaya, T. G., Zhang, R., Molkov, Y. I., Rybak, I. A. and Smith, J. C. (2016) Perturbations of respiratory rhythm and pattern by disrupting synaptic inhibition within pre-botzinger and botzinger complexes. *eNeuro* **3**, 1-24.

Marchenko, V. and Rogers, R. F. (2009) GABAAergic and glycinergic inhibition in the phrenic nucleus organizes and couples fast oscillations in motor output. *Journal of Neurophysiology* **101**, 2134-2145.

Marchenko, V. and Rogers, R. F. (2007) Temperature and state dependence of dynamic phrenic oscillations in the decerebrate juvenile rat. *American Journal of Physiology - Regulatory Integrative Comparative Physiology* **293**, R2323-R2335.

Marchenko, V. and Rogers, R. F. (2006a) Time-frequency coherence analysis of phrenic and hypoglossal activity in the decerebrate rat during eupnea, hyperpnea, and gasping. *American Journal of Physiology - Regulatory Integrative Comparative Physiology* **291**, R1430-R1442.

Marchenko, V. and Rogers, R. F. (2006b) Selective loss of high-frequency oscillations in phrenic and hypoglossal activity in the decerebrate rat during gasping. *American Journal of Physiology - Regulatory Integrative Comparative Physiology* **291**, R1414-R1429.

Marchenko, V. and Sapru, H. N. (2003) Cardiovascular responses to chemical stimulation of the lateral tegmental field and adjacent medullary reticular formation in the rat. *Brain Research* **977**, 247-260.

Marlinskii, V. V. and Voitenko L. P. (1992) Participation of the medial reticular formation of the medulla oblongata in the supraspinal control of ocomotor and postural activities in the guinea pig. *Neuroscience and Behavioral Physiology* **22**, 336-342.

Martínez-Gálvez, G., Zambrano, J. M., Diaz Soto. J. C., Zhan, W. Z., Gransee, H. M., Sieck, G. C. and Mantilla, C. B. (2016). TrkB gene therapy by adeno-associated virus enhances recovery after cervical spinal cord injury. *Experimental Neurology* **276**, 31-40.

Medvedev, O. S. and Stepochkina, N. A. (1975) Effect of phenamine and gutimine and gutimine on adaptive changes in arterial pressure occurring during skeletal muscle contraction. *Biulleten Eksperimentalnoi Biologii I Meditsiny* **80**, 41-44.

Meehan, C. F., Grondahl, L., Nielsen, J. B. and Hultborn, H. R. (2012) Fictive locomotion in the adult decerebrate and spinal mouse *in vivo*. *Journal of Physiology* **590**, 289-300.

Molkov, Y. I., Rubin, J. E., Rybak, I. A. and Smith, J. C. (2017) Computational models of the neural control of breathing. *Wiley Interdisciplinary Reviews. Systems Biology and Medicine* **9**, 2.

Montano, N., Lombardi, F., Gnecchi Ruscone, T., Contini, M., Finocchiaro, M. L., Baselli, G., Porta, A., Cerutti, S. and Malliani, A. (1992) Spectral analysis of sympathetic discharge, R-R interval and systolic arterial pressure in decerebrate cats. *Journal of the Autonomic Nervous System* **40**, 21-31.

Morgado Valle, C., Baca, S. M. and Feldman, J. L. (2010) Glycinergic pacemaker neurons in preBötzinger complex of neonatal mouse. *Journal of Neuroscience* **30**, 3634-3639.

Morgado Valle, C. and Beltran Parrazal, L. (2017) Respiratory rhythm generation: the whole is greater than the sum of the parts. *Advances in Experimental Medicine and Biology* **1015**, 147-161.

Mueller, P. J., Fyk-Kolodziej, B. E., Azar, T. A. and Llewellyn-Smith, I. J. (2019) Subregional differences in GABAA receptor subunit expression in the rostral ventrolateral medulla of sedentary versus physically active rats. *Journal of Comparative Neurology* **528**, 1053-1075.

Nam, H. and Kerman, I. A. (2016) Distribution of catecholaminergic presympathetic-premotor neurons in the rat lower brainstem. *Neuroscience* **324**, 430-445.

Okromelidze, L., Tsuboi, T., Eisinger, R. S., Burns, M. R., Charbel, M., Rana, M., Grewal, S. S., Lu, C. Q., Almeida, L., Foote, K. D., Okun, M. S. and Middlebrooks, E. H. (2020) Functional and Structural Connectivity Patterns Associated with Clinical Outcomes in Deep Brain Stimulation of the Globus Pallidus Interneus for Generalized Dystonia. *AJNR American Journal of Neuroradiology*. doi:10.3174/ajnr.A6429 [Epub ahead of print]

Ogundele, O. M., Lee, C. C. and Francis, J. (2017) Thalamic dopaminergic neurons projects to the paraventricular nucleus-rostral ventrolateral medulla/C1 neural circuit. *Anatomical record* **300**, 1307-1314.

O'Hara, T. E. Jr. and Goshgarian, H. G. (1991). Quantitative assessment of phrenic nerve functional recovery mediated by the crossed phrenic reflex at various time intervals after spinal cord injury. *Experimental Neurology* **111**, 244-250.

Opris, I., Dai, X., Johnson, D. M. G., Sanchez, F. J., Villamil, L. M., Xie, S., Lee-Hauser, C. R., Chang, S., Jordan, L. M. and Noga, B. R. (2019) Activation of Brainstem Neurons During Mesencephalic Locomotor Region-Evoked Locomotion in the Cat. *Frontiers in Systems Neuroscience* **13**, 69.

Pagni, C. A., Albanese, A., Bentivoglio, A., Broggi, G., Canavero, S., Cioni, B., Rose, M. D., Simone, C. D., Franzini, A., Lavano, A., Landi, A., Meglio, M., Modugno, M., Romanelli, L., Romito, L. M., Sturiale, C., Valzania, F., Zeme, S. and Zenga, F. (2008) Results by motor cortex stimulation in treatment of focal dystonia, Parkinson's disease and postictal spasticity. The experience of the Italian Study Group of the Italian Neurosurgical Society. *Acta Neurochirurgica Supplement* **101**, 13-21.

Palisses, R., Persegol, L., Viala, D. and Viala, G. (1988) Reflex modulation of phrenic activity through hindlimb passive motion in decorticate and spinal rabbit preparation. *Neuroscience* **24**, 719-728.

Palisses, R., Perségol, L. and Viala, D. (1989) Evidence for respiratory interneurones in the C3-C5 cervical spinal cord in the decorticate rabbit. *Experimental Brain Research* **78**, 624-632.

Petrenko, A. B., Yamakura, T., Sakimura, K. and Baba, H. (2014) Defining the role of NMDA receptors in anesthesia: are we there yet? *European Journal of Pharmacology* **723**, 29-37.

Pickering, A. E. and Paton, J. F. (2006) A decerebrate, artificially-perfused in situ preparation of rat: utility for the study of autonomic and nociceptive processing. *Journal of Neuroscience Methods* **155**, 260-271.

Polentes, J., Stamegna, J. C., Nieto-Sampedro, M. and Gauthier, P. (2004) Phrenic rehabilitation and diaphragm recovery after cervical injury and transplantation of olfactory ensheathing cells. *Neurobiology of Disease* **16**, 638-653.

Pollock, L. J. and Davis, L. (1930) The reflex activities of a decerebrate animal. *Journal of Comparative Neurology* **50**, 377-411.

Porter, W. T. (1895). The path of the respiratory impulse from the bulb to the phrenic nuclei. *Journal of Physiology* **17**, 455-485.

Rajshekhar, G., Gorthi, S. S. and Rastogi, P. (2009) Strain, curvature, and twist measurements in digital holographic interferometry using pseudo-Wigner-Ville distribution based method. *Review of Scientific Instruments* **80**, 093107.

Reinoso, M. A., Sieck, G. C. and Hubmayr, R. D. (1996) Respiratory muscle coordination in acute spinal dogs. *Respiration Physiology* **104**, 29-37.

Rezaee, Z., Kaura, S., Solanki, D., Dash, A., Srivastava MVP, Lahiri, U., and Dutta, A. (2020) Deep Cerebellar Transcranial Direct Current Stimulation of the Dentate Nucleus to Facilitate Standing Balance in Chronic Stroke Survivors - A Pilot Study. *Brain Science* **10**. pii: E94. doi: 10.3390/brainsci/10020094

Reynolds, C. A., O'Leary, D. S., Ly, C., Smith, S. A. and Minic, Z. (2019) Development of a decerebrate model for investigating mechanisms mediating viscero-sympathetic reflexes in the spinalized rat. *American Journal of Physiology - Heart and Circulatory Physiology* **316**, H1332-H1340.

Richardson, C. A. and Mitchell, R. A. (1982) Power spectral analysis of inspiratory nerve activity in the decerebrate cat. *Brain Research* **233**, 317-336.

Richardson, C. A. (1986) Unique spectral peak in phrenic nerve activity characterizes gasps in decerebrate cats. *Journal of Applied Physiology* **60**, 782-790.

Rhoton, A. L. Jr. (2000a) Cerebellum and fourth ventricle. *Neurosurgery* **47**, S7-27.

Rhoton, A. I. Jr. (2000b) The Foramen Magnum. *Neurosurgery* **47**, S155-S193.

Rybak, I. A., Molkov, Y. I., Jasinski, P. E., Shevtsova, N. A. and Smith, J. C. (2014) Rhythmic bursting in the pre-Bötzinger complex: mechanisms and models. *Progress in Brain Research* **209**, 1-23.

Rybak, I. A., Shevtsova, N. A., St-John, W. M., Paton, J. F. and Pierrefiche, O. (2003) Endogenous rhythm generation in the pre-Bötzinger complex and ionic currents: modelling and *in vitro* studies. *European Journal of Neuroscience* **18**, 239-257.

Sapru, H. N. and Krieger, A. J. (1979) Cardiovascular and respiratory effects of some anesthetics in the decerebrate rat. *European Journal of Pharmacology* **53**, 151-158.

Sapru, H. N. and Krieger, A. J. (1978) Procedure for the decerebration of the rat. *Brain Research Bulletin* **3**, 675-679.

Schreihofer, A. M. and Guyenet, P. G. (1997) Identification of C1 presympathetic neurons in rat rostral ventrolateral medulla by juxtacellular labeling *in vivo*. *Journal of Comparative Neurology* **387**, 524-536.

Seyedabadi, M., Li, Q., Padley, J. R., Pilowsky, P. M. and Goodchild, A. K. (2006) A novel pressor area at the medullo-cervical junction that is not dependent on the RVLM: efferent pathways and chemical mediators. *Journal of Neuroscience* **26**, 5420-5427.

Sherrington, C. S. (1898) Decerebrate rigidity, and reflex coordination of movements. *Journal of Physiology* **22**, 319-332.

Sherrington, C. (1906) The integrative action of the nervous system. Yale University Press: New Haven.

Shintani, Y., Terao, Y. and Ohta, H. (2010) Molecular mechanisms underlying hypothermia-induced neuroprotection. *Stroke Research Treatment* **2011**, 809874.

Sholomenko, G. N., Funk, G. D. and Steeves, J. D. (1991) Locomotor activities in the decerebrate bird without phasic afferent input. *Neuroscience* **40**, 257-266.

Sica, A. L. and Gandhi, M. R. (1990) Efferent phrenic nerve and respiratory neuron activities in the developing kitten: spontaneous discharges and hypoxic responses. *Brain Research* **524**, 254-262.

Silverman, J., Garnett, N. L., Giszter, S. F., Heckman, C. J. 2nd, Kulpa-Eddy, J. A., Lemay, M. A., Perry, C. K. and Pinter, M. (2005) Decerebrate mammalian preparations: unalleviated or fully alleviated pain? A review and opinion. *Contemporary Topics in Laboratory Animal Science* **44**, 34-36.

Sivertsen, M. S., Perreault M. C. and Glover J. C. (2016) Pontine reticulospinal projections in the neonatal mouse: internal organization and axon trajectories. *Journal of Comparative Neurology* **524**, 1270-1291.

Smith, J. C., Ellenberger, H. H., Ballanyi, K., Richter, D. W. and Feldman, J. L. (1991) Pre-Bötzinger complex: a brainstem region that may generate respiratory rhythm in mammals. *Science* **254**, 726-729.

Spetzler, R. F., Nakaji, P., Kalani, Y. (2015) Neurovascular Surgery. New York, New York: Thieme.

Stornetta, R. L. (2009) Neurochemistry of bulbospinal presympathetic neurons of the medulla oblongata. *Journal of Chemical Neuroanatomy* **38**, 222-230.

Stornetta, R. L., Sevigny, C. P., Schreihofer, A. M., Rosin, D. L. and Guyenet, P. G. (2002) Vesicular glutamate transporter DNPI/VGLUT2 is expressed by both C1 adrenergic and nonaminergic presympathetic vasomotor neurons of the rat medulla. *Journal of Comparative Neurology* **444**, 207-220.

Sun, M. K., Young, B. S., Hackett, J. T. and Guyenet, P. G. (1988) Reticulospinal pacemaker neurons of the rat rostral ventrolateral medulla with putative sympathoexcitatory function: an intracellular study *in vitro*. *Brain Research* **442**, 229-239.

Takakusaki, K., Chiba R., Nozu, T. and Okumura, T. (2016) Brainstem control of locomotion and muscle tone with special reference to the role of the mesopontine tegmentum and medullary reticulospinal systems. *Journal of Neural Transmission (Vienna)* **123**, 695-729.

Tan, Z. G., Zhou, Q., Huang, T. and Jiang, Y. (2016) Efficacies of globus pallidus stimulation and subthalamimc nucleus stimulation for advanced Parkinson's disease: a meta-analysis of randomized controlled trials. *Clinical and Interventional Aging* **11**, 777-786.

Tang, X., Hu, T. and Snyder, J. S. (2010) The aortic and carotid sinus baroreflexes contribute equally to control blood pressure and heart rate variabilities. *The FASEB Journal* **24**, lb1-1065.27.

Taylor, J. S., Neal, R. I., Harris, J., Ford, T. W. and Clarke, R. W. (1991). Prolonged inhibition of a spinal reflex after intense stimulation of distant peripheral nerves in the decerebrated rabbit. *Journal of Physiology* **437**, 71-83.

Tenney, S. M. and Ou, L. C. (1977) Ventilatory response of decorticate and decerebrate cats to hypoxia and CO2. *Respiration Physiology* **29**, 81-92.

Thornton, E. W. and Van-Toller, C. (1973) Operant conditioning of heart-rate changes in the functionally decorticate curarised rat. *Physiology and Behavior* **10**, 983-988.

Tonkovic-Capin, M., Krolo, M., Stuth, E. A., Hopp, F. A. and Zuperku, E. J. (1998) Improved method of canine decerebration. *Journal of Applied Physiology* **85**, 747-750.

Tsuchimochi, H., Hayes, S. G., McCord, J. L. and Kaufman, M. P. (2009) Both central command and exercise pressor reflex activate cardiac sympathetic nerve activity in decerebrate cats. *American Journal of Physiology - Heart and Circulatory Physiology* **296**, H1157-H1163.

Tsuchimochi, H., McCord, J. L., Hayes, S. G., Koba, S. and Kaufman, M. P. (2010) Chronic femoral artery occlusion augments exercise pressor reflex in decerebrated rats. *American Journal of Physiology - Heart and Circulatory Physiology* **299**, H106-H113.

van Brederode, J. F. and Berger, A. J. (2008) Spike-firing resonance in hypoglossal motoneurons. *Journal of Neurophysiology* **99**, 2916-2928.

Vassal, F., Dilly, D., Boutet, C., Bertholon, F., Charier, D. and Pommier, B. (2019) White matter tracts involved by deep brain stimulation of the subthalamic nucleus in Parkinsono's disease: a connectivity study based on preoperative diffusion tensor imaging tractography. *British Journal of Neurosurgery* 1-9 doi: 10.1080/02688697.

Viala, D., Persegol, L. and Palisses, R. (1987a) Relationship between phrenic and hindlimb extensor activities during fictive locomotion. *Neuroscience Letters* **74**, 49-52.

Viala, D., Viala, G., Persegol, L. and Palisses, R. (1987b) Changeover from alternate to synchronous bilateral pattern of the phrenic bursts entrained by fictive locomotion in the spinal rabbit preparation. *Neuroscience Letters* **78**, 318-322.

Viala, D., Vidal, C. and Freton, E. (1979) Coordinated rhythmic bursting in respiratory and locomotor muscle nerves in the spinal rabbit. *Neuroscience Letters* **11**, 155-159.

Vinit, S. and Kastner, A. (2009) Descending bulbospinal pathways and recovery of respiratory motor function following spinal cord injury. *Respiratory Physiology and Neurobiology* **169**, 115-122.

Von Bezold, A. and Hirt, L. (1867) Über die physiologischen Wirkungen des essigsauren Veratrine. *Unters Physiol Lab Wurzburg* **1**, 73-122.

Waites, B. A., Ackland, G. L., Noble, R. and Hanson, M. A. (1996) Red nucleus lesions abolish the biphasic respiratory response to isocapnic hypoxia in decerebrate young rabbits. *Journal of Physiology* **495**, 217-225.

Wilson, J. R., Vardaris, R. M., and Schweikert, G. E. 3rd. (1975) Technique for chronic electrode or cannula implantation in decorticate animals. *Physiology and Behavior* **14**, 875-877.

Woods, J. W. (1964) Behavior of chronic decerebrate rats. *Journal of Neurophysiology* **27**, 635-644.

Woolf, C. J. (1984) Long term alterations in the excitability of the flexion reflex produced by peripheral tissue injury in the chronic decerebrate rat. *Pain* **18**, 325-343.

Yang, A. I., Buch, V. P., Heman-Ackah, S. M., Ramayya, A. G., Hitti, F. L., Beatson, N., Chaibainou, H., Yates, M., Wang, S., Verma, R., Wolf, R. L. and Baltuch, G. H. (2020) Thalamic deep brain stimulation for essential tremor: relation of the dentato-rubro-thalamic tract with stimulation parameters. *World Neurosurgery* pii: S1878-S8750(20)30047-4 [Epub ahead of print]

Yasargil G. M. and Sandri C. (1990) Topography and ultrastructure of commissural interneurons that may establish reciprocal inibitory connections of the Mauthner axons in the spinal cord of the tench, Tinca tinca L. *Journal of Neurocytology* **19**, 111-126.

Yates, B. J., Balaban, C. D., Miller, A. D., Endo, K., Yamaguchi, Y. (1995) Vestibular inputs to the lateral tegmental field of the cat: potential role in autonomic control. *Brain Research* **689**, 197-206.

Zhou, D., Huang, Q., Fung, M. L., Li, A., Darnall, R. A., Nattie, E. E. and St. John, W. M. (1996). Phrenic response to hypercapnia in the unanesthetized, decerebrate, newborn rat. *Respiration Physiology* **104**, 11-22.

Zielinski, A. T. and Gebber, G. L. (1975) Basis for late expiratory spinal inhibition of phrenic nerve discharge. *American Journal of Physiology* **228**, 1690-1694.

Zimmer, M. B. and Goshgarian, H. G. (2005) Spontaneous crossed phrenic activity in the neonatal respiratory network. *Experimental Neurology* **194**, 530-540.

Zimmer, M. B. and Goshgarian, H. G. (2006) Spinal activation of serotonin 1A receptors enhances latent respiratory activity after spinal cord injury. *Journal of Spinal Cord Medicine* **29**, 147-155.

Zimmer, M. B. and Goshgarian, H. G. (2007) GABA, not glycine, mediates inhibition of latent respiratory motor pathways after spinal cord injury. *Experimental Neurology* **203**, 493-501.

Zuperku, E. J., Stucke, A. G., Krolikowski, J. G., Tomlinson, J., Hopp, F. A. and Stuth, E. A. (2019) Inputs to medullary respiratory neurons from a pontine subregion that controls breathing frequency. *Respiratory Physiology and Neurobiology* **265**, 127-140.